Regulation of Piezo1 channels and its impact on cell division

Julia Carrillo García

TESIS DOCTORAL UPF / 2021

DIRECTORES DE LA TESIS:

Dr. Miguel Ángel Valverde de Castro

Dr. José Manuel Fernández-Fernández

Departamento de Ciencias Experimentales y de la Salud

Universitat Pompeu Fabra Barcelona

Abstract

Despite recognizing for a long time that some physiological responses depend on forces and membrane shape changes, it is not until the current decade that a deeper insight into the underlying proteins and cascades has taken place. The mechanosensitive ion channel Piezo1 is pointed out as one of the major and essential front-line proteins in the response to forces. Its regulation has been in the spotlight of recent mechanobiological studies. We now know that Piezo1 can be modulated by external and internal global forces. However, little is known about its regulation by local membrane-binding proteins. Here, we present a step further in the understanding of how cells can regulate their mechanical response through specialized membrane-shaping proteins, the BAR domain-containing proteins. We showed by an electrophysiological study that two BAR proteins, Pacsin3 and Amphiphysin, can decrease the inactivation rates of Piezo1 currents leading to an overall increase in the mechanical response of the channel. We next investigated the relevance of Pacsin3/Piezo1 interplay in the context of cytokinesis, a mechanical process widely influenced by forces. Using a microendothelial cell model and cell imaging, we revealed an important contribution of these proteins and calcium in the proper endosomal vesicle trafficking to the intercellular bridge connecting the two daughter cells, with subsequent effects in the localization of the abscission machinery. These results underline Piezo1 as an important mechanotransductor during cytokinesis but also present a model of regulation that might be important in more physiological events.

Resumen

A pesar de reconocer durante un largo tiempo que las fuerzas y los cambios en la forma de la membrana influyen en algunas respuestas fisiológicas, no ha sido hasta la década actual que se han empezado a entender las proteínas y cascadas implicadas en estos procesos. El canal iónico mecanosensible Piezo1 ha sido señalado como una de las proteínas principales y fundamentales en la respuesta mecánica de la célula. Su regulación está en el foco de los estudios actuales de mecanobiología. Ahora sabemos que Piezo1 puede ser modulado por fuerzas externas e internas. Sin embargo, se conoce poco acerca de su regulación a través de proteínas de unión a membrana. Aquí, presentamos un paso adelante en el entendimiento de cómo las células son capaces de regular la respuesta mecánica del canal a través de proteínas con un dominio BAR, especializadas en remodelar la membrana. A través de un estudio electrofisiológico, hemos demostrado que dos de ellas, Pacsin3 y Anfifisina, son capaces de disminuir la tasa de inactivación de Piezo1 provocando un aumento general de la respuesta mecánica del canal. A continuación, hemos investigado la relevancia de la relación Pacsin3/Piezo1 en el contexto de la citocinesis, un proceso ampliamente influenciado por las fuerzas. Utilizando un modelo celular microendotelial y técnicas de microscopía, hemos desvelado una importante contribución de estas proteínas y del calcio en el tráfico de vesículas endosomales al puente intercelular que conecta las dos células hijas, con consiguientes efectos en la localización de la maquinaria de abscisión. Estos resultados no sólo destacan el papel de Piezo1 como mecanotransductor en el proceso de citocinesis, también presentan un modelo de regulación que podría ser clave en otros procesos fisiológicos.

Preface

The study of Piezo1 has expanded our understanding of cell physics in cellular signaling. Membrane mechanics (stiffness, thickness, tension, and curvature) rule the behavior of Piezo1 and are pivotal to organ development and cell proliferation. Furthermore, the role of calcium in these processes has widely been studied. In this context, this work aims to find new regulators of the Piezo1 channel within proteins involved in membrane dynamics as well as their implications in the mechanical process of cell division.

This thesis begins with the introduction of three major subjects. The first subject concerns a review of the main characteristics of the Piezo1 channel and its mechanotransduction. Then, the most relevant modulators of membrane mechanics are presented addressing their role in Piezo1 response. In this section, we outline a group of proteins required for membrane-shaping dynamics, the BAR proteins, which are recently related to mechanosensitive channels. The third subject delves into the process of cell division, highlighting the main mechanical changes controlling the mitotic machinery and approaching the topic to the engagement of Piezo1.

The results of this thesis are divided into two chapters. In the first chapter, we demonstrate through patch-clamp and calcium imaging techniques that Piezo1 inactivation is modulated by the concave membrane-binding protein Pacsin3. Combining directed mutagenesis with functional studies and co-immunoprecipitation analyses, we determine the interaction between these proteins, delimiting the responsible regions within Pacsin3 and Piezo1 structures. Furthermore, we demonstrate that this interplay is required for the proper localization of Piezo1 in the cell membrane. We also show that another concave protein, Amphiphysin, can also similarly regulate Piezo1

inactivation. However, the convex protein IRSp53 lacks this ability, suggesting a shape-dependent mode of regulation.

In the second chapter, we demonstrate that the interplay between Piezo1 and Pacsin3 is involved in the response to mechanical forces exerted during cytokinesis. We show that both proteins are located at the intercellular bridge connecting daughter cells. The knockdown of these proteins with specific siRNAs increases cell multinucleation and bridge length. Similarly, the use of Piezo1 inhibitors or calcium chelators also impairs cytokinetic completion, standing out the role of this second messenger in the process. Under these conditions, we find a defective Rab11-FIP3 endosomal delivery to the intercellular bridge, mislocalizing proteins from the abscission machinery, such as ESCRT-III and its binding-partner ALIX.

Finally, the implication of these results is discussed emphasizing its relevance in cell physiology and pathophysiology in the context of current research in mechanobiology.

Glossary

AFM atomic force microscopy
Ca^{2+} Calcium
CED C-terminal extracellular domain
CTD C-terminal domains
ECM extracellular matrix
ENaC/DEG/ASIC epithelial sodium channel/degenerin/acid-sensing ion channel
ERM ezrin-radixin-moesin
ESCRT endosomal sorting complex required for transport
FAK focal adhesión kinase
HS-AFM high-speed atomic force microscopy
ICB intercelular bridge
IH inner helix
K-fibers kinetochore fibers
MBCD methyl-beta-cyclodextrin
MSC mechanosensitive ion channel
MT1-MMP Membrane-type 1- matrix metalloproteinase
NO nitric oxid
nPo open probability
OH Outer helix
PDE1 phosphodiesterases 1
PIP phosphatidylinositol phosphate
PIP2 phosphatidyl 4,5-bisphosphate
PKA Protein kinase A
PKC protein kinase C
PM plasma membrane
PRD Proline rich domain
PUFA polyunsaturated fatty acid
S1P sphingosine 1-phosphate
SH3 src-homology 3
STOML3 stomatin-like protein-3
T50 half activation
THU transmembrane helical units
TIRF Total internal reflection fluorescence
TM transmembrane helix
TRP Transient receptor potential
τ_{inact} time constant of inactivation
3D three-dimensional

Table of contents

1. Introduction

One of the biggest challenges that researchers have faced over the years is understanding how changes in cellular architecture and extracellular environment influence the behavior of tissues and organs. Our body is constantly subjected to a wide variety of stimuli in daily life. In this context, physical forces play an important role in how we perceive the world. Hearing surrounding noises, touching surfaces or the conscious awareness of body position are ways to transmit external and internal information to our brains through specialized sensory systems. Moreover, other unconscious internal forces originate in our body as a consequence of the cell microenvironment, such as substrate rigidity, topology, adhesiveness, and cell-cell contacts. All these mechanical stimuli are known to trigger specific responses that are essential for many cellular processes. Understanding how physical forces coordinate physiological responses has emerged as a promising multidisciplinary field, known as Mechanobiology.

The study of the mechanical properties of cells has revealed outstanding clues on how forces can control the fate of organ development, cell differentiation, and motility (Mammoto et al., 2013; Wolfenson et al., 2019). Many studies associate aberrant mechanical conditions to a wide variety of diseases, such as cancer or heart failure, pointing to the importance of these processes (Elosegui-Artola et al., 2014; Lyon et al., 2015; Northey et al., 2017; Pardo-Pastor et al., 2018). Thanks to mechanobiology we have a better understanding of how tissues and organs exhibit unique material properties, three-dimensional forms, and compartmentalization, answering important questions difficult to assess only with genetics and biochemistry.

Unlike chemical signals, which commonly involve a traditional receptor/ligand interaction, physical forces often result in cellular

deformations, challenging the identification of the molecules in charge of force transduction. Those molecules are called mechanosensors and form a heterogeneous group of proteins that share the ability to sense mechanical signals and translate them into biochemical signalings.

We can find mechanosensors in all the cells of our body. However, some organs are subjected to higher levels of mechanical stress and, in consequence, are equipped with specific cell types enriched in certain mechanosensors. One example is blood vessels, where endothelial cells respond to changes in blood flow, a shear stress force that can induce cell polarization and migration (Wojciak-Stothard & Ridley, 2003). In the kidney, mechanosensors from epithelial cells respond to changes in hydrostatic and osmotic pressure by modulating ion transport or endocytic functions (Raghavan et al., 2016). Developing neurons are fitted with large actin-supported extensions at the tip of neurites or axons commissioned to explore the microenvironment through the formation of point contact adhesions and under the regulation of calcium (Ca^{2+}) signaling (Raghavan & Weisz, 2016). Furthermore, fibroblast remodeling activities of the extracellular matrix (ECM) provide collagen deformation fields and local pulling sensed by macrophages that migrate towards the force source, traveling through several hundreds of micrometers (Pakshir et al., 2019). Moreover, contractile muscle cells from the uterus are subjected to one of the biggest mechanical loads occurring in the human body, including organ remodeling during pregnancy and postpartum, the weight of the fetus during gestation or vigorous contractions during partition (Myers & Elad, 2017). Many other cells have similar capacities to specialize against concrete forces. The diversity of mechanosensory elements with distinct biomechanical properties provide a mechanism for specificity in mechanotransduction.

Interestingly, Kim and colleagues have grouped mechanosensors following two models: the “tethered model” and the “lipid bilayer model” (C.-G. Lim et al., 2018). Within the tethered model, proteins undergo conformational changes in consequence of a pulling force, exhibiting binding protein site for open conformational stabilization, releasing signaling molecules, or exposing important regions for enzymatic activity (Collins et al., 2012; Hinz, 2015; Seddiki et al., 2018; Snyder et al., 2017). On the other hand, the force acting upon cells, such as stretching or bending, can cause deformation of entire cells and in this context, lipid bilayers are important sensors of mechanical stress. Transmembrane proteins are tightly coupled with nearby lipids. This configuration allows changes in the physical properties of the lipid bilayer to affect the conformation of some integral membrane proteins, and vice versa (Corradi et al., 2018; R. Phillips et al., 2009). It is what they called “the lipid bilayer model”. Among these transmembrane proteins, mechanosensitive ion channels (MSCs) are one of the most important force-transducing elements as they can convert mechanical stimuli into electrochemical intracellular signals within milliseconds, which is essential for processes requiring short time responses (Martinac & Cox, 2017). In the next section, I will focus on the biophysical principles that underlie the innate force-sensing ability of the MSCs in our cells.

1.1 Mechanosensitive ion channels

MSCs were discovered in the first instance in the context of neuroscience. The idea of mechano-electrical molecular switches arose from the observation that stretching of the muscle cells can depolarize the sensory nerve endings, triggering action potentials (Katz, 1950; Loewenstein, 1959). However, it was not until 30 years later that researchers uncovered the molecular nature of those switches. Thanks to the emergence of the patch-clamp technique, they were capable for the first time to directly measure single MSC currents in frog and chick muscle cells (Brehm et al., 1984; Guharay & Sachs, 1984; Hamill, 1983). MSCs were described as pore-forming transmembrane proteins shaped to facilitate the passage of specific ions in response to an increase in membrane tension (Fig. 1A). These ions not only create an electrical signal in the cell but also act as important cellular messengers, outlining the role of Ca^{2+}. Since their emergence, numerous *in vitro* assays have been developed to apply different types of physical forces to MSCs, revealing a diversity of activating forms, such as suction, shear stress, pulling/pushing, or matrix deflection, and distinct degrees of mechanical sensitivity (Fig. 1B,C).

Due to the difficulties arising from the study of these physical events, such as artifactual signals, a wide variety of techniques have been carried out to identify *bona fide* MSC. Genetic tools, such as siRNA screening technologies or directed mutagenesis, explore alterations of the mechanical cell response to identify reliable MSC proteins. Isolating MSCs in artificial lipid bilayers has been another strategy for the discovery of inherently mechanosensitive proteins. This is the case of the bacterial mechanosensitive MscL/S, the eukaryotic potassium channels TRAAK and TREK or the cation nonspecific Piezo1 channel (Brohawn et al., 2014; S. Sukharev et al., 2001; S. I. Sukharev et al., 1994; Syeda et al., 2016).

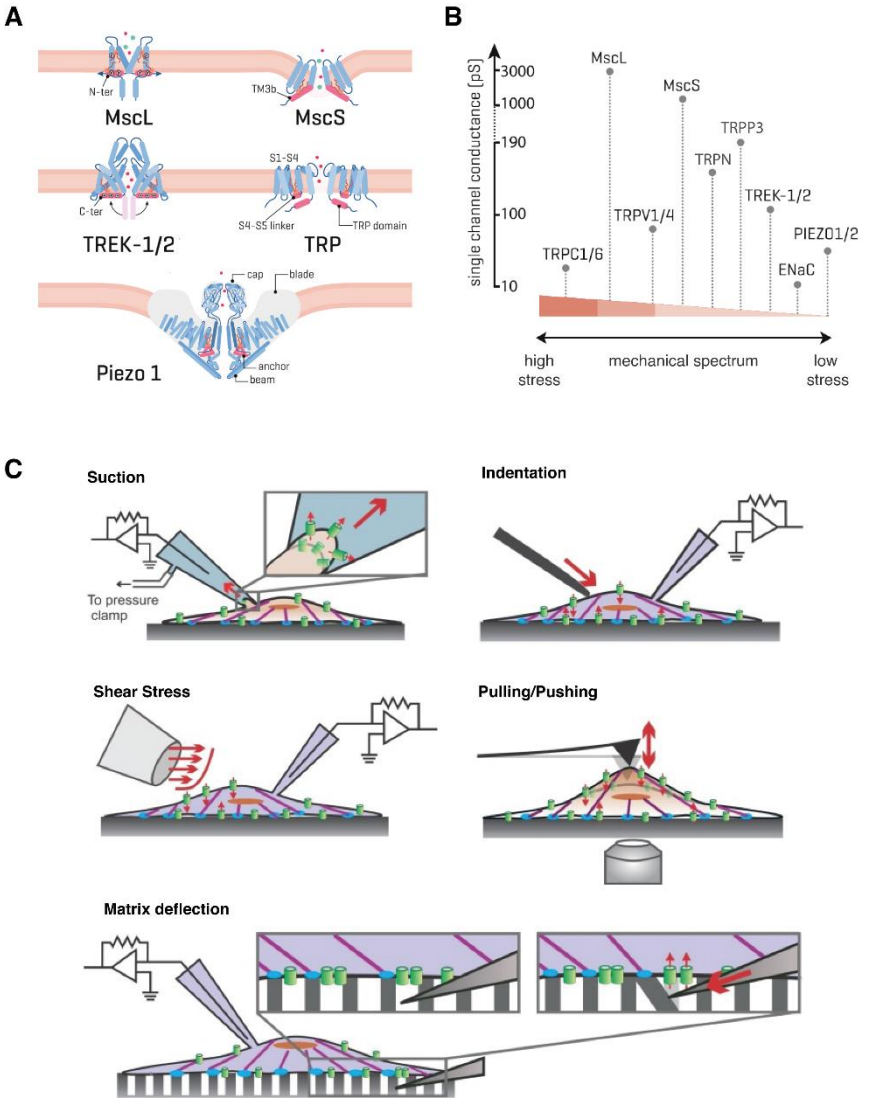

Fig. 1. Mechanosensitive ion channels. (A) Schematic structure of distinct MSCs (adapted from (Bavi et al. 2017)) (B) Spectrum of mechanical sensitivity of MSCs examined by the patch-clamp technique (adapted from (Cox, Bavi, and Martinac 2017)). (C) Some of the current outside-in mechanical techniques to stimulate MSCs (adapted from (Nourse and Pathak 2017)).

To date, the epithelial sodium channel/degenerin/acid-sensing ion channel (ENaC/DEG/ASIC) family has also been associated with mechanical sensing but there is a lack of solid evidence supporting its intrinsically mechanical gating (Carattino & Montalbetti, 2020). Other MSC proteins, such as the transient receptor potential (TRP) channel family, have been linked to mechanical processing, although many of them are insensitive *per se* to mechanical tension (Nikolaev et al., 2019). Those studies suggest that MSCs can also be indirectly activated by mechanical stress, assisted by upstream or downstream molecules, and acting as amplifiers of cellular mechanosensory signals. Under this definition, the list of ion channels implicated in mechanosensation continues to grow.

In this thesis, I will focus on the above-mentioned Piezo1 channel, a recently discovered cation-permeating MSC, which belongs to the first family of MSCs identified in mammals that is both necessary and sufficient for body mechanical sensing, as it will be seen in the next section.

1.1.1 Piezo1 expression and function

Piezo proteins are a fascinating MSC family formed by two members: Piezo1 and Piezo2. These proteins are evolutionarily conserved in animals, plants, and protozoa, but no orthologs can be found in bacteria or yeast (Coste et al., 2010). In mammals, Piezo proteins are encoded by the family with sequence similarity 38 (*FAM38*) genes, also called *PIEZO* genes. These genes share no sequence homology to other known ion channel families or other protein classes, compromising their identification by comparison with other MSC sequences. Instead, their identification as a mechanosensor was conducted with a knockdown study of dozens of candidate genes in Neuro2A sensitive cells, based on transcript enrichments

of this cell line. They further tested the knockdowns for losses of mechanical current activation, discovering Piezo1 and Piezo2 as essential players of the process (Coste et al., 2010).

PIEZO1 and *PIEZO2* genes encode large proteins with a broad expression pattern. At a cellular level, Piezo is present in the plasma membrane (PM), accumulating in dynamic membrane protrusions, such as lamellipodia, filopodia, or axonal growth cones (Koser et al., 2016; Jing Li et al., 2014; Sugimoto et al., 2017). Some studies suggest that these proteins can also be localized in the endoplasmic reticulum, although it remains controversial whether they have a functional role or if it is part of the trafficking process (McHugh et al., 2010; T. Zhang et al., 2017). Piezo1 is found in abundant levels in the vascular and central nervous system, skin, bladder, lung, kidney, and colon. Piezo2 expression is predominant in the peripheral nervous system, skin, bladder, lung, and colon.

Mutations in these proteins are related to multiple diseases. Gain-of-function mutations in the human *PIEZO1* gene can cause dehydrated stomatocytosis, whereas *PIEZO1* loss of function cause lymphatic dysplasia (Albuisson et al., 2013; Fotiou et al., 2015; Lukacs et al., 2015), highlighting the functional importance of this channel in red blood cell function and vessels. Recent studies have related Piezo1 to migraine and chronic pain, which are conditions of mechanical hypersensitivity and allodynia, processes originally mediated by MSC proteins (Della Pietra et al., 2020). Loss of function mutations of *PIEZO2* cause proprioception defects, scoliosis, arthrogryposis, perinatal respiratory distress, and muscle weakness (Delle Vedove et al., 2016; Haliloglu et al., 2017; Masingue et al., 2019). Additionally, high *PIEZO1* or *PIEZO2* expression levels are correlated with poorer prognosis of cancer and increased metastasis (Pardo-Pastor et al., 2018; Yang et al., 2016; Zhou et al., 2020).

Their function is essential in mammals, as shown by constitutive knockout experiments of *PIEZO1* or *PIEZO2* in mice, that cause embryonic lethality (Jing Li et al., 2014; Ranade et al., 2014; Woo et al., 2014). This is not the case of the other known mammalian inherent MSCs, TRAAK, and TREK. Indeed, the triple knockout of TREK-1/TREK-2/TRAAK do not impair mice survival (Schwingshackl et al., 2017). These results point to the requirement of Piezo1 and mechanical forces in physiology.

The Piezo family has been related with virtually all the mechanical processes, including touch, proprioception, pain, the control of plastic changes in different organs, bone homeostasis, stem cell differentiation, neuronal cell development, volume cell regulation, migration, and cell division (Cahalan et al., 2015; Gudipaty et al., 2017; Hung et al., 2016; Pathak et al., 2014; Lijun Wang et al., 2020; Woo et al., 2015). However, the molecular mechanisms and downstream effectors of Piezo currents are not always well understood.

Focusing on Piezo1, which is the subject of this thesis, its presence is critical for the control of vascular development. The Ca^{2+} influx through Piezo1 induced by flow is responsible for stress fiber organization and alignment in the direction of force. This occurs through the activation of the Ca^{2+} binding protein calpain, which in turn regulates cell alignment via proteolytic cleavage of actin and focal adhesion proteins (Jing Li et al., 2014; Ranade et al., 2014). Piezo1 is also necessary for ATP release, promoting vasodilation through nitric oxide (NO) production, which is essential for long-term regulation of vascular tone and blood pressure (Cinar et al., 2015; S. Wang et al., 2016). Despite knowing the downstream signaling of this process, involving purinergic receptor activation and AKT, we still do not fully understand the process of Piezo1-mediated ATP release. Besides, the synergic relation of mechanical shear stress and the

soluble mediator sphingosine 1-phosphate (S1P) can also activate Piezo1 inducing the translocation and activation of the membrane-type 1- matrix metalloproteinase (MT1-MMP) (Kang et al., 2019). MT1-MMP mediates ECM degradation leading to the sprouting of new vessels. This process of angiogenesis increases by enhancing wall shear stress, suggesting a new possible therapeutic strategy for angiogenesis-related diseases based on Piezo1 modulation.

Piezo1 can also modulate other channels, such as the potassium channel KCa3.1 (Cahalan et al., 2015). Ca^{2+} entry across Piezo1 forms a complex with calmodulin that activates KCa3.1, promoting the outgoing traffic of potassium ions and water molecules. This results in cell shrinkage, a process needed for red blood cell volume regulation in response to shear flow or the passage of erythrocytes through narrow blood vessels.

Furthermore, Ca^{2+}-mediate Piezo1 signaling can influence the nuclear localization of transcriptional regulators, such as YAP, which in turn promotes the expression of genes implicated in different processes, such as cell differentiation and substrate stiffness sensing. This mechanism is reported in weight-induced mechanical loading response in skeletal cells (Lijun Wang et al., 2020). Piezo1-mediated Yap translocation to the nucleus is also found in stem cells in response to traction forces, influencing neuronal or glial specification in a substrate stiffness-dependent manner (Pathak et al., 2014).

Another interesting function of Piezo1 is its ability to modulate different cell migration modes, depending on microenvironment conditions. Migration is a dynamic process of actin polymerization and turnover, involving the formation of specialized structures in charge of cell motility. These structures are lamellipodia, filopodia, and focal adhesions, whose formation requires the participation of three distinct pathways triggered by

Rac1, Cdc42, and RhoA, respectively (J. Liu et al., 2015). These pathways coordinate actin dynamics and activate myosin-II and integrin-based adhesions (Pasapera et al., 2015; Sandquist et al., 2006; Woodham et al., 2017). Single migrating cells respond to different degrees of confinement by the regulation of these proteins to optimize cell motility (Hung et al., 2013). Unconfined migration requires Rac1 signaling, whereas under physical confinement cells migrate in a RhoA/myosin II-dependent fashion (Hung et al., 2013; Y.-J. Liu et al., 2015). It has recently been discovered that cells can differentially balance these pathways by sensing the degree of confinement thanks to the activation of Piezo1. Ca^{2+} entry through active Piezo1 channels associates to calmodulin, which binds and activates phosphodiesterases 1 (PDE1), downregulating protein kinase A (PKA) (Hung et al., 2016). PKA is a known regulator of Rho proteins, which inactivates RhoA by phosphorylation and activates Rac1 through β_1 integrin signaling (Newell-Litwa & Horwitz, 2011; O'Connor & Mercurio, 2001). Thus, Piezo1 activation by mechanical confinement forces leads to a strong RhoA output, which acts in synergy with the actomyosin network. These results highlight the undeniable relevance of Piezo1 in the mechanical process of confined migration, with notable implications in metastasis.

Myosin II phosphorylation can also activate Piezo1 through force-producing adhesions, in the absence of external mechanical forces (Ellefsen et al., 2019; Pathak et al., 2014). The mechanism that has been suggested is that cellular traction forces, generated by Myosin-II motors along actin filaments are tethered to integrin-based focal adhesions, increasing local membrane tension that activates nearby Piezo1 channels (Ellefsen et al., 2019). Cells can use this system for probing the stiffness of the extracellular matrix modulating cell migration, but also promoting wound healing and immune function (Discher et al., 2005).

Piezo1 has also been recently involved in the homeostatic control of the cell number (Gudipaty et al., 2017). In the epithelium, cell turnover occurs at some of the highest rates in the body. Some studies on this tissue have revealed that barrier function, the first line of defense in innate immunity, is maintained by a constant regulation of cell number, based on cell division and extrusion of damaged and living cells (Eisenhoffer et al., 2012). To extrude, the cell produces and secrete S1P, which binds to the G-protein-coupled receptor Sphingosine 1 Phosphate receptor 2 ($S1P_2$) of the adjacent cells, activating a RhoA signaling (Spindler et al., 2010). Then, RhoA mediates the formation of a contractile actomyosin ring. Contraction of the neighboring cells squeezes the middle cell out while forming intercellular junctions between the new adjacent cells, preventing gaps to the epithelial barrier. Interestingly, while in damaged cells S1P production is stimulated by an apoptotic stimulus, in crowded areas cell extrusion involves mechanical stimulation of Piezo1. Indeed, impairing Piezo1 by chemical or genetic approaches induces the formation of cell masses in developing zebrafish embryos, at sites where cells would extrude (Eisenhoffer et al., 2012; Gudipaty et al., 2017). Researchers of this study theorize that Piezo1 signaling is upstream of S1P production and secretion. However, as presented before, S1P seems to regulate in turn Piezo1 activity. Thus, there is the possibility that a positive feedback process involves those proteins.

In the same context of epithelial barrier maintenance, Piezo1 stretch-activated channels have also been related to cell division by promoting cell cycle progression from the G2 phase to mitosis (Gudipaty et al., 2017). These results suggest a unique ability to regulate two opposing processes, depending on Piezo1 stimulus, levels, and localization. This is of relevant interest to understand the normal growth of organs, but also for cancer research as approximately 90% of cancers arise from epithelial tissues, and a misregulation in this fine-tuning of cell turnover could complicate the

scenario. Further in the introduction, I will inquire into the underlying mechanisms of Piezo1 control on cell division and the unanswered question surrounding this process, as it represents one of the objects of study of this thesis.

1.1.2 Piezo1 structure and gating mechanism

Although a wide variety of MSC has been discovered over the last years in all types of living forms, only a few of them have a known 3D structure. The lack of homology to any known channel, together with its atypical physical properties, turns the Piezo channels into one of the greatest challenges for structural biology. Although the complete topology of Piezo channels has not yet been determined, structural studies using cryo-EM, electron microscopy data, structure-guided mutagenesis with electrophysiological characterizations, and computational prediction models, are closed to achieve the precise structure of Piezos (Fig. 2A).

Piezo channels are one of the largest ion channels identified to date, with more than 2500 amino acids, and an unusually large number of 38 transmembrane helix (TM), which assembled into a homotrimeric structure (Coste et al., 2010; Ge et al., 2015; Q. Zhao et al., 2018). These TMs shape a gigantic pore-forming protein that exhibits a unique propeller-shaped architecture with three blades (Fig. 2B). Each blade is formed by 9 tandem transmembrane helical units (THUs) of 4 TMs each (Ge et al., 2015; Q. Zhao et al., 2018). The TM37, called outer helix (OH), and the TM38, called the inner helix (IH), of each monomer, are distributed enclosing a ~ 8 Å conducting pore. This region contains specialized residues that act as a transmembrane tunnel for cation influx (Li Wang et al., 2019). The C-terminal extracellular domain (CED) is a large extracellular loop

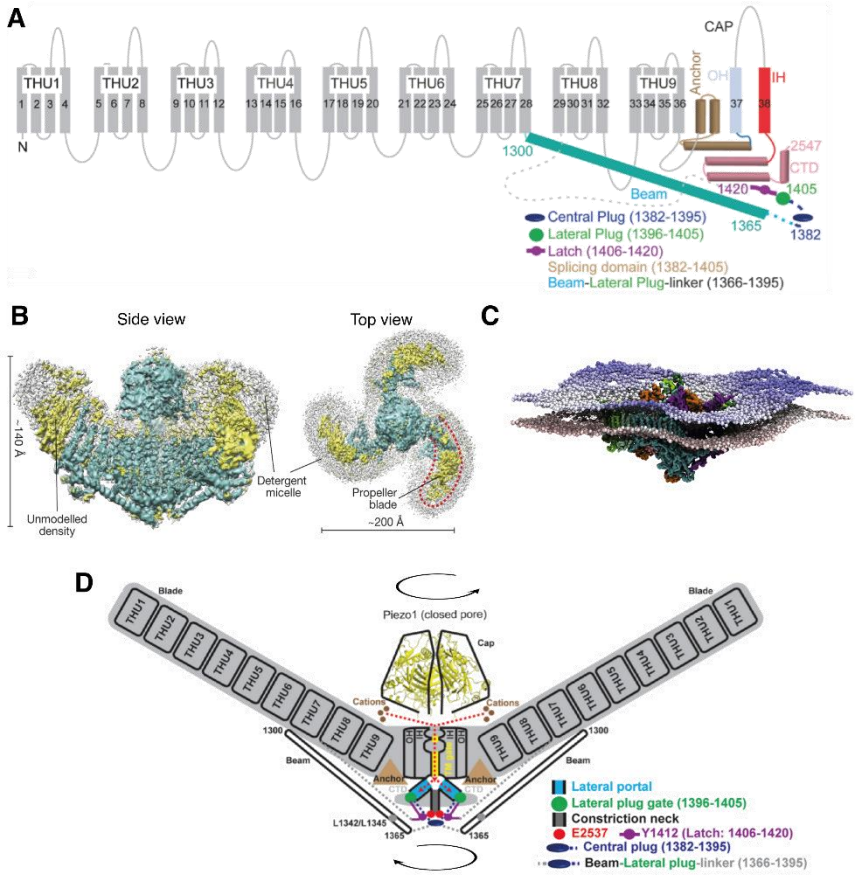

Fig. 2. Piezo1 structure and domain arrangement. (A) Topological model of Piezo1 (adapted from (Geng et al. 2020)). Dashed lines indicate structurally undefined regions. (B) Side and top views of the Piezo1 surface density map (adapted from (Saotome et al. 2018)). (C) Simulation of the bowl-shaped hallmark of Piezo1 in the plasma membrane (adapted from (Chong et al. 2021)). (D) Proposed gating mechanism of the Piezo1 channel (modified from (Geng et al. 2020)). Red dashed lines represent the ion-conducting pathway. Black arrows indicate the rotation direction for the opening of each gate.

connected to the OH and the IH. Each CED of the trimer assembles to form the “cap” of the channel (Fig. 2D) (Ge et al., 2015). In the intracellular side

of the protein, we can find the beams, 9-nm long lateral rods, connecting the blades mechanically to the center of the trimeric complex, and the C-terminal domains (CTD) of each unit (Fig. 2A).

The central pore region, including IH and OH helix, CEDs, and CTDs, is essential for the cationic specificity of the channel and for its gating mechanism. The CTDs form a vertical constriction neck along the central axis, connecting to three lateral portals extending from the central pore (Yubo Wang & Xiao, 2018). Curiously, the intracellular ion-conducting pathway and selectivity of the channel occur through these three lateral portals, instead of the vertical constriction neck (Fig. 2D). Mutating 9 residues of the lateral portals can convert the cation-selective Piezo1 channel into an anion-selective channel (Geng et al., 2020). Also, mutations in the lateral plug (1396-1405), which physically blocks the lateral ion-conducting portals, simultaneously affect ion permeation and channel gating (Geng et al., 2020). Besides, the three lateral plugs are sealed through a "latch" domain (1406-1420). Mutations in this region alter channel conductance, i.e. the flux of ions across the membrane (Geng et al., 2020). This "plug-and-latch" mechanism is suggested to coordinate the gate of the channel, which in turn is allosterically controlled by the cap. It has been demonstrated that deleting some residues from the cap (2393-2397) resulted in a marked reduction of the maximal amplitude of currents, while conserving normal protein expression at the PM (Q. Zhao et al., 2016). Moreover, a central plug (1382-1395) physically blocks the bottom part of the constriction neck and links the proximal end of the beam domain to the intracellular pore, forming a lever-like structure controlled by the blades (Fig. 2D) (Geng et al., 2020; Saotome et al., 2018; Q. Zhao et al., 2018). This mechanism is essential for coordinating a second gate of the channel. Thus, Piezo1 is thought to have a dual-gating mechanism, controlled on one side by the cap, and on the other side by the peripheral blade-beam

apparatus (Li Wang et al., 2019). The cap seems to control the central gate by transmitting to the pore-lining IH and OH a lateral anticlockwise movement, while the blades open the channel twisting in a clockwise manner (Fig. 2D). This duality probably allows the channel to be activated by distinct types of forces with a modality-specific gating. Interestingly, deleting the cap region completely abolished whole-cell currents evoked by poking, suggesting that an intact structure of the channel is needed for both modalities (Li Wang et al., 2019). However, to confirm this remarkable gating mechanism, structures of the fully open state of the channel are needed, as all the structural studies are based on its closed conformation.

These two gates also determine the inactivation properties of the Piezo1 currents. During mechanical stimulation, Piezo kinetics are characterized by an instantaneous rise of current intensity, reaching the maximal amplitude, followed by a slower decay characteristic of channel inactivation, transitioning toward pore closure, i.e. deactivation. In the IH, residues L2475 and V2476 of Piezo1 form a hydrophobic constriction site defined as an inactivation gate (J. Wu et al., 2017; Zheng et al., 2019). Also, a single lysine residue (K2479) in the IH confers a voltage dependence of inactivation (Lewis & Grandl, 2020; Moroni et al., 2018; J. Wu et al., 2017). This implies that following a mechanical stimulation, depolarization favors the stabilization of the open state, slowing inactivation and deactivation. It has been suggested that the cap can allosterically modulate channel inactivation through transmitting structural changes to the connected IH, acting as a coupling unit between force-sensing and inactivation (J. Wu et al., 2017; Q. Zhao et al., 2016). Indeed, some mutations in the CED, such as M2225R and R2456H, cause a slowdown in channel inactivation, without affecting unitary conductance (Q. Zhao et al., 2016). However, other domains, such as the CTDs, also contribute to the inactivation process, pointing towards more inactivation modalities.

Most of the Piezo1 mutations in diseases alter their inactivation, indicating the critical role of these kinetics in normal physiology (Albuisson et al., 2013; C. Bae et al., 2013). Furthermore, inactivation is one of the main differences between Piezo1 and Piezo2 channels, which despite sharing only 42% of sequence homology, the overall structures are very similar (Coste et al., 2010). Piezo1 has a slower inactivation than Piezo2, which could explain their disparate roles in physiology (Coste et al., 2010). Accordingly, understanding inactivation is crucial for unlocking the pathophysiology of some diseases, but also to clarify the physiological function of Piezo currents and their possible modulation by intracellular regulatory proteins or lipids modifying the pore region structure.

Tandem THUs form the force-sensing blades which extend from the central OH-IH pair to the periphery. Interestingly, the three blades can move independently, which might be of relevant interest for the physical response, as a force applied in the membrane is unlikely to be equally distributed among the three subunits (Q. Zhao et al., 2018). Indeed, asymmetric tension can be transmitted to the central axis and then be redistributed to the three lateral plug gates for coordinating the gate of Piezo (Geng et al., 2020). These transmembrane blades are relevant for the mechanosensing and transduction, but also for inducing positive local membrane curvature, i.e. towards the cytoplasm (Fig. 2C). A recent study has demonstrated that Piezo1 adopts different degrees of curvature in lipid vesicles of different sizes (Lin et al., 2019). Furthermore, using high-speed atomic force microscopy (HS-AFM) imaging, the same researchers have analyzed the deformability of Piezo1 under force stimulation. The results suggest that Piezo1 can be reversibly flattened into the membrane plane. This deformation could explain how lateral membrane tension can be converted into a conformational change to gate the Piezo1 channel. A question arises from this fact, as to whether proteins that affect membrane

curvature could modulate these tension-dependent conformational changes. This represents a major objective of this thesis and will be developed in the first chapter of results.

1.1.3 Piezo1 regulation and pharmacology

Piezo1 response to mechanical forces can be modulated by endogenous mechanisms. Curiously, it has been demonstrated that only a minor fraction of Ca^{2+} elevation induced by Piezo1 activation directly occurs by regular Piezo1 influx. Instead, the majority of the Ca^{2+} signal results from upstream or downstream amplification mechanisms (W. Lee et al., 2014).

The mechanical activation of Piezo1 can be influenced by some chemical properties, such as pH. Patch-clamp experiments recording Piezo1 currents at low pH (~6.3) have demonstrated that channel activation is inhibited through the protonation of a region involved in the open to inactivate transition (Bae et al., 2015). Indeed, mutant channels that do not inactivate are pH independent. Besides, pH does not directly affect membrane mechanics, as no changes in membrane capacitance, i.e. the dielectric properties of the bilayer, have been observed during negative pressure stimulation (suction). Researchers have indicated that this modulation could represent an important protective mechanism to microenvironment acidification under some pathological stress conditions.

Piezo1 activity may also be modulated by post-translational modification, produced during protein biosynthesis or by specific enzymes in the PM. Previously, it has been mentioned that the mechanical activation of the Piezo1 channel is enhanced by S1P. This regulation seems to involve the activation of the Src kinase protein. Researchers hypothesize that Src, activated by S1P, could phosphorylate Piezo1 at Ser1621 and Thr1626, a

region close to the beam, sensitizing Piezo1 to mechanical stimulation (Kang et al., 2019). Although it is not the first time that Piezo1 phosphorylation has been reported, the relevance of phosphorylation is still not confirmed and more studies are needed (Zuccala et al., 2016). Furthermore, a recent study suggests that Piezo1 undergoes N-linked glycosylation of two residues from the cap, N2294 and N2331 (Jinyuan Li et al., 2021). This glycosylation state of the channel seems necessary for its trafficking to the membrane.

In addition to the above-mentioned S1P, other proteins in the vicinity of membranes, or being part of them, are important Piezo1 modulators. SERCA, the sarcoplasmic/endoplasmic reticulum Ca^{2+} ATPase, interacts near the PM with a linker region of Piezo1 beside the CTD (T. Zhang et al., 2017). This interaction suppresses Piezo1 activity by impairing the mechanogating of the channel. As SERCA is necessary for cytosolic Ca^{2+} recycling into the sarcoplasmic or endoplasmic reticulum stores, this control of Piezo1 activity could be essential for maintaining Ca^{2+} homeostasis after mechanical activation. Moreover, this interplay has been related to the control of eNOS phosphorylation and Piezo1-dependent migration of endothelial cells (T. Zhang et al., 2017).

Piezo1 can also be indirectly regulated by proteins and lipids that modify membrane mechanics. One example is the stomatin-like protein-3 (STOML3), which binds to cholesterol in cholesterol-rich membrane fractions adding tension to membranes. This tightening facilitates the force transferring to Piezo1, sensitizing channel activation in response to mechanical stimulation (Poole et al., 2014; Qi et al., 2015). From a pathophysiological point of view, some studies have related allodynia with the crosstalk between low-threshold mechanoreceptors, such as Piezo1, and the nociceptive circuits (Lolignier et al., 2015). Since it is known that

cholesterol depletion attenuates the tactile allodynia in mice, STOML3/cholesterol/Piezo1 rapport could be an interesting target for chronic pain treatment. Furthermore, some studies have proved that the lipid composition of the membrane can modify the mechanical response of Piezo1, which will be discussed in more detail later (Borbiro et al., 2015; Romero et al., 2019). Nevertheless, there is still a long way to go to understand the relationships among these biological factors and the key structural domains implicated in those processes.

Piezo1 can also be regulated by pharmacological molecules. The first chemical activator of Piezo1 has been identified in a screening of ~3.25 million compounds, revealing one promising candidate named Yoda1, in honor of the ally of force in cinema (Syeda et al., 2015). Syeda and colleagues have demonstrated that Yoda1 added to artificial cell membranes, containing no other cellular components apart from Piezo1, can trigger a Ca^{2+} influx. Indeed, they have proved that Yoda1 affects the sensitivity and the inactivation kinetics of mechanically stimulated Piezo1 currents. It has been later proved that Yoda1 binds directly to Piezo1 in a region between the pore module and the blades, acting as what authors describe as a “molecular wedge” (Botello-Smith et al., 2019). This union facilitates force-induced conformational changes leading to pore opening in the presence of sub-threshold mechanical stimuli. It is interesting to note that some mutants prevent chemical activation, maintaining mechanical sensitivity, and vice versa (Coste et al., 2015; Yanfeng Wang et al., 2018). Thus, it may be attractive to study how chemical and mechanical activation could be sensed by independent transduction pathways. Since then, some other synthetic small agonists of Piezo1 have been identified using high throughput screening. However, none of them possess higher potency than Yoda1 (Yanfeng Wang et al., 2018). By contrast to Piezo1, no chemical activators are known up to date for Piezo2.

Some pharmacological inhibitors of Piezo1 currents have also been identified. Ruthenium red and gadolinium are the first compounds to be proved as chemical inhibitors of Piezo1 currents, as they are known blockers of many MSCs (Coste et al., 2010). However, their lack of specificity towards Piezo1 and the absence of studies determining their mechanism of inhibition handicap their use as experimental or clinical tools. In 2011, GsMTx4, a spider venom peptide, has been shown to inhibit Piezo1 currents by its effect on membrane mechanics (Bae et al., 2011; Gnanasambandam et al., 2017). GsMTx4 is suggested to bind relaxed membrane surfaces distorting their structure. From a physical point of view, the main theory for understanding Piezo1 inhibition is that, after membrane stretching, lateral pressure in the lipids is reduced and the peptide could penetrate deeper into the membrane, leading to partial relaxation of the outer monolayer (Suchyna et al., 2004). This induces that the positive membrane curvature near the channel, generated by its intrinsic structure, is relieved so that greater membrane tension would be necessary to activate Piezo1. Conversely, GsMTx4 is shown to activate some inherently MSCs, such as TREK or the bacterial MscL (Kamaraju et al., 2010; Suchyna, 2017). Indeed, the binding of GsMTx4 to the outer membrane can induce negative curvature tension in resting surrounding membranes, activating these channels. This interesting observation appeals to understanding the functional relevance of the positive local membrane curvature generated by the structure of Piezo1, by contrast to the rest of MSCs known.

Researchers have been searching for inhibitors of Piezo1 that specifically bind to the channel. Recently, they have synthesized an antagonist of Yoda1-induced activation of Piezo1, named Dooku1, in honor of its enmity with Yoda (Evans et al., 2018). Dooku1 is derived from the structure of Yoda1 and thus, its antagonistic activity is through reversible competition for similar binding sites. These synthetic molecules represent an important

advance for the understanding of Piezo1 structure and would be helpful for functional studies. However, the pursuit of specific chemical regulators of Piezo1 and understanding how changes in mechanical properties concretely affect MSC activity, are questions that are still being assessed.

1.2 Membrane dynamics

MSCs are embedded in PMs, and thus, are in constant rapport with membrane dynamics. As highly dynamic structures, PMs control the exchange of matter, energy, and information with the extracellular microenvironment. Around one-third of the coded information of our genomes corresponds to membrane proteins (Wallin & Von Heijne, 1998). Thus, understanding the complex interrelationships between these proteins and lipids and their spatial and temporal regulation is essential to understand many physiological processes, such as vesicular trafficking, cell-cell communication, motility, and cell division.

In the context of mechanobiology, membranes are regularly subjected to internal and external forces, which are rapidly and precisely translated into local deformations, membrane remodeling, or protein signaling. These modifications lead to changes in membrane parameters such as tension, thickness, and curvature. In addition to MSCs, cells are subjected to other important force-transducing elements, which are the extracellular matrix, the cytoskeleton, and lipids. Interestingly, all these 3 elements have shown a strong rapport with MSC function. Additionally, the cell is equipped with scaffold proteins that connect these elements, sensing and stabilizing membrane dynamics. How MSCs precisely interact with these constituents is a question that remains incompletely understood. The next section of this

introduction will address the main characteristics of these cellular mechanics, and their interplay with MSCs, with the focus on Piezo1.

1.2.1 Force-transducing cellular components

Piezo1 channels are inherently activated by mechanical stimulation, as demonstrated by patch-clamp recordings in membrane patches, membrane blebs, and in reconstituted lipid bilayer systems (Cox et al., 2016; Lewis & Grandl, 2015; Syeda et al., 2016). Those experiments isolate Piezo1 from the effect of the ECM and the cytoskeleton, but not from lipid structural influences. However, the three of them have been shown to induce changes in the mechanosensitive properties of Piezo1, as well as to other MSCs, acting as important force-transducing cellular components.

Extracellular matrix

The ECM is a complex network of fibrillar and non-fibrillar macromolecules, which provides a three-dimensional (3D) scaffold where different cell types are embedded forming tissues. The ECM is highly specialized, providing not only structural integrity but also communicating and dictating functions to resident cells via chemical and mechanical signals. Thanks to this ECM-cell liaison, the ECM can regulate cellular processes such as proliferation, differentiation, or migration (L. R. Smith et al., 2018; Yamada et al., 2019).

Its composition is surprisingly dynamic, varying among tissues, over time, during normal tissue repair, and under some pathological conditions. Many macromolecules forming the ECM can directly interact with cell surface

receptors, acting as important chemical cues for signaling processes. Among the principal constituents of the ECM are collagen, elastin, and fibronectin, which can assemble into fibrils conferring tensile strength to the ECM. Non-fibrillar molecules, as glycoproteins, proteoglycans, and hyaluronan, endow the ECM with compressive resistance. Thus, these components also represent important physical cues, contributing to ECM rigidity, density, porosity, and topography. However, the molecular mechanisms controlling cell adaptation to these physical changes are not fully understood.

The close rapport between MSCs and ECM has been studied over the last years. Piezo1 has been identified as a key element for cellular matrix stiffness sensing and remodeling. A stiffer mechanical environment has been linked to an upregulation of Piezo1 expression in some tumors, correlating to a worse cancer prognosis (Chen et al., 2018). Besides, a recent study using *Piezo1*-deficient mice has revealed that mechanically activated Piezo1 can control the expression of some types of collagens through the modulation of the transcriptional regulator YAP, coordinating ECM remodeling and subsequently tissue stiffness (Lijun Wang et al., 2020). In turn, matrix stiffening provides a mechanical microenvironment to activate Piezo1. An experiment using beads coated with ECM proteins and mounted to atomic force microscopy (AFM) cantilever, has demonstrated that Piezo1 is sensitized to pulling forces only in presence of ECM proteins (Gaub & Müller, 2017). This enhanced calcium signal can not be reproduced with concanavalin A coated beads, a non-ECM protein that adheres to carbohydrates from the cell surface. These results indicate that Piezo1 sensitization is mediated by the binding of specific matrix proteins, such as collagen. However, it remains to be investigated whether collagen modulates Piezo1 response by direct binding or indirectly by a neighboring membrane protein signaling.

One protein implicated in mediating Piezo1-ECM crosslink is integrin. Integrins are located in cell surfaces and represent one of the principal cellular components controlling ECM mechanics (Schwartz, 2010). They are tethered to the ECM by its extracellular domain, with different binding specificities for matrix components, including collagen, fibronectin, laminin, and proteoglycans. Their cytoplasmic tails are connected to actin through adaptor proteins, such as talin or tensin. This results in a physical transmission of mechanical and chemical signals from the ECM to the cytoskeleton, and vice versa. Integrins are involved in the intracellular recruitment of important kinases, such as Src kinases or focal adhesion kinases (FAK), and other scaffold proteins, promoting cell adhesion, motility, proliferation, and differentiation (C. Kim et al., 2011). Indeed, Piezo1 activity at focal adhesions has been shown to activate integrin-FAK signaling via Ca^{2+} mediated FAK phosphorylation promoting the formation of focal adhesions (Albarrán-Juárez et al., 2018; X. Chen et al., 2018). This mechanism can explain the increase in matrix stiffness sensing mediated by Piezo1 activity. Thus, Piezo1 is involved in a feedforward positive control between matrix stiffening and sensing of stiffness, which can be a contributing factor in tumor tissue malignancy or fibrosis.

Cytoskeleton

Another native cellular structure that must be considered in MSC mechanotransduction is the cytoskeleton. Together with the ECM, the local arrangement of the cytoskeleton largely determines membrane forces. The cytoskeleton is formed by a highly structured and dynamic network of three types of filaments: actin, microtubules, and intermediate filaments. These filaments are connected and regulated by the association of a wide variety of cytoskeletal proteins. These proteins orchestrate the assembly and

disassembly of filaments arming cells with structural support necessary to regulate cell shape and movement. Besides, the cytoskeleton-associated proteins can interact with MSCs to modulate their tension sensitivity. This interplay between MSCs and the cytoskeleton has been linked to important cytoskeletal functions such as endocytosis and vesicle transport, migration, adhesion, and cell division (Abe & Puertollano, 2011; Gudipaty et al., 2017; Hung et al., 2016; Jetta et al., 2021).

Since the discovery of MSCs, researchers have tried to understand the role of the cytoskeleton in the activity of Piezo1 channels. Interestingly, they have noticed that Piezo1 activated in bleb-attached patches, which lack cytoskeletal connections, are more sensitive to tension than in cell-attached patches, where the cytoskeletal components are presumably maintained (Cox et al., 2016). Besides, knocking out filamin, a scaffold protein connecting actin to membrane proteins, increases Piezo1 sensitivity to mechanical stimuli (Retailleau et al., 2015). These results reveal a mechanoprotective role of the cytoskeleton on Piezo1, which represents a key mechanism for preventing uncontrolled channel gating in resting cells.

By contrast, disrupting the entire actin filaments with cytochalasin D results in a reduction of whole-cell Piezo1 currents activated by indentation of a concrete region of the cell surface (Gottlieb et al., 2012). Given that Piezo1 can be activated in the absence of the cytoskeleton, these results suggest that the cytoskeleton also participates in a force transmission along the membrane, sensitizing Piezo1 channels distant from the source of membrane deformation.

Moreover, thanks to high signal-to-noise techniques, such as the total internal reflection fluorescence (TIRF) microscopy, Piezo1 Ca^{2+} flickers have been detected at the cell-substrate interface in the absence of mechanical stimulation (Ellefsen et al., 2019; Pathak et al., 2014). These

endogenous Piezo1 flickers are enriched in the vicinity of force-producing adhesions. Indeed, the inhibition of myosin II, which regulates actin filament contraction, impairs these spontaneous Piezo1 activities (Pathak et al., 2014). Taken together, these results indicate that Piezo1 can be activated by an increase in membrane tension generated in traction forces coming from a pre-stressed cytoskeleton. This mechanism could allow the cell to explore its environment, acting as a sensor at the cell-matrix interface. However, the detailed mechanisms regarding how these intracellular forces are directly or indirectly transmitted to Piezo1 require further studies.

The most consensual theory to explain the full gating mechanism of Piezo1 is that the "tether model" works in combination with "the force through lipid" model (Gaub & Müller, 2017). This theory arises from the observation that Piezo1 can be activated independently of the ECM and the cytoskeleton, by forces transmitted through the lipid bilayer. Thus, understanding how Piezo1 interacts with lipids is essential to fully understand the activation process.

Lipids

Lipid membrane composition can not only modulate the activity and localization of constitutive proteins, but also the mechanical properties of the lipid bilayer. Changes in thickness, elasticity, and transbilayer pressure have been found to affect the activity of all MSCs, including TRP channels, TREK, TRAAK, Msc, and Piezo1 (Brohawn et al., 2014; Ciardo & Ferrer-Montiel, 2017; Cox & Gottlieb, 2019; Ridone et al., 2018). These studies combine different techniques of spectroscopy with patch-clamp functional characterization of MSC currents, demonstrating that an increase in unsaturated lipids leads to a decrease in membrane thickness which reduces

the tension required for the opening of MSCs. Additionally, the level of unsaturation increases the area/lipid relation, promoting channel relaxation, which in some MSCs is translated to the stabilization of the open state, which is the case of MscS (Pietro Ridone et al., 2018).

In the case of Piezo1, lipids can influence the three states of the channel (closed, open, and inactivated) without necessarily binding to the channel or altering the cytoskeleton (Cox & Gottlieb, 2019). As previously mentioned, a decrease in positive membrane curvature, by outer monolayer relaxation, likely induced by the amphipathic molecule GsMTx4, inhibits the closed to open transition of Piezo1 after mechanical stimulation. This is supported by the fact that the proteolytic cleavage of the protein APP results in an amphipathic Aβ peptide, which can inhibit Piezo1 currents similarly to GsMTx4, without any interaction with the channel (Gottlieb et al., 2019). Besides, it has been shown that saturated fatty acids increase membrane lipid order, stiffening the bilayer. In consequence, the Piezo1 channel requires a greater mechanical stimulus to be activated. In contrast, polyunsaturated fatty acids (PUFAs) tend to increase lipid disorder, allowing the transmission of force to the pore module (Q. Zhao et al., 2018).

Interestingly, not only the cell-intrinsic lipid profile is responsible for MSC modulation, but also changes in the fatty acid metabolism (Ridone et al., 2018). Dietary fatty acids can integrate into membranes controlling thickness and fluidity and modulating Piezo1 mechanical response (Romero et al., 2019). The results of this study have demonstrated that supplementing membranes with margaric acid, a saturated fatty acid found in dairy and fish, increases membrane rigidity and bending stiffness. This inhibits endogenous Piezo1 currents by affecting its mechanosensitivity. By contrast, long PUFAs present in meat and fish, can affect Piezo1 inactivation without modifying current magnitudes nor channel sensitivity

to mechanical stimulation. However, different PUFAs with similar structures can cause a different outcome on Piezo1 inactivation, slowing or accelerating such kinetics. This effect on inactivation appears to stem from an allosteric modulation of the coupling between the CED and the inner pore helix. The distinct impact in inactivation of different PUFAs stills unexplained, though it could be possible that the number of unsaturations allows them to interact with a different layer of the membrane or to implicate additional players, such as specialized proteins or changes in cholesterol content (Sherratt & Preston Mason, 2018; Turk & Chapkin, 2013). These results can explain the discrepancy in Piezo1 kinetics between cell types. Furthermore, researchers point towards an important therapeutic strategy for reverse pathological Piezo1 gain-of-function mutations through supplementation with fatty acids (Pietro Ridone et al., 2018).

Similarly, cholesterol can affect fluidity, lipid order, and bending rigidity of membranes depending on lipid chain saturation, as well as cytoskeletal membrane interactions (Khatibzadeh et al., 2013; Pan et al., 2009). Depletion of cholesterol with methyl-beta-cyclodextrin (MBCD), produces a reduction of Piezo1 mechanosensitivity, comparable to the effect of saturated fatty acids (Qi et al., 2015; P. Ridone et al., 2019). These results have been observed even in membranes with undetectable amounts of STOML3 (P. Ridone et al., 2019). Thus, cholesterol can affect Piezo1 activity by STOML3 dependent and independent mechanisms. However, it must be determined how this effect is through membrane mechanic changes, by direct binding of cholesterol to Piezo1, or by a mix of both.

Indeed, some lipids such as phosphatidylinositol phosphates (PIPs), seem to directly interact with Piezo channels, throughout their propellers. However, these studies are based on computational simulations and must be experimentally confirmed (Buyan et al., 2019; Chong et al., 2019). Some

of the effects of PIPs on Piezo1 activity have already been studied. A depletion of phosphatidyl 4,5-bisphosphate (PIP2) has been linked to a reduction of Piezo1 activity (Borbiro et al., 2015). Thus, PIPs are a major focal point for mechanobiology, also for their contribution to important mechanical processes such as migration or cell division (Echard, 2012; C.-Y. Wu et al., 2014).

Solving the relation of Piezo1 with lipids is an essential question to understand how membrane tension is propagated through phospholipid bilayers. The lipid dome shape induced by the Piezo1 structure can in turn store significant potential energy, in the form of curvature changes (Haselwandter & MacKinnon, 2018). This membrane footprint can not only amplify the sensitivity of Piezo1 to tension but also recruit other bending proteins specialized to detect membrane curvatures, such as the BAR domain proteins.

1.2.2 Bar-domain proteins

The ability of membranes to adopt different degrees of curvature is essential for the cellular architecture, defining its morphology, organelles, and local membrane subdomains. Moreover, the budding of membrane vesicles during endocytosis, the formation of tubular cytoplasmic projections during cell migration, or the emergence of the intercellular bridge (ICB) in the course of cytokinesis are examples of the pivotal role of membrane curvature in physiological processes.

Membrane curvatures can be generated in different ways and degrees. Usually, the asymmetric lipid or protein composition along the two lipid leaves of the bilayer is responsible for low membrane bending. However, the formation of highly curved membranes is an active process that requires

specialized protein networks and sometimes the cytoskeleton. One of these membrane-sculpting proteins is the family of BAR domain-containing proteins.

BAR domain proteins are a unique group of proteins involved in membrane reshaping and fission. They are specialized in bending membranes by coupling to the internal face of the bilayer and altering the underlying lipid organization, acting as a mold. This is possible thanks to a singular arched shape, responsible not only for inducing membrane curvature but also for sensing and binding to bending regions. In consequence, they can be found as part of essential cellular processes such as endocytosis, migration, or cytokinesis.

Their physical environment is central to understanding their distinct properties. Indeed, they are influenced by protein density on the membrane, membrane tension, and membrane shape. These parameters can control their fate by modulating their level of oligomerization or their interaction with other proteins. Their similarities with MSCs in function and localization, open the way to a new paradigm. Uncovering how MSCs and Bar domains could interact with each other is key to understanding potential physiological processes in which this cooperation could take place.

Types and structure

The BAR domain proteins are ubiquitous proteins highly conserved in eukaryotes, and recently identified in prokaryotes (D. A. Phillips et al., 2020). Within the BAR proteins, members are grouped into classical BARs, I-BARs, N-BARs, and F-BARs. Commonly, these families of proteins combine a membrane-remodeling BAR domain with additional

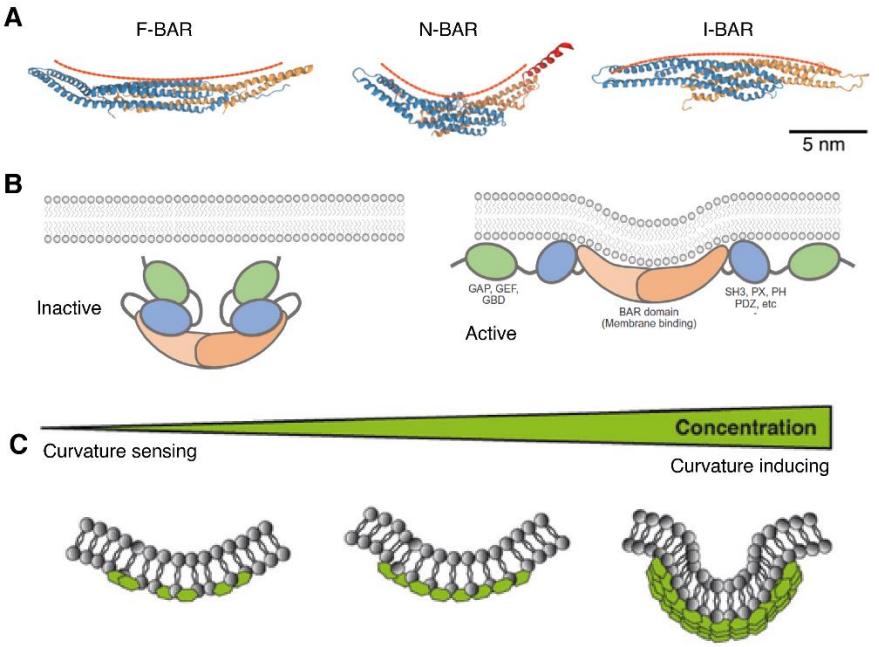

Fig. 3. Characteristics of BAR-domain proteins. (A) Different intrinsic curvatures degrees of BAR-domain proteins (modified from (Simunovic et al. 2015)). Note the positive curvature of the F-BAR and N-BAR domains, in contrast to the negative curvature of the I-BAR domain. Red line represents the PM. (B) Representation of the inactive and active state of a prototypical concave BAR-domain protein (modified from (Carman and Dominguez 2018)). (C) Function of BAR-domains depending on protein density on the membrane, ranging from curvature sensing to curvature inducing (modified from (Johannes, Wunder, and Bassereau 2014)).

protein-protein or protein-lipid interaction extensions and/or catalytic domains. All these factors are responsible for the biological coupling of different membrane curvature states to specific cellular responses. The BAR domain consists of a characteristic banana-shaped coiled-coil core formed by 2 anti-parallel dimers with 3 α-helices each one (Fig. 3A) (Masuda & Mochizuki, 2010). The disruption of hydrophobic interactions among dimers impairs BAR protein functionality and is used by cells to

regulate their membrane remodeling activity (Dislich et al., 2011; Gortat et al., 2012). One face of the Bar domain contains positively charged residues that interact with the negatively charged lipid headgroups of the inner surface of membranes. The orientation of positive charges, the degree of bending and twisting of the 3 helices and their angle of dimerization mainly determine the type of membrane curvature sensed.

Classical BARs, F-BARs, and N-BARs have a concave structure attracted by positive membrane curvatures, forming invaginations. N-BAR proteins, such as Amphiphysin or Endophilin, are characterized by an amphipathic N-terminal α-helix preceding the BAR domain, that inserts into the membrane and participates in membrane curvature generation (Cui et al., 2013). Some F-BAR proteins, such as Pacsins, present a similar insert, the wedge loop (Bai et al., 2012; Q. Wang et al., 2009). However, F-BAR domains are enough for membrane binding through electrostatic interactions. The wedge loop seems to be necessary for the interaction between dimers, modifying tubules diameters (Frost et al., 2008; Henne et al., 2007). Some "classical" BARs have additional domains implicated in protein-membrane interactions, such as the BAR-PH module found in ASAP/ACAP-family members and the PX-BAR module of sorting nexins, which can bind phosphoinositides from the membrane (Fig. 3B). In contrast to the N-terminal signature of N-BAR, those domains only dictate protein localization, explaining their predilection for early endosomes (Zhong et al., 2005). Another important difference between classical BARs, F-BARs, and N-BARs is their degree of curvature and their predilection for distinct membrane types (Daum et al., 2016; Frost et al., 2008). N-BARs are attracted to higher curved membranes than "classical" BARs, which in turn generate narrower tubules than F-BARs. Indeed, F-BARs are the most elongated domains with shallower curvatures and thus, usually stabilize membrane structures with larger diameters.

Conversely, I-BARs are slightly convex, sensing and promoting negative bending, leading to the formation of protrusions. Exceptionally, some members of the F-BAR family, such as Pacsin2, also have the ability to induce filopodia-like structures. Researchers have suggested that this protein may differ from the "canonical" F-BAR domains by a different surface distribution of positively charged residues (Guerrier et al., 2009). Interestingly, a study indicates that 2 members of the I-BAR family, MIM and ABBA, also insert an amphipathic helix into the membrane surface, contributing to the larger diameter of the tubular structures formed *in vitro (Saarikangas et al., 2009)*.

Moreover, these proteins contain complementary features that determine their oligomerization, their interaction with other proteins, and ultimately, their role in membrane remodeling. Generally, BAR proteins tend to be part of a multiprotein complex, rather than existing in isolation. Indeed, BAR domain proteins interact with each other to form a sophisticated network that acts as a scaffold to sculpt liposomes, tubular structures, and projections (Fig. 3C). Some studies demonstrate via electron microscopy experiments how BAR domain proteins interconnect. F-BARs can assemble by lateral and tip-to-tip interactions, while N-BARs assemble mainly through interactions between their N-terminal amphipathic helices (Shimada et al., 2007; Frost et al., 2008; Mim et al., 2012). In the case of I-BARs, they form lateral and end-to-end interactions responsible for their sculpting ability (Nepal et al., 2020). Besides, some BAR proteins also present auxiliary domains enabling the interaction with distinct proteins, including the domains SH3, PDZ, ArfGAP, RhoGEF, and RhoGAP. These domains not only instigate the formation of protein complexes essential for many cellular processes but also direct target proteins to specific localizations. Additionally, they promote an autoinhibited configuration of BAR proteins in resting conditions, covering the membrane-binding

surface of the BAR domain (Fig. 3B). This is possible thanks to intramolecular interactions between the auxiliary domains, regulating protein activity. Thus, these domains are critical to understanding the many functions of BAR proteins.

Function and regulation

Besides the principal function of BAR proteins, which is to provide scaffolding that imposes shape and tension on membranes, they also render structural support to cytoskeletal proteins. Some of their domains act as linkers between actin dynamics and membrane rearrangements.

The SH3 (src-homology 3) domain is the most common motif, present in ~50% of all BAR proteins. It allows BARs to interact with proteins containing a proline-rich domain (PRD) of the PXXP type, such as actin-related proteins WASP, WAVE, Arp2/3, and formin. SH3 recruits these assembly factors, connecting membrane dynamics and curvature changes to the cytoskeleton. Additionally, some BAR proteins can regulate RhoGTPase activity, playing a significant role in actin dynamics. As an example, RhoGEF and RhoGAP catalytic domains are present in several BAR proteins and act like cellular switches of Rho GTPases, promoting the transition between the inactive GDP-bound state to the active GTP-bound state, and vice versa (Bos et al., 2007). The regulation of Rho GTPase activity has been reported for all members of the I-BAR family, including IRSp53, and in some members of the F-BAR family, such as the Pacsin2 isoform (Kreuk et al., 2011; K. B. Lim et al., 2008). These Rho GTPases regulate in turn actin assembly during cell cycle, cell polarity, cell migration, and endocytosis.

Besides binding to cytoskeletal assembly factors, the SH3 can alternatively bind to dynamin, a GTPase responsible for endocytosis. In turn, dynamin can regulate the activity of those BAR proteins by inducing a conformational change that relieves them from their autoinhibitory configuration. Afterward, active BAR proteins are ready to bind to membrane surfaces. Such regulation is observed in Amphiphysin, Endophilin, and Pacsin (Meinecke et al., 2013; Rao et al., 2010). This mechanism may also explain how BAR proteins can be regulated for switching between binding to actin filaments and to membranes during endocytosis. Indeed, some BAR proteins have a bidirectional interaction with both actin cytoskeleton and dynamin. This enables BAR proteins to drive clathrin-dependent and -independent endocytosis (Boucrot et al., 2015; Itoh et al., 2005; Sathe et al., 2018). However, the role of BAR proteins in endocytosis has also been reported in a dynamin-independent fashion, such as IRSp53-mediated endocytosis (Sathe et al., 2018).

Furthermore, some BAR proteins, members of the FES/FER F-BAR family, possess tyrosine kinase domains that promote the phosphorylation of downstream effectors, including cytoskeletal proteins. This ability has been associated with cell development, survival, migration, and inflammatory mediator release (Craig, 2012). Curiously, cellular kinases can also phosphorylate residues from BAR proteins regulating their membrane remodeling capacity. As an example, the phosphorylation of Ser75 of Endophilin has been identified with the deeper incorporation of its N-terminal amphipathic helix into the membrane (Ambroso et al., 2014). This regulates their mechanism of membrane curvature induction, shifting from vesiculation to tubulation. IRSp53 is also regulated by the phosphorylation of two threonines. In this case, the phosphorylated state of IRSp53 creates a binding site for the protein 14-3-3, triggering the inactivation of the I-BAR (Robens et al., 2010). This mechanism is in

charge of downregulating filopodia dynamics during migration (Kast & Dominguez, 2019). Moreover, the phosphorylation of Pacsin2 by the protein kinase C (PKC) has been proposed to reduce its membrane binding capacity, enabling its recruitment by dynamin, and thus promoting endocytosis (Senju et al., 2015). In this case, phosphorylation is proposed to determine the type of function conducted by the BAR protein, whether stabilization or scission of the membrane vesicle. Interestingly, it has been discovered that this phosphorylation can be induced by increases in membrane tension.

Indeed, mechanical stress plays an important role in BAR protein regulation. Researchers have found that external physical forces applied on the membrane, such as tension and friction, impact the ability of BAR domain proteins to remodel membranes (T. Nishimura et al., 2018). Membrane tension seems to be an inhibitory factor for BAR domain assembly, as shown by the induction of cluster geometry alteration (Shi & Baumgart, 2015; Simunovic & Voth, 2015). By contrast, mechanical forces appear to increase the binding of BAR proteins to the membrane (Z. Chen et al., 2015; Shi & Baumgart, 2015). This effect of forces on BAR domain oligomerization suggests a role of BAR dimers as mechanosensor proteins. Additionally, a binding site for SH3 has been found in some MSCs, such as members from the ENaC and TRP family (Cuajungco et al., 2006; Rotin et al., 1994).

Moreover, the amphipathic helix insertion of N-BAR and Pacsins can promote lipid packing defects (Hatzakis et al., 2009; H. Zhao et al., 2013). Thus, these BAR proteins could increase MSCs activity similarly to polyunsaturated phospholipids. Recent studies demonstrate that BAR domains can selectively bind to phosphoinositides through their positively charged amino acids or by membrane-binding auxiliary domains

(Moravcevic et al., 2015; Saarikangas et al., 2009; Schöneberg et al., 2017). Indeed, PIP2 can release some F-BAR from their autoinhibitory state, promoting membrane insertion and bending (Kelley et al., 2015). In addition to regulating membrane geometry, this allows BAR lattices to induce PIP2 clustering and lipid-phase separation generating extremely stable lipid microdomains (H. Zhao et al., 2013). In these microdomains, the lateral diffusion of lipids is strongly suppressed. This increase in lipid order is known to affect the mechanical response of the cell, for example, decreasing mechanosensation of Piezo1. Thus, a better understanding of how individual and oligomerized BAR protein affects membrane mechanics and their relationship with MSCs could lead to a better understanding of cell mechanotransduction.

Pacsin3 and MSCs

Pacsin3 belongs to a subfamily of F-BAR proteins, constituted by three isoforms (Fig. 4A) (Sumoy et al., 2001). Despite being identified as an important coordinator of membrane mechanics, Pacsin3 is the last reported isoform and the least well-known. Interestingly, it has been discovered a novel role for Pacsin3 on MSC regulation.

The three isoforms of Pacsin are associated with the sensing and remodeling of positive membrane curvatures. Phylogenetic analyses suggest that *PACSIN3* emerges from the gene duplication of a *PACSIN1/2* ancestor (Fig. 4B) (Kessels & Qualmann, 2004). Their main differences reside in their tissue distribution, some extra motifs in their structure, and a few functional divergences. While Pacsin2 expression is ubiquitous, Pacsin1 expression is almost restricted to the brain (Modregger et al., 2000). To date, Pacsin3 has been detected in almost all tissues, enriched in the heart, skeletal muscle,

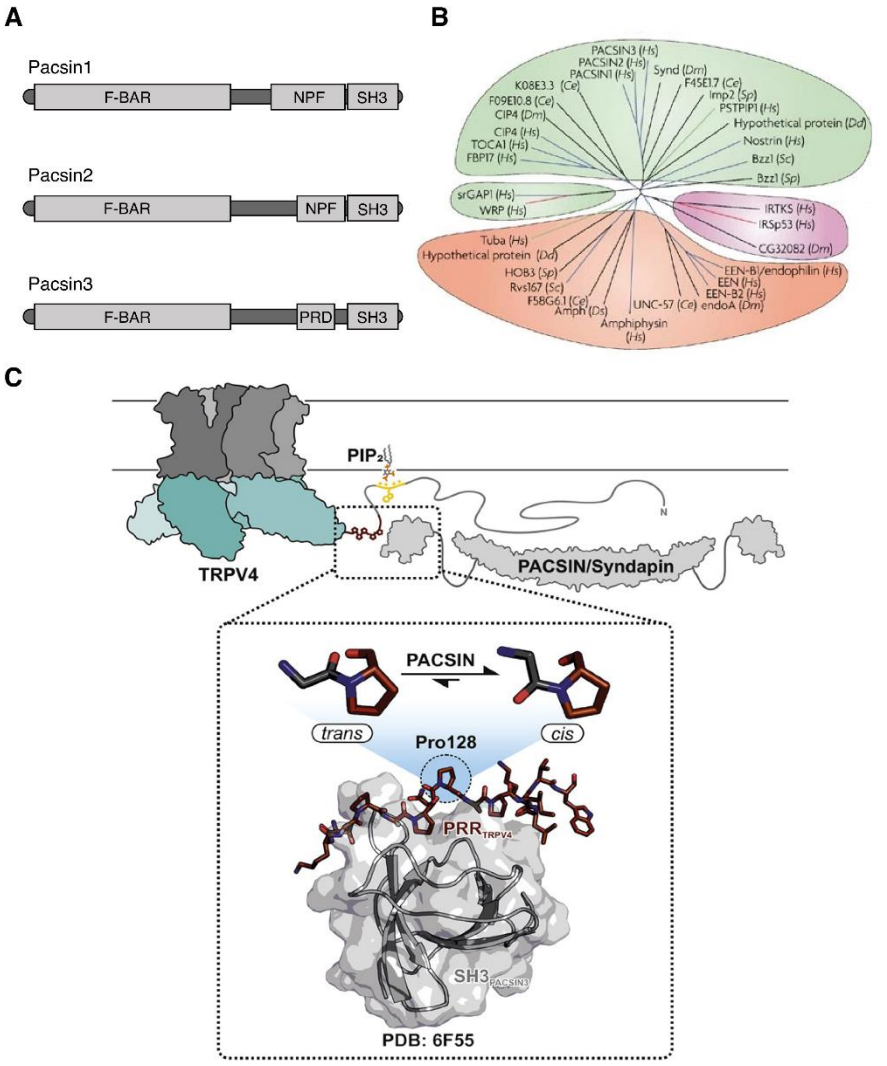

Fig. 4. Characteristics of Pacsin isoforms and their interaction with the TRPV4 channel. (A) Domain structure organization of the three Pacsin isoforms. (B) Pacsin phylogeny within the context of BAR-domain proteins (adapted from (Takenawa and Suetsugu 2007)). (C) Model of the interaction between the Pacsin1-3 SH3 domain and the TRPV4 PRD domain (adapted from (Goretzki et al. 2018)).

and lung (Sumoy et al., 2001). Regarding their structure, all Pacsin isoforms are constituted by an elongated F-BAR domain with an S-shaped concave conformation and a C-terminal SH3 protein-protein interaction domain. Additionally, all of them have a wedge loop which seems to mediate lateral interaction among dimers and, to a lesser extent, membrane insertion (Wang et al., 2009). Indeed, some specific residues found in Pacsin3 increase the rigidity of the wedge loop leading to lower membrane curvatures and higher tubule diameters than those induced by Pacsin1 and 2 (Bai et al., 2012). Moreover, Pacsin3 structure differs from the rest of isoforms by containing a proline-rich region, possibly coupling other SH3 proteins, and lacking NPF motifs, which mediates the interaction with the eps15-homology domain for vesicle formation and recycling (Fig 4A) (Guilherme et al., 2004; Cuajungco et al., 2006).

Their F-BAR domain is also suggested to participate in homo- and hetero-oligomerization of Pacsins (Kessels & Qualmann, 2004). This capacity of clustering is important during endocytosis, as they act as an adaptor lattice linking the endocytic machinery with the actin cytoskeleton. Their binding to actin effectors, such as N-WASP, stimulates actin polymerization for a proper vesicle formation (Kreuk et al., 2011; Ritter et al., 1999). Pacsins link dynamin to the neck of budding vesicles in the last step of endocytosis, triggering membrane scission. However, the co-distribution of all Pacsin isoforms with dynamin is partial (Modregger et al., 2000). Furthermore, at high concentrations, Pacsins inhibit the endocytic process (Modregger et al., 2000; Simpson et al., 1999). Specifically, Pacsin3 may also inhibit endocytosis through its PRD domain, by interaction with the SH3 of dynamin displacing important interactors from the endocytic machinery (Cuajungco et al., 2006). All these results suggest additional functions of Pacsins besides endocytosis.

Despite missing RhoGAP and RhoGEF domains, Pacsins are linked to the control of Rac1 inactivation. Interestingly, the same function is described for Piezo1, while TRPV4, in contrast, is shown to promote the activation of Rac1 (Ou-Yang et al., 2018). Pacsins interact with the C-terminal of Rac1 through its SH3 domain (Kreuk et al., 2011). This interaction seems to regulate Rac1 internalization, as it is dependent on dynamin activity (Kreuk et al., 2011; Schlunck et al., 2004). Researchers suggest that Pacsins can contribute to targeting Rac1 to sites for GAP-mediated inactivation. This is supported by the increase of the GTP-bound state of Rac1 with the knockdown of Pacsin2. By contrast, the I-BAR IRSp53 has the reverse function, it links the activated Rac1 to WAVE, stimulating actin polymerization (Abou-Kheir et al., 2008; Miki et al., 2000). This suggests a potential role of Pacsins in cell adhesion, migration, and division.

Furthermore, Pacsins are revealed as potential interactors of MSC. A yeast two-hybrid screen has allowed the discovery of a new partnership between Pacsin and the mechanosensitive TRPV4 channel (Fig. 4C) (Cuajungco et al., 2006). TRPV4 is a nonspecific cation channel, which triggers cellular signaling upon mechano-osmotic stimulation. Mechanical forces indirectly activate TRPV4, most probably through second messengers (Fernandes et al., 2008; Nikolaev et al., 2019; Nilius et al., 2003). Organ-mediated osmosensation of TRPV4 influences important processes such as nociception or vascular function (Alessandri-Haber et al., 2008; C.-K. Chen et al., 2018). Several other modulators have been reported for TRPV4, including heat and lipids, such as the polyunsaturated arachidonic acid (Berna-Erro et al., 2017; Güler et al., 2002). The interaction of Pacsins with this channel occurs between their SH3 domain and a triple-proline motif of TRPV4 (Cuajungco et al., 2006). The same study shows that other TRP channels, such as TRPV2 and the non-MSC TRPV1, do not display any alteration of their subcellular distribution when co-expressed with Pacsins.

These results are in line with the absence of this triple-proline motif in the rest of TRPs. Remarkably, only the co-expression of TRPV4 with Pacsin3, but not Pacsin1 and 2, induces an increase in the PM localization of TRPV4. This membrane accumulation of TRPV4 can be explained by the blockade of endocytosis by dynamin sequestration through the exclusive PRD domain of Pacsin3. This mechanism could be shared with other MSCs to prevent their internalization in regions of high membrane curvature and thus, modulating mechanotransduction without being removed.

Pacsin3 has not only been implicated in the regulation of MSC localization but it also inhibits TRPV4 mechanosensation (D'hoedt et al., 2008). The binding of an active Pacsin3 to TRPV4 is necessary for this purpose, as the SH3 mutant and the lack of the F-BAR domain avoids all inhibitory activity independently (D'hoedt et al., 2008; Garcia-Elias et al., 2013). The interaction of Pacsin3 with the N-terminal region of the channel, which is an important determinant for mechanical-induced activation, seems to be responsible for preventing TRPV4 gating (Fig. 4C). This N-tail is also a PIP2-binding site, which is required for the mechanical activity of TRPV4 (Garcia-Elias et al., 2013). This competition between Pacsin3 and PIP2 for a TRPV4-binding site could be an important regulatory instrument for mechanotransduction. Thus, Pacsin3 acts as a membrane adaptor modulating the activity and localization of TRPV4. Whether this capacity of Pacsin3 is also regulating other MSCs and its implication in mechanical processes, such as cell division, remains to be explored.

1.3 Mitotic forces

Cell division is a central process in the life of a cell. This process is influenced by different physical and biochemical signals that orchestrate the separation of the cell content into two genetically equivalent daughter cells. During the mitotic phase, the cell undergoes important morphological changes which require forces such as surface tension, osmotic pressure, and spontaneous curvature. This triggers a stress-induced cellular remodeling under the action of the cytokinetic machinery, the extracellular matrix, and the PM (Atilla-Gokcumen et al., 2014; Dix et al., 2018; Fink et al., 2011). Uncovering how dividing cells integrate these elements and the specific mechanosensors implicated in this network is a primary question to understand cell division.

Recently, several studies have pointed to Piezo1 as one of the main ion channel regulators of cell cycle progression. Piezo1 is involved in the G0/G1 to S transition through the Ca^{2+}-mediated phosphorylation of Akt 4 (Han et al., 2019; Nam et al., 2019). Similarly, TRPV4 and TRPM7 have been shown to influence the transition from G0/G1 to S (Nam et al., 2019; Yee et al., 2011). Additionally, mechanically activated Piezo1 has been related to the Ca^{2+}-dependent phosphorylation of ERK1/2, triggering the transition from G2 to M (Gudipaty et al., 2017). However, there is a lack of knowledge regarding the activity of Piezo1 and other MSCs during the inherent mechanical events characteristic of the mitotic phase.

Furthermore, the dividing cell is regulated by 2 important transient elevations of cytosolic Ca^{2+} concentration modulating signaling pathways that control mitotic progression. The first one is reported during the transition from metaphase to anaphase, while the second one takes place during cytokinesis. This Ca^{2+}-mediated regulation of cell division occurs directly, or indirectly through Ca^{2+}-binding proteins, promoting gene

expression, enzymatic activity, or vesicle fusion (Chircop et al., 2010; Sarah E. Webb & Miller, 2017). However, the mechanism by which calcium signal is generated during the mitotic phase and its downstream effectors are not well understood. Besides, the versatility of Ca^{2+} signaling, characterized by its multiplicity of targets, adds complexity to the study.

Many of these mitotic processes involving Ca^{2+}, such as cytoskeletal and membrane remodeling, are closely synchronized with mitotic forces. In turn, BAR domain proteins and MSCs have a considerable contribution to these processes during cell life. Thus, it is plausible that these proteins are activated and related through mitotic forces at some point in cell division.

1.3.1 Mitotic cell rounding

The first change in shape is observed during early mitosis, where cells experience what is known as mitotic cell rounding. This shape alteration triggers changes in the mechanical properties of the cell, increasing cell surface tension, cortical stiffness, and osmotic pressure (Fig. 5A). This morphological change is necessary to prepare space for the correct mitotic spindle formation in charge of the alignment of chromosomes during metaphase. This is supported by the fact that under strict physical confinement, the ability of cells to round is impaired, triggering severe defects in spindle assembly (Lancaster et al., 2013).

During mitotic entry, cells undergo a remodeling of cell-substrate adhesions which starts in the early prophase. Focal adhesions connecting the cell to the ECM are disassembled through the inactivation of the small GTPase Rap1, increasing surface tension (Dao et al., 2009; Dix et al., 2018). However, cells remain weakly connected to the underlying substrate by

integrin-rich retraction fibers providing molecular memory to facilitate daughter cell re-spreading (Dix et al., 2018). These retraction fibers are formed by thin bundles of actin filaments and integrin, which lack some of the conventional focal adhesion components in charge of traction force generation. In consequence, the total force exerted by mitotic cells on the substrate is restricted to a few nanonewtons (Burton & Taylor, 1997; Fink et al., 2011). Under these conditions, MSCs are in a resting state. For instance, Piezo1 has a half activation T50 of 1.4 ± 0.1 mN/m, which represents a high degree of sensitivity compared to other MSCs, such as MscS (T50 ~ 5 mN/m) and MscL (T50 ~ 10 mN/m) (Fig. 1B) (Lewis & Grandl, 2015). Thus, the ECM-cell interface is a minimum force-generating element in this phase of mitosis.

Some computational models have tried to closely monitor the distribution of forces occurring throughout this process (Koyama et al., 2012; Poirier et al., 2012). In those models, cells are represented as a viscoelastic material. The results suggest that rendering uniform protrusions across the cell-substrate boundary, in the absence of adhesions, generates a surface tension leading to a rounded shape. However, protrusions are not sufficient to explain the maintenance of circularization *in vivo*. Additionally, surface forces generated during mitotic rounding have been studied thanks to an AFM cantilever (Fischer-Friedrich et al., 2014; Ramanathan et al., 2015). These experiments demonstrate that a cortical tension is generated by the actomyosin network, performed in parallel to cellular protrusions (Fig. 5A).

This cortical actomyosin is mediated by cytoskeletal regulators, such as Rho GTPases, which undergo an accurate temporal localization and activation. While Rac1 inactivation is required during all the steps of mitosis, RhoA is the primary driver of cortical tension during cell rounding. Its downstream effectors, mDia1 and ROCK, control actin filament

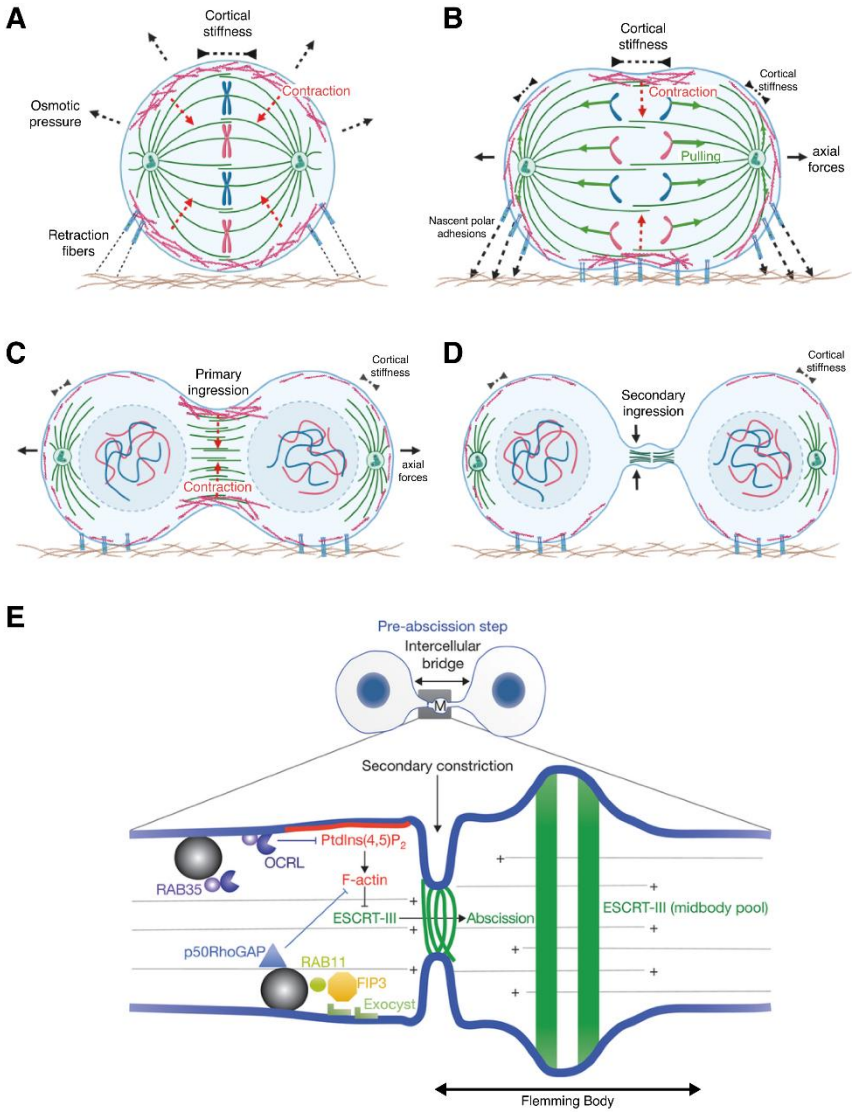

Fig. 5. Mitotic forces and biochemical signaling orchestrating cellular shape changes. (A-D) Physical forces controlling cell division during (A) metaphase, (B) anaphase, (C) telophase and (D) cytokinesis. Arrows indicate the sense of forces. (E) Abscission machinery managing the final cut of the membrane at the midbody (M) (modified from (Echard 2012)). Note the formation of the secondary ingression site through the delivery of endosome vesicles, which also mediate F-actin clearance from the midbody and the recruiting of components from the ESCRT machinery.

organization and contractility, respectively. The formin mDia1 promotes the assembly of long actin filaments along the membrane creating a thin but strong cortex (Cao et al., 2020). ROCK phosphorylates myosin II which progressively accumulates at actin filaments. Knockdown of myosin II dramatically reduces the ability of cells to apply surface tension (Toyoda et al., 2017). However, increasing the RhoA/myosin II-mediated contractility with the RhoA activator Calpeptin induces the formation of blebs in mitotic rounded cells (Ramanathan et al., 2015). This suggests that intermediate levels of contractility are necessary to obtain maximum cortical tension without inducing instability. These levels are achieved thanks to the controlled phosphorylation of RhoGEF Ect2 by the kinase Cdk1 (Su et al., 2011).

This Ect2-RhoA pathway confers a cytoskeletal rigidity that is transferred to the PM thanks to protein linkers, such as ezrin-radixin-moesin (ERM) proteins (Diz-Muñoz et al., 2010; Kunda et al., 2008). ERM proteins firmly connect the contractile actin network with the lipid bilayer, preventing bulge outgrowth and transmitting actomyosin force to lipids. Interestingly, ERM proteins have a predilection for bent membranes but do not have the ability to sense nor deform curvature alone. Recently, a study has demonstrated that the ERM protein Ezrin, requires the interaction with the I-BAR IRSp53 to tether the actin cytoskeleton to negatively-curved membranes (Tsai et al., 2018). This suggests a potential structural role of I-BARs in actomyosin tension transmission to lipid configuration.

Actomyosin forces generate an increase in surface tension, from 0.2 mN/m during interphase to 1.6 mN/m during metaphase (Fischer-Friedrich et al., 2014). In theory, this level of tension could activate low-threshold MSCs such as Piezo1. However, the contribution of membrane tension to overall surface tension in rounded cells is less than 0.2 mN/m, similar to resting

membranes (Fischer-Friedrich et al., 2014; Morris & Homann, 2001). This is explained since surface tension increased, generated by the actomyosin network, is coupled to an increase in membrane stiffness (Fischer-Friedrich et al., 2014; Kelkar et al., 2020). Indeed, rounded cells display resistance to local and whole-cell membrane deformation (Maddox & Burridge, 2003; Matthews et al., 2012). Moreover, metaphase cells treated with blebbistatin, which inhibits myosin II contraction, and latrunculin A, which depolymerize actin filaments, display an increase in membrane deformability up to the same levels as an interphase cell (Stewart et al., 2011). An increase in membrane stiffness is associated with the inhibition of the mechanosensitive response of many MSCs, such as Piezo1 and MscS (Romero et al., 2019; Xue et al., 2020). These data suggest that the actomyosin cortex may have a mechanoprotective role in preventing MSC activity during this phase of mitosis.

This membrane stiffening is caused by a ~10-fold increase of the intracellular pressure, manifested during the transition from prophase to prometaphase (Fischer-Friedrich et al., 2014). This results in a mild swelling by water and ion influx through the Na-H exchanger (Son et al., 2015; Zlotek-Zlotkiewicz et al., 2015). This volume change is constrained by the cortical force, which retains a certain level of osmotic pressure impeding the cortical mesh to collapse under its own contraction (Stewart et al., 2011). In agreement with the previous results regarding lipid tension in mitotic rounded cells, mild hypotonic swelling does not alter membrane tension or the adhesion of the membrane to the underlying cytoskeleton but causes an increase in the membrane elastic modulus, translated by membrane stiffening (Ayee & Levitan, 2018). Additionally, researchers suggest that this generates a more homogenous and less viscous cytoplasm environment, which may help to chromosome segregation along the

equatorial spindle. This balance of forces is maintained until anaphase, where a new force hierarchy rules membrane shape.

1.3.2 Furrow ingression and contraction

After anaphase onset, mitotic forces redistribute to position a division plane between the two bunches of segregating chromosomes. This division plane positioning is controlled by the formation of new polar adhesions, by the assembly of an actomyosin ring in the equatorial region, and by changes in polar cortical tension, which together orchestrate mitotic spindle elongation, and the progression of furrow ingression.

Initially, axial forces start to increase thanks to the creation of new polar adhesions (Fig. 5B) (Burton & Taylor, 1997; Dix et al., 2018; Sedzinski et al., 2011). These adhesions are directed by the integrin-rich retraction fibers that remain linking the cell to the extracellular matrix after metaphase rounding. This creates a driving force for the beginning of axial elongation, where the isotropic cortical tension starts to polarize (Poirier et al., 2012). At the equatorial pole, the curvature starts to transition from the intrinsic negative curvature of rounded mitotic cells to a positive curvature characteristic of the cleavage furrow ingression (Fig. 5B). This causes an increase in polar cortical tension as the curvature rises, while the furrow deforms (Matzke et al., 2001; Poirier et al., 2012). The radial component begins to dominate while the axial component decreases. These polar contractile forces and adhesions are essential to slow down furrow ingression and maintain cell shape during this process.

Cell shape control at the polar cortex is driven by bleb formation (Roubinet et al., 2011; Taneja et al., 2020). When the surface tension increases at the poles, blebs act as valves releasing cortical contractility. Activated Piezo1 and calcium signaling have shown to be important mechanisms for bleb

formation (Blaser et al., 2006; Srivastava et al., 2020). Interestingly, when chelating intracellular Ca^{2+} with Bapta-AM or extracellular calcium with Ca^{2+}-free mediums, blebs still form and regulate cell shape oscillations during this phase of mitosis (Sedzinski et al., 2011). Thus, researchers exclude a mechanosensing cascade responsible for mitotic blebbing formation. These results suggest that Piezo1 and other calcium MSCs are poorly localized, or inhibited, in the membrane poles during furrow ingression. Instead, this process is mediated by astral microtubules, which deactivate mDia1 from the poles, decreasing membrane stiffness and allowing blebbing for the regulation of internal hydrostatic pressure (A. Chen et al., 2021).

Moreover, it has been demonstrated that at this point of mitosis, traction forces at the poles remain scarce (Burton & Taylor, 1997). Thus, low forces are generated from the ECM-cell adhesions, supporting reduced mechanotransduction at the poles during anaphase. Interestingly, traction forces appear towards the equatorial region of the dividing cell (Burton & Taylor, 1997; Uroz et al., 2019). These traction forces control the kinetics of the central furrow ingression. In resting condition, they could instigate the deformability of the furrow, assisting division. However, in dividing cells subjected to a mechanical load, equatorial traction forces slow down cell division by strengthening furrow adhesion to the ECM. Thus, this involves a mechanosensitive pathway, but the mechanosensors implicated in this process are not yet known. Although adhesions and traction forces may be sufficient for furrow ingression, as demonstrated by computational models and experiments with adherent cells lacking cortical contractility, other mitotic forces work in parallel to promote furrow progression.

The axial force led to a reduction of metaphase anti-poleward forces, which allows the movement of bi-oriented chromosomes towards the opposite

spindle poles. The primary source of force generation for pulling chromosomes is the depolymerization of kinetochore fibers (k-fibers) (Fig. 5B). These fibers connect the spindle poles to the centromere of each chromosome through long microtubules. K-fiber depolymerization occurs mainly in the kinetochore end, a mechanical sensor system that feels the right tension at microtubules to induce chromatid separation (Suzuki et al., 2016). Microtubule depolymerization also occurs at centrosomes but to a smaller extent and is dispensable for the process (Vukušić et al., 2017). At this point, some microtubules of the mitotic spindle are released from the centrosomes and positioned at the equatorial region. The sliding of microtubules is produced through dynein motor proteins bridging k-fibers (Vukušić et al., 2017). As they slide, the interpolar microtubules push apart neighboring k-fibers, contributing to chromosome movement. Together with new polymerized microtubules, they start bundling forming the spindle midzone (Douglas & Mishima, 2010). At this step, cortical forces seem not necessary for chromosome segregation and spindle elongation. However, the polar cortex increases intracellular pressure helping physical displacement of the spindle (Sedzinski et al., 2011). Additionally, astral microtubules seem to directly contact the equatorial cortex through dynein, which generates cortical pulling forces (K.-Y. Lee et al., 2015). Cortical pulling, in cooperation with a regulatory signal from the central spindle, contributes to the positioning of the division plane (Taneja et al., 2016; Werner et al., 2007).

At the central spindle, a complex of proteins assembles forming the centralspindlin. The centralspindlin is a heterotetramer consisting of dimers of 2 distinct proteins, a kinesin-like protein, MKLP1, and a Rho GTPase-activating protein, MgcRacGAP. This complex is needed to complete microtubule bundling at the midzone and to promote RhoA activation (Hutterer et al., 2009; Y. Nishimura & Yonemura, 2006; Somers & Saint,

2003; Yüce et al., 2005). The progressive inactivation of the kinase Cdk1, in charge of maintaining cortical tension, releases a phosphorylation site in RhoGEF Ect2 for the kinase Plk1 (Neef et al., 2007). In turn, Plk1 mediates the binding of Ect2 to MgcRacGAP, promoting its recruitment at the equatorial region and the formation of an actomyosin ring by RhoA activation (Su et al., 2011). Calmodulin is accumulated at the equatorial plane and is thought to participate in a Ca^{2+}-mediated assembly of the central spindle (C. J. Li et al., 1999; W. M. Li et al., 2008; Yu et al., 2004). Thus, the transient elevation of Ca^{2+} observed at the onset of cytokinesis could be necessary for the formation of the equatorial complex. The contractility of the actomyosin ring assists in turn radial deformation of the division plane (Fig. 5B).

The centralspindlin is tethered to the PM through the C1 domain of the MgcRacGAP protein, which binds to phosphoinositide lipids (Lekomtsev et al., 2012). Other scaffold proteins, such as anillin and septin, link the actomyosin network to the PM to stabilize the contractile ring (Benaud et al., 2015; Piekny & Glotzer, 2008; van Oostende Triplet et al., 2014). Additionally, a study has demonstrated that Syndapin, the ortholog of Pacsins in *Drosophila*, mediates anillin binding to the curved membrane around the contractile ring (Takeda et al., 2013). Interestingly, Syndapin is maintained until the end of cytokinesis, suggesting further roles. This scaffolding activity of Syndapin could be mimicked by some of the Pacsin human isoforms. Indeed, Pacsin2 has been involved in a similar function (C. M. Smith & Chircop, 2012).

This association to the PM increases surface tension similar to the metaphase cortex (Matzke et al., 2001; Reichl et al., 2008). As the contraction increases, the membrane beneath the actomyosin ring stiffens, thus controlling furrow kinetics. At the same time, traction forces

connecting the furrow to the extracellular matrix start to disappear, allowing the detachment of the cleavage furrow from the matrix (Fig. 5C) (Burton & Taylor, 1997). The lack of ECM-cell connections, together with the membrane stiffening during contraction could establish a hostile environment for the activation of MSCs. At this point, daughter nuclear envelopes start forming, and chromosomes deconden se.

Thus, the matrix compression starts to propagate towards the central region, indicating a change in the cortical tension gradient (Fig. 5C). The axial cortical tension continues to decrease, increasing poles' deformability. Protrusions and adhesions guide in turn re-spreading and polarized cell migration of the two nascent daughter cells, preventing recession of the cleavage furrow. Several studies have demonstrated that cells with a compromised actomyosin cortex still can undergo abscission thanks to the adhesion-mediated migration of the two daughter cells (Kanada et al., 2005; Nagasaki et al., 2009). Moreover, it is known that in the absence of myosin II, ring contractility can be supplied by a combination of adhesion and protrusion-mediated stresses (Kanada et al., 2005; Zang et al., 1997). These results suggest that the contractile actomyosin ring could be dispensable for cytokinesis under certain circumstances.

The membrane pursues ingression during telophase and cytokinesis, compressing the midzone and associated microtubules. Failure in controlling forces that govern furrow positioning and ingression leads to asymmetric cell division, which results in two daughter cells with dramatic differences in size (Ou et al., 2010). The mechanical parameters that characterize this final step of mitosis ultimately determine cytokinetic abscission (W. Zhang & Robinson, 2005).

1.3.3 Abscission

During late cytokinesis, a new priority obeys in membrane mechanics intending to separate the two nascent daughter cells. The cytokinetic machinery is assembled at the midbody to mediate biochemical and physical cutting of the bridge connecting the new cells (Fig. 5D,E). As the nuclear envelope is already generated, and chromatin decondensed, failure in the control of this final step of cytokinesis often triggers the recession of the furrow leading to a unique multinucleated cell. Genomic unbalance involves serious risks for tissue viability and is implicated in various diseases, such as cancer, blood disorders, and female infertility (Lacroix & Maddox, 2012). Thus, understanding the mechanics underlying the abscission process is crucial for therapeutic purposes.

The contraction of the actomyosin ring proceeds to form a microtubule-rich ICB, known as the midbody (Fig. 5D,E). The midbody length increases, while the contractile furrow narrows around the central spindle, reaching a thickness of 0.4-1.4 µm and completing the first membrane ingression (Petsalaki & Zachos, 2016). This compression results in a protein accumulation at the center of the midbody referred to as the Fleming Body. Proteomic studies have estimated more than 100 proteins accumulated in this region and flanking regions within the ICB (Skop et al., 2004). This makes the Flemming Body a thicker structure, around 1-2 µm, which acts as a scaffold platform for assembling and activating signaling proteins in charge of abscission (Fig. 5E).

Dephosphorylation events upon mitotic exit are thought to be necessary to localize many of these proteins to the midbody. One example is dynamin II, which is first phosphorylated by Cdk1 on serine 764 during mitosis, holding the protein at the centrosome (Thompson et al., 2004). This phosphorylation is not associated nor required for endocytosis or

centrosome cohesion but instead is targeted by the Ca^{2+}-activated phosphatase calcineurin (Chircop et al., 2011). This calcineurin-dependent dephosphorylation seems to assist dynamin II relocalization at the midbody. Both calcineurin and dynamin II are required for the completion of cytokinesis (Chircop et al., 2010; Thompson et al., 2002). Using dynamin II phospho-mimetic mutants, and dynamin II siRNA or inhibitors, an abscission delay or blockage is observed, increasing the number of multinucleated cells (Chircop et al., 2011; Joshi et al., 2010). Interestingly, calcineurin localization at the midbody is not altered during these experiments, suggesting that its localization to the midbody is not sufficient to complete cytokinesis, and depends on dynamin II activity.

Dynamin II dephosphorylation may promote its interaction with specific binding proteins which would retain the protein in this region of the membrane and/or stimulate its GTPase activity. BAR proteins, such as Pacsin, are known binding partners of dephosphorylated dynamin, suggesting the possibility that Pacsins are implicated in cytokinetic abscission (Anggono et al., 2006). However, the presence of dynamin is not always required for the activity of BAR proteins during cytokinesis. In yeast, the F-BAR Cdc15 is directly dephosphorylated by calcineurin at the division plane, linking the actomyosin contraction to the septum biosynthesis during the last step of cytokinesis (Martín-García et al., 2018). Its mammalian F-BAR homolog, PSTPIP1, is also involved in cytokinesis, but its dephosphorylation is thought to drive actomyosin ring disassembly (Angers-Loustau et al., 1999; Spencer et al., 1997). Additionally, other BAR proteins, such as Amphiphysin, are also mitotically phosphorylated and targeted later by calcineurin (Bauerfeind et al., 1997; Floyd et al., 2001). Although their role in cell division is not well understood, these results delve into the implication of concave BAR proteins in the process of abscission.

Following the completion of cleavage furrow ingression and ICB formation, the actomyosin ring disassembles by a process involving cytoskeletal and membrane remodeling. Actin filaments are disassembled by the inactivation of RhoA through the action of a complex formed by the kinase PKCε and the protein 14-3-3 (Saurin et al., 2008). Additionally, the disruption of the actomyosin ring is also assisted by the fusion of recycling endosomal and post-Golgi vesicles transported by Rab GTPases to the midbody and targeted by the exocyst tethering complex (Fielding et al., 2005; Gromley et al., 2005). These vesicles are required for the post-furrowing terminal steps of cytokinesis (Fig. 5E). Their lack impairs ICB stability and abscission, promoting multinucleation and increasing the time required for abscission (Kouranti et al., 2006; Wilson et al., 2005). Rab11-FIP3 vesicles deliver important abscission proteins to the ICB such as p50RhoGAP, which catalyzes the inactivation of RhoA (Schiel et al., 2012). Actin depolymerization decreases cortical surface tension increasing the deformability of the midbody. Additionally, the fusion of these vesicles increases lipid surface contributing to a gradual narrowing of the flanking regions of the Flemming body. Rab35 vesicles aid membrane remodeling by delivering PIP2, and thus, changing the lipid composition of the midbody membrane (Kouranti et al., 2006). In turn, PIP2 increases membrane bridge stability and recruits cytoskeletal proteins essential for scission, such as the scaffold protein septin (Emoto et al., 2005). Conversely, anillin is properly localized at the midbody using a dominant-negative mutant of Rab35 (Rab35-S22N) (Kouranti et al., 2006). Rab35 and Rab11 modulate independently different endocytic recycling pathways, indicating that distinct vesicle trafficking events are individually required for cytokinesis (Zerial & McBride, 2001). These remodeling events progressively create a region of high positive curvature known as secondary ingression site, where the ICB is thinned to around 100 nm in the

proximities of the Flemming body, pointing to the final region for abscission (Fig. 5E) (Schiel et al., 2011).

As the Flemming Body is not contractile, it is unable to prompt abscission on its own. Thus, it is endowed with a complex machinery required to mediate the final cut at the secondary ingression site (Wollert et al., 2009). This machinery is constituted by proteins from the endosomal sorting complex required for transport (ESCRT), and auxiliary ESCRT-interacting partners, such as the Bro-domain containing protein ALIX and the centrosomal protein CEP55. CEP55 is thought to bind to MKLP1 at the midbody promoting the simultaneous recruitment of TSG101 (ESCRT-I) and ALIX into two cortical rings at the Flemming body (Lee et al., 2008; Morita et al., 2007; Zhao et al., 2006). However, within some cell types and organisms lacking CEP55, it is suggested that ALIX can directly bind to proteins from the centralspindlin complex (Lie-Jensen et al., 2019; Tedeschi et al., 2020). In turn, Tsg101 and ALIX trigger CHMP4B (ESCRT-III) recruitment, which assembles into a filamentous spiral that extends from the Flemming body to the secondary ingression site (Fig. 5E). Finally, the ATPase VPS4 controls CHMP4B turnover, facilitating membrane squeezing, while the ATPase spastin severs microtubule bundles (Errico et al., 2002; Mierzwa et al., 2017).

The spatial and temporal regulation of this machinery is crucial for the correct outcome of membrane abscission. Rab11-FIP3 endosomes not only mediate the secondary membrane ingression but also the further recruitment of some elements of the abscission machinery, such as the ESCRT-III protein, CHMP4B (Schiel et al., 2012). When the recruitment of CHMP4B to the midbody fails, the secondary ingression can be initiated but the membrane regresses to its original width disrupting cytokinesis (Schiel et al., 2012). These results suggest that the secondary ingression site is formed

before CHMP4B recruitment. Similarly, impairing Rab11-FIP3 function by p50RhoGAP knockdown block actin disassembly inhibiting CHMP4B localization at the secondary ingression site. Additionally, FIP3 mediates the delivery of the protein SCAMP3, a known interactor of Tsg101 (Schiel et al., 2012). Thus, the triple role of Rab11-FIP3 vesicles, mediating secondary ingression, actin clearance, and the delivery of the Tsg101-binding protein SCAMP3, seems to be the main responsible for CHMP4B recruitment. However, depletion of Tsg101 has a weaker cytokinetic effect compared to ALIX or Rab11-FIP3 depletion (Carlton & Martin-Serrano, 2007; Morita et al., 2007). Thus, it has been proposed that the function of this protein is limited to stabilized ALIX at the midbody or that CHMP4B localization could be compensated via ALIX (Christ et al., 2016).

Nevertheless, it stills a long way to go to understand the concrete spatiotemporal regulation of the abscission machinery. Important questions arise around this subject, such as how the endosomal vesicle trafficking affects the localization of other proteins from the abscission complex. Moreover, the curvature and membrane tension changes during actomyosin disassembly and secondary ingression could involve a mechanosensory signaling. In consequence, one of the subjects of this thesis is trying to reveal the nature of some of the mechanosensors implicated in the regulation of this process.

2. Objectives

1. To evaluate possible regulation of the Piezo1 channel by BAR domain-containing proteins.

2. To study the implication of Piezo1 and the BAR domain-containing protein Pacsin3 in the process of cytokinesis.

3. To examine Pacsin3/Piezo1 interplay in the orchestration of the abscission machinery.

3. Methods

Materials

Drugs, antibodies, oligonucleotides, and plasmids used in this thesis are described in table S1. from chapter 2, except for the following plasmids:

PLASMIDS	SUPPLIER	REFERENCE
pcDNA3-AMPH1	Addgene 47390	
pEGFP-IRSp53		Provided by Dr. Giorgio Scita (University of Milan, Italy)
pcDNA3-PASCIN3-ΔFBAR-YFP	Own plasmid	Generated based on pcDNA3-myc-Pacsin3 provided by Markus Ploman (University of Cologne, Germany)
CFP-PACSIN3-P415L	Own plasmid	Generated based on pcDNA3-myc-Pacsin3 provided by Markus Ploman (University of Cologne, Germany)

Table 1. Annex table S1 (chapter 2).

Cell culture

Cell lines collected were cultured at 37°C and 5% CO2 and grown in the indicated media (Table 2). All cells were plated in collagen type I (354236, Cultek, 10 μg/mL in 0.02 M acetic acid, 1h and 37ºC) coated chambers, coverslips, or 35 mm MatTek glass-bottom dishes. Cells were synchronized in G2/M using 100 nM of nocodazole (Sigma) in complete medium for 16-20h or with a double block procedure (16h-8h-16h). After this, cells were released 2h before experiments with normal medium and treated with the specified drugs.

CELL LINE	SUPPLIER /REFERENCE	MEDIUM
HEK293	Sigma	DMEM High Glucose (Life Technologies) with 10% FBS, 1% Pen/Strep
HMEC	ATCC®	MCDB-131 (Gibco) with 15% FBS, 1% Pen/Strep, 0.1 µg/mL hydrocortisone, 12 ng/mL EGF, 2 mM L-glutamine (G7513, Sigma)
Fibroblasts	GM05565	DMEM High Glucose (Life Technologies) with 10% FBS, 1% Pen/Strep
MDA-MB-231-BrM2	Provided by Dr. Joan Massagué	DMEM High Glucose (Life Technologies) with 10% FBS, 1% Pen/Strep, 1% GlutaMAX
HELA	ECACC	DMEM High Glucose (Life Technologies) with 10% FBS, 1% Pen/Strep

Table 2. Cell lines and supplemented culture media.

Plasmid and siRNA transfections

HEK293 cells were transfected for 48h using polyethylenimine (PEI, Polysciences, 23966; ratio 5:1 PEI:DNA) and following manufacturer's protocol with the pair of plasmids (ratio 1:1) indicated in each experiment: Piezo1, pcDNA3, Pacsin3, Amphiphysin, or IRSp53. Transient knockdowns in HMEC and fibroblasts were performed using Lipofectamine RNAiMAX (Thermo; ratio 1:1 LIPO:DNA diluted in OPTIMEM (Gibco)) and following manufacturer's instructions. Plasmid transfection in HMEC was conducted with Lipofectamine 3000 (Thermo; ratio 1:1 LIPO:DNA diluted in OPTIMEM) following the manufacturer's instructions. After 2-3 hours with transfection mediums, cells were cultured with their respective growth medium. Experiments were conducted 1-3

days after transfection. Knockdown of Piezo1 in MDA-MB-231BrM2 cells was obtained using lentivirus as previously described (Pardo-Pastor et al., 2018). In brief, HEK293 were transfected with 2 µg pMD2-G + 4 µg pSPAX2 and 5 µg pLKO.1-shPIEZO1 or pLKO.1-scramble (Table S1) using lipofectamine 3000 (Invitrogen). After collection, centrifugation, and titration, lentiviral supernatants were used to infect MDA-MB-231BrM2 cells. MDA-MB-231BrM2-shPIEZO1 and MB-231BrM2-scramble stable cell lines were generated by selection with 1 µg/mL puromycin.

Electrophysiological recordings

Whole-cell patch-clamp recordings were performed in a bath solution containing (in mM) 140 NaCl, 2.5 KCl, 1.2 $CaCl_2$, 0.5 $MgCl_2$, 5 glucose and 10 HEPES (adjusted to pH 7.45 with NaOH). Tip resistance of borosilicate glass patch pipettes was 1-5 MΩ and contained (in mM) 140 CsCl, 0.3 Na_3GTP, 4 Na_2ATP, 1 EGTA, 10 HEPES (adjusted to pH 7.3 with Tris). Patches were held at a membrane potential of −80 mV using an Axopatch 200 A (Molecular Devices, U.S.A.). Cells were mechanically stimulated by membrane indentation generated by the upward motion (Δ 1 µm, 200 ms, every 10 s) of a fire-polished glass probe driven by a piezoelectric controller (E-665, Physik Instrumente). Currents were sampled at 10 kHz and filtered at 1 kHz 20 using pClamp10.5 software (Axon Instruments).

Cell-attached patch-clamp recordings were performed with a bath solution containing (in mM) 140 KCl, 1 $MgCl_2$, 10 glucose, and 10 HEPES (adjusted to pH 7.3 with Tris). Borosilicate glass patch pipettes (2-3 MΩ) were filled with a solution containing (in mM) 130 NaCl, 5 KCl, 1 $CaCl_2$, 1 $MgCl_2$, 10 TEA-Cl, 10 HEPES (adjusted to pH 7.45 with NaOH). Piezo1 activity was assessed stimulating cells with negative pressure (suction) using a High-

Speed Pressure Clamp (HSPC-1, ALA Scientific Instruments). The protocol used for macrocurrent recordings consisted of successive negative pulses from -10 to -60 mmHg (Δ 10 mmHg, 250 ms, every 10 s). The protocol used to evaluate channel recovery from inactivation involved 2 successive pulses (30 mmHg, 100 ms) with an increased space interval. For single-channel recordings, a pre-pulse of -8 mmHg was used to mechanically stimulate the cells. Piezo1 agonist Yoda1 (20 μM) was added to the pipette solution when specified. Membrane potential was held at -80 mV using an EPC10-USB patch-clamp amplifier (HEKA Elektronik). Currents were recorded with PatchMaster software at 10 kHz and low-pass-filtered at 0.7 kHz.

Inside-out patch-clamp recordings were performed with a bath solution containing (in mM) 140 KCl, 1 MgCl2, 10 Glucose and 10 Hepes (adjusted to pH 7.3 with Tris). Glass patch pipettes (2-3 MΩ) were filled with a solution containing (in mM) 130 NaCl, 5 KCl, 1 $CaCl_2$, 1 $MgCl_2$, 10 TEA-Cl and 10 HEPES (adjusted to pH 7.45 with NaOH). As in cell-attached configuration, patches were stimulated by suction with negative pressure pulses ranging from -10 to -60 mmHg (Δ 10 mmHg, 250 ms, every 10 s). Currents held at -80 mV were acquired at 10 kHz and low-pass-filtered at 0.7 kHz using an EPC10-USB patch-clamp amplifier (HEKA Elektronik).

All experiments were run 2 days after transfection at room temperature (22-26ºC). Data were analyzed using Igor Pro 8 (WaveMetrics) and MATLAB. Due to the biphasic kinetics of the currents, the time constant of inactivation τ_1 (τ_{inact}) was obtained by fitting the results to a double exponential curve between the peak current and the end of the stimulus, according to the next equation:

$$I = I_0 + A_1 \exp\left(\frac{t - t_0}{\tau_1}\right) + A_2 \exp\left(\frac{t - t_0}{\tau_2}\right).$$

Calcium imaging

Cytosolic Ca^{2+} changes were measured in 50% confluent cells cultured in a silicone chamber (STB-CH-04, STRETX Inc.) and loaded with 4.5 µM Fura 2-AM (Thermo) as previously described (Fernandes et al., 2008). Isotonic bath solutions contained 140 mM NaCl, 2.5 mM KCl, 1.2 mM $CaCl_2$, 0.5 mM $MgCl_2$, 5 mM glucose, and 10 mM HEPES (adjusted to pH 7.3 with NaOH). Chambers were subjected to 2 consecutive mechanical uniaxial stretchings (40% and 80% of the initial chamber length, 0.5 s duration, 8 min delay). The fluorescence ratio (F340/F380) was monitored by HCImage software (Hamamatsu Photonics). Alternatively, cells were loaded with the single wavelength Ca^{2+} dye Calbryte, as previously described (Venturini et al., 2020). Signals were always normalized to steady-state values prior to stimulation.

Confocal microscopy

For localization studies, HMEC and MDA-MB-231-BrM2 cells were seeded in coverslips, fixed with 4% PFA (20 min at 37ºC), permeabilized with 0.5% Triton X-100 (Sigma) in PBS (5 min) and blocked in 5% BSA in PBS (1 h at room temperature). Coverslips were incubated sequentially with primary antibodies (Table S1) overnight at 4ºC, secondary antibodies (Table S1) for 1 h at room temperature, and DAPI for 10 min to visualize cell nuclei, all diluted in 1% BSA in PBS 1x. The PM was stained with a pretreatment of 20 min of concanavalin A (1:50; in ice-cooled PBS), before cell fixation. Coverslips were mounted with Fluoromount (0100-01, Southern Biotech). Cells were examined with a Leica TCS-SP8 confocal microscope with a 63× 1.40 immersion oil objective. Image processing was performed with ImageJ software (National Institute of Health). Piezo1, CHMP4B, ALIX, Cep55, Beclin-1 and ALG-2 intensities at the

intercellular bridge were quantified using a plot line along the α-tubulin staining.

Live microscopy

For time-length measurements during cell cycle, HMEC cells were plated at 70-90% confluence in a 24-well plate and imaged in a Zeiss Cell Observer HS microscope, with a 10× objective, while maintained at 37ºC and 5% CO_2 using the microscope incubator. Time-lapse images (13-15 z-sections, 5 µm apart) were acquired every 10-15 min, over 24h. Videos were processed with ImageJ and cytokinesis start time and the abscission time were manually calculated based on cell morphology. For time-lapse using GenEPI, HMEC cells were seeded in 35-mm glass-bottom dishes and experiments were performed 48h post-transfection and synchronization in a Leica TCS-SP8 confocal microscope with a 40× 1.40 immersion oil objective, using a resonant scanner and a HyD detector. Experiments were performed at 37º C and 5% CO2 using an Okolab portable incubation system. Images were acquired every 7 min for 16h.

Co-immunoprecipitation and western blot

Co-immunoprecipitation assay was performed as previously described (Doñate-Macian et al., 2020). In brief, cell lysates were prepared using 1% Triton X-100 lysis buffer supplemented with 10% of protease inhibitor cocktail (Thermo) for 30 min at 4ºC. After centrifugation at 10.000g for 5 min at 4ºC, the supernatant was incubated with equilibrated GFP-Trap beads (gta-20, ChromoTek) or RFP-Trap beads (gta-10, ChromoTek) for 2h at 4ºC. The immunoprecipitated beads were centrifuged and washed 4 times with PBS 1x and denatured with SDS-PAGE sample buffer (NP0007,

Invitrogen) for 10 min at 70 ºC. The immunoprecipitated proteins were analyzed by western blotting with a SDS-PAGE in Tris-acetate 3-8% precast gels (EA0375BOX, Invitrogen). Soluble fractions from cell lysis were used as input. Membranes were blocked with 5% non-fat-dry milk in TTBS. Then, incubation with primary antibody anti-Myc or anti-GFP (Table S1) (overnight at 4ºC) and secondary antibodies peroxidase-conjugated anti-rabbit IgG or anti-mouse IgG (1:2000, 1h at RT) were performed in the same blocking buffer. Detection was performed using the enhanced chemiluminescence (ECL) detection kit (1705061, Clarity Biorad). For co-immunoprecipitation of endogenous proteins in HMEC, cell extracts were centrifuged at 14.000g at 4ºC for 10 min to remove aggregates. Solubilized proteins were incubated overnight with an anti-Piezo1 antibody. Immuno-complexes were then incubated with 50 µL of protein G beads for 2 hours at 4ºC.

Quantitative real-time PCR

For RNA isolation, NucleoSpin RNA isolation kit (740955, Macherey-Nagel) or NZY Total RNA Isolation kit (MB13402, NZYTech) were used. For cDNA synthesis, SuperScript III reverse transcriptase system (18080044, Thermo) was used. Quantitative real-time PCR was performed using SYBR Green (4367659, Applied Biosystems) in a QuantStudio 12K Flex system (Applied Biosystems) with the specific human primers shown in Table S1. GAPDH was used as a housekeeping gene for the quantification of relative gene expression using $2^{-\Delta\Delta Ct}$.

Mutagenesis

FIP3 Asp residues in EF-1 (D215/D217/D219) and EF-2 (D247) coordinating Ca^{2+} binding were mutated to Ala (FIP3-4DA) on the pEGFP-

C1-FIP3 plasmid. Mutations were introduced by site-directed mutagenesis using the QuikChange kit (Stratagene), with primers shown in Table S1.

Statistical analysis

Data in all figures are shown as mean ± S.E.M. Statistics and graphics were performed using GraphPad Prism. Normality was assessed with a Shapiro-Wilk omnibus normality test. Data with normal distributions were analyzed with a Student's unpaired t-test between two groups or one-way analysis of variance (ANOVA) followed by Bonferroni or Dunnett post hoc tests across multiple groups. Data that did not assume Gaussian distributions were analyzed using a Mann–Whitney's U test between two groups or Kruskal–Wallis followed by Dunn's post hoc test for multiple groups. $P < 0.05$*, $P<0.01$** and $P<0.001$***.

4. Results

Chapter 1: Pacsin3 impairs the inactivation of the Piezo1 channel increasing its mechanical response.

The mechanical activation of Piezo1 is enhanced by concave BAR proteins through the impairment of channel inactivation.

BAR domain proteins are important sensors and inductors of membrane curvature (Frost et al., 2009). Changes in membrane shaping are on the physical basis of the mechanical activation of Piezo1 (Liang & Howard, 2018). This opens up the possibility of a substantial interplay between both mechanosensitive pathways. To investigate this scenario, we performed an electrophysiological study in HEK293 cells overexpressing Piezo1 and proteins belonging to the three families of mammalian BAR domain-containing proteins: Pacsin3 (F-BAR), Amphiphysin (N-BAR), and IRSp53 (I-BAR). To evaluate the effect of these proteins in Piezo1 response, we stimulated the cells with different mechanical inputs under distinct patch-clamp configurations: a) whole-cell recordings of Piezo1 currents in cells poked with a glass probe (Fig. 1-3), b) cell-attached Piezo1 single-channel recordings using a pressure-clamp controller (Fig. 2-3). We noticed that co-transfection of Piezo1 with either Pacsin3 or Amphiphysin induced larger Piezo1 whole-cell currents (Fig. 1B, F, C, and J) in cells mechanically stimulated with a blunt glass probe. Additionally, stimulating cell-attached patches by a slight suction pulse through the recording pipette triggered a significant increase in the open state probability of Piezo1 under the co-transfection of Pacsin3 (nPo 0.34 ± 0.04) or Amphiphysin (nPo 0.35 ± 0.03), compared to pcDNA3 (nPo 0.18 ± 0.02) (Fig. 2A, B). This increase was no longer observed 2 min after the pulse, indicating a time-dependent phenomenon (Fig. 2C). A very similar result was obtained when treating the cells with 20 µM of Yoda1 (nPo 0.44 ± 0.05) (Fig. 2). Yoda1 is known for its capacity to interact with Piezo1 and decelerate its inactivation phase (Botello-Smith et al., 2019). Our result suggested that the concave BAR proteins Pacsin3 and Amphiphysin could be impairing the inactivation kinetic of Piezo1 similarly to its agonist Yoda1. To study this hypothesis,

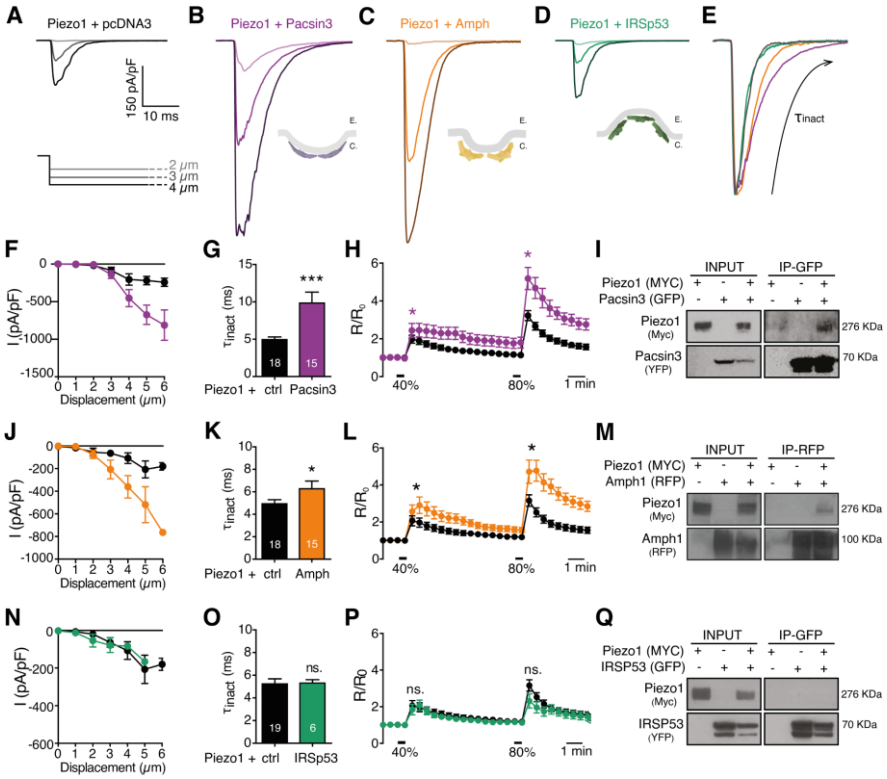

Fig. 1. Concave BAR proteins increase Piezo1 whole-cell currents and Ca^{2+} influx. (A-D) Representative whole-cell Piezo1 currents in HEK293 cells stimulated with a poking pipette performing consecutive mechanical steps of 1 µm. Cells co-transfected with Piezo1 and (A) pcDNA3, (B) Pacsin3, (C) Amphiphysin, or (D) IRSp53. Currents recorded at a holding potential of -80 mV. (B-D) are accompanied by schematic representations of the corresponding tested BAR domains and their bending effect on the relaxed membranes (gray). "E" extracellular, "C" cytoplasm. (E) Normalized whole-cell Piezo1 traces from A-D (colors maintained) in response to 2 µm mechanical indentation. "τ_{inact}" represents the inactivation time constant of currents. (F,J,N) Mean peak whole-cell Piezo1 currents in HEK293 cells overexpressing Piezo1 and pcDNA3 (black; N=17-33), Pacsin3 (F; purple; N=18), Amphiphysin (J; orange; N=14), or IRSp53 (N; green; N=6). Cells stimulated with increased mechanical displacement of the poking pipette of 1 µm. (G,K,O) Mean inactivation time constant (τ_{inac}) of whole-cell currents in F, J, and N, respectively. Means ± S.E.M. of the number of cells indicated in each bar. Statistical significance was evaluated using a Student's unpaired t-test. (H,L,P) Mean intracellular Ca^{2+} responses

to 2 consecutive uniaxial stretching pulses (40% and 80% of the initial chamber length) in HEK293 cells loaded with Fura-2-AM and transfected with Piezo1 and pcDNA3 (black; N=48) Pacsin3 (H; purple; N=17), Amphiphysin (L; orange; N=28) or IRSp53 (P; green; N=35). Data are means ± S.E.M. and the statistical significance was calculated for the area under the curve of each mechanical step using Kruskal-Wallis followed by Dunn's post hoc. (I,M,Q) Co-immunoprecipitation assays of Piezo1-myc with the indicated BAR proteins tagged with YFP or RPF.

we fitted the inactivation phase of whole-cell Piezo1 currents, i.e. the decay phase (arrow in Fig. 1E), to a double exponential. We observed an increase in the time constant of inactivation (τ_{inact}) from 4.9 ± 0.4 ms in cells transfected with Piezo1 and pcDNA3 to 9.8 ± 1.4 ms when the channel was co-transfected with Pacsin3 (Fig. 1G) or 6.2 ± 0.7 ms with Amphiphysin (Fig. 1K). Changes in inactivation time-course were also studied in cell-attached Piezo1 macrocurrents induced by negative pressure pulses from -10 to -60 mmHg (ΔP = -10 mmHg). In line with the previous results, macropatches from cells overexpressing Piezo1 and Pacsin3 displayed an increase in τ_{inact}, like in the case of cells treated with 20 µM of Yoda1 (Fig. 3A, B). However, channel sensitivity was not affected by the presence of Pacsin3 (Fig. 3C). Thus, concave BAR proteins might hamper the shift from the open to the inactivated state and/or impaired inactivation state promoting the reopening of the channel. Either way, the channel would spend more time in its open conformation after mechanical stimulation (Fig. 2). This could explain the rise in the mechanical response of whole-cell currents (Fig. 1F, J), on account of a better synchronization of open channels along the membrane. Consistent with the patch-clamp analysis, Ca^{2+} imaging experiments showed an increase in Ca^{2+} influx in the presence of Pacsin3 or Amphiphysin following uniaxial stretching of cells (Fig. 1H, L).

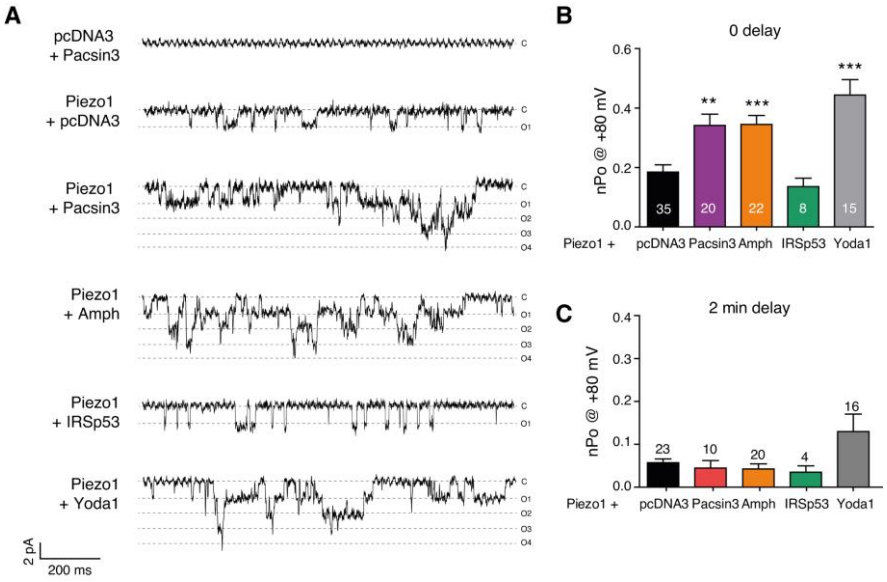

Fig. 2. Concave BAR proteins increase Piezo1 open probability in a time-dependent manner. (A) Representative single-channel recordings of Piezo1 currents in HEK293 cells recorded in cell-attached configuration after stimulation with a negative pressure pulse of -8 mmHg for 10 sec. Cells were transfected with the indicated constructs and the membrane potential was held at -80 mV during the recording. Yoda1 was added to the pipette solution at 20 μM. "C" close state, "O" open states. (B,C) Mean open probability (nPo) calculated from the cell-attached patches (shown in A), (B) just after stimulation, and (C) 2 min after stimulation. Mean ± S.E.M. of nPo obtained from the number of patches indicated in each bar. Statistical significance was assessed using Kruskal-Wallis followed by Dunn's post hoc.

By contrast, the convex IRSp53 did not affect Piezo1 current density (Fig. 1N), inactivation kinetics (Fig. 1D, E, O), open probability (Fig. 2) nor Piezo1-mediated Ca^{2+} signal (Fig. 1P) compared to control cells. Besides, HEK293 cells transfected only with BAR proteins and pcDNA3, displayed significantly smaller currents (Fig. 3A and Fig. 2A), proving that mechanically-induced currents were specifically mediated by Piezo1.

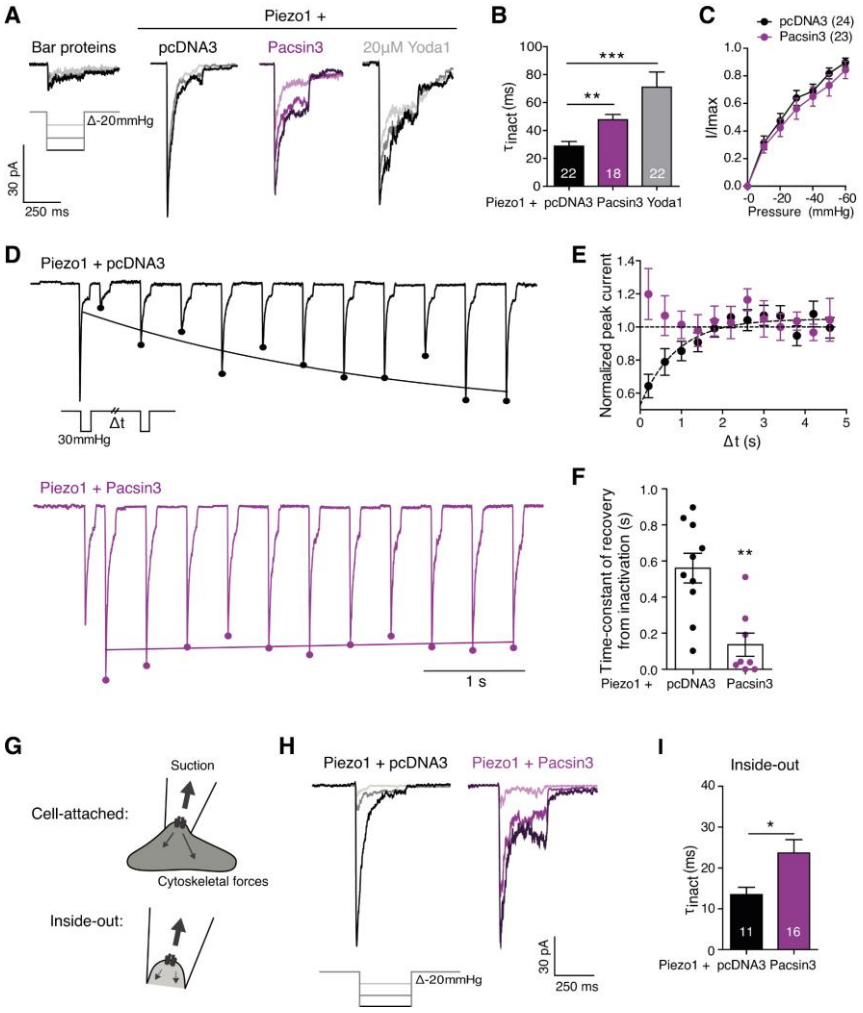

Fig. 3. Pacsin3 slows down Piezo1 inactivation independently of the effect of the cytoskeleton and increases channel recovery from inactivation. (A) Typical cell-attached Piezo1 MA in HEK293 cells stimulated with negative pulses from -10 to -60 mmHg (only -20, -40, and -60 mmHg pulses are represented) for 250 ms. Cells co-transfected with Piezo1, pcDNA3, and Pacsin3 as indicated. Yoda1 treatment was added to the pipette solution at 20 µM. (B) Mean inactivation time constant (τ_{inac}) from cell-attached MA shown in A. (C) Pressure responses curves comparing cells transfected with Piezo1 plus pcDNA3 or Pacsin3. Peak current values (I) are normalized to the maximal current (Imax) for each cell. (D) Representative traces of cell-attached Piezo1 MA stimulated with a protocol consisting of 2 consecutive negative pressure pulses of -30

mmHg for 100 ms, separated by an increasing delay. The second MA was normalized to the first peak. All the sweeps were concatenated to a single trace and fitted to a monoexponential equation. Cells were transfected with the indicated constructs. (E) Normalized means of the second MA peak shown in C for Piezo1 + pcDNA3 (black; N=13) or Piezo1 + Pacsin3 (purple; N=11), with their corresponding fitting. (F) Average of time-constants of recovery from inactivation for each cell, as shown in C, overexpressing Piezo1 + pcDNA3 (black; N=10) or Piezo1 + Pacsin3 (purple; N=8). (G) Scheme of the influence of the cytoskeleton in mechanically activated cells in cell-attached patch-clamp configuration compared to inside-out. (H) Representative MA of inside-out patches from cells transfected with the indicated constructs, mechanically stimulated as in A. (I) Mean inactivation time constant (τ_{inac}) of inside-out currents represented in G. Note that the effect of Pacsin3 in Piezo1 inactivation is maintained even when the cytoskeletal component is reduced. Data are represented as mean ± S.E.M. and statistics were evaluated with a Kruskal-Wallis followed by Dunn's post hoc (B) or a Mann–Whitney's U test (F,I). The membrane potential inside the patch was held at -80 mV in all the electrophysiological recordings.

Deepening on the effect of Pacsin3 on Piezo1 currents, we investigated the recovery from inactivation of the channel in cell-attached patches (Fig. 3D-F). Following a short control negative pressure pulse of -30 mmHg, a second suction of the same magnitude was performed in the patch, increasing sequentially the time between stimuli. By so doing, we tested the time needed for the current to recover the amplitude obtained with the initial pulse. After normalizing to the first control peak and superimposing the second pulses, we fitted the results to an exponential curve (Fig. 3D, E). Piezo1 currents normally take approximately 2 seconds to fully recover due to the transition between the open-inactivate-close states before being able to open again. However, we noticed that, in presence of Pacsin3, Piezo1 was able to recover to values similar to those obtained with the first pulse almost immediately (Fig. 3E). This was traduced by a significant reduction of the time-constant recovery from inactivation from 0.56 ± 0.06 s for cells

co-transfected with Piezo1 and pcDNA3 to 0.10 ± 0.06 s for cells co-transfected with Piezo1 and Pacsin3 (Fig. 3F). Thus, Piezo1 spends about threefold less time in the inactivated state in presence of Pacsin3. Once again, these results supported a disruption in the inactivated state of Piezo1 in presence of Pacsin3, which would allow the channel to be reactivated faster. As Pacsins can interact with actin-binding proteins, which are known to assist endocytosis through membrane pulling of the vesicles, we wondered if the effect of Pacsin3 on Piezo1 activity may be influenced/mediated by the cytoskeleton. To test this idea, we performed an electrophysiological analysis of Piezo1 macrocurrents in an inside-out configuration, which entailed a reduced influence of the cytoskeletal component in the total force exerted on membranes (Suchyna et al., 2009) (Fig. 3G). Similar to the cell-attach and whole-cell electrophysiological experiments, we observed a slowdown in Piezo1 inactivation in the presence of Pacsin3, with an almost 2-fold increase in τ_{inact} (Fig. 3H, I). Thus, Pacsin3 regulation on Piezo1 is mainly mediated by membrane tension and not by cytoskeletal forces.

Pacsin3 increases the mechanosensitive response of the Piezo1 channel by interaction through its SH3 domain.

Considering the impact of different BAR-domain-containing proteins on Piezo1 activity we evaluated their interaction by co-immunoprecipitation assays. Using an antibody against GFP to immunoprecipitate the BAR-domain proteins, we detected Piezo1 as a co-precipitant of Pacsin3 (Fig. 1I) and Amphyphisin (Fig. 1M), but not of IRSp53 (Fig. 1Q). At present we can not distinguish whether the lack of interaction between Piezo1 and IRSp53 is due to the structural impediment for binding of convex protein in the vicinity of the concave membrane footprint generated by Piezo1 or is

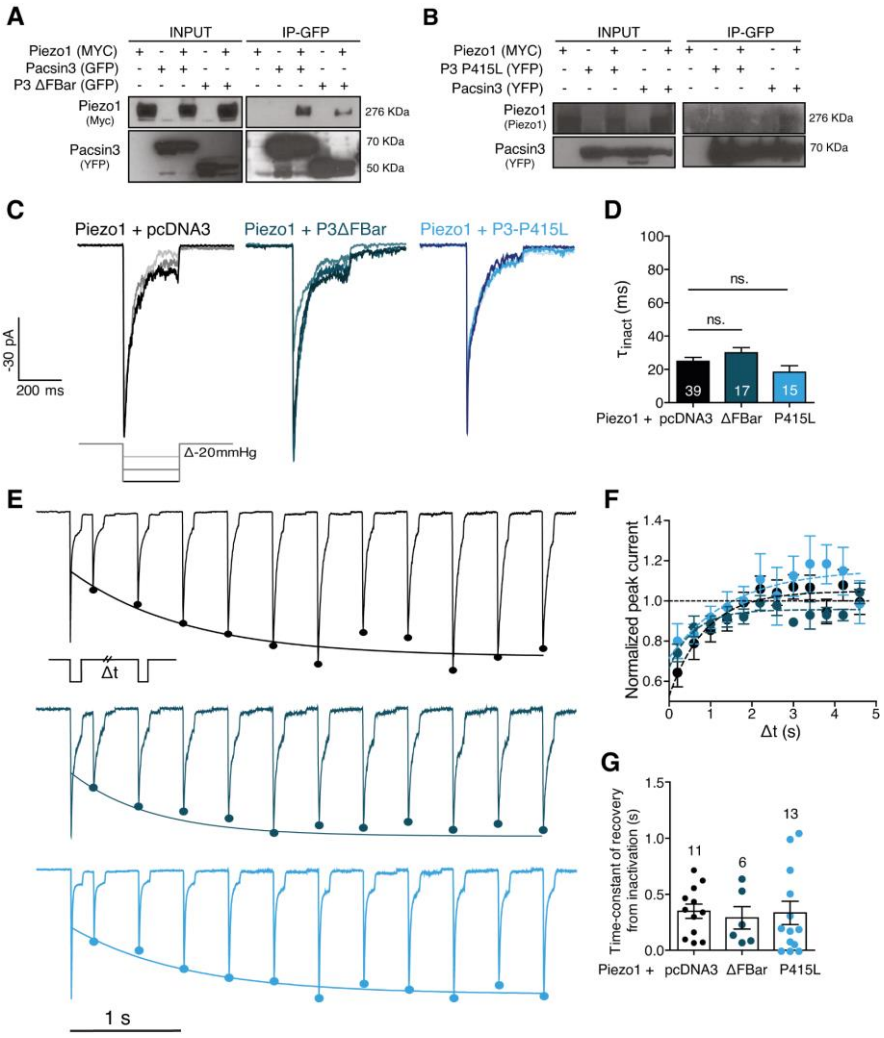

Fig. 4. Pacsin3 interacts with Piezo1 through its SH3 domain affecting channel inactivation parameters thanks to its F-BAR domain. (A) Co-immunoprecipitation of Piezo1-myc and Pacsin3-CFP or Pacsin3 mutant lacking the F-BAR domain (P3ΔFBAR), expressed in HEK293 cells. (B) Co-immunoprecipitation of Piezo1-myc and Pacsin3-YFP or the mutant P415L (SH3) of Pacsin3, expressed in HEK293 cells. (C) Representative traces of cell-attached Piezo1 MA in HEK293 cells expressing the indicated constructs and stimulated with negative pressure pulses from -10 to -60 mmHg (only -20, -40, and -60 mmHg pulses are illustrated) for 250 ms. (D) Mean inactivation time constant (τ_{inact}) from cell-attached patches represented in C. (E) Representative traces of cell-attached Piezo1 MA

stimulated with a protocol of recovery from inactivation performed in HEK293 cells overexpressing Piezo1 and pcDNA3 (black), P3ΔFBAR (dark blue) or Pacsin3-P415L (light blue). MA peaks fitted to a monoexponential equation represented with a curve. (F) Normalized mean peak of E, for Piezo1 + pcDNA3 (black; N=11), Piezo1 + P3ΔFBAR (dark blue; N=6) or Piezo1 + Pacsin3-P415L (light blue; N=13) with the corresponding fitting. (G) Average of time-constants of recovery from inactivation for each cell shown in F. Mean ± S.E.M. for the number of cells indicated in each bar or at the legend. Statistical significance was tested using a Kruskal-Wallis followed by Dunn's post hoc. Cell patches were held at a membrane potential of -80 mV.

due to specific domains of IRSp53. Further evaluation of Piezo1 interaction with BAR-domain proteins was focused on Pacsin3. The BAR domain is required for binding to and bending of membranes and the SH3 domain is required to interact with its partners (Q. Wang et al., 2009). We generated Pacsin3 mutants lacking the BAR domain (Pacsin3-ΔF-BAR) (Garcia-Elias et al., 2013) or carrying the P415L substitution in the SH3 domain (Pacsin3-P415L) that renders Pacsin3 unable to interact with its binding partners (Cuajungco et al., 2006). We reasoned that Pacsin3-ΔF-BAR will provide information about the relevance of the Pacsin3 interaction with the membrane to modulate Piezo1 activity and the Pacsin3-P415L mutant will provide information about the need for direct interaction between Pacsin3 and Piezo1 to modulate channel activity. First, we demonstrated that Pacsin3-ΔF-BAR, but not Pacsin3-P415L, co-immunoprecipitated with Piezo1 (Fig. 4A, B), although neither of them modified Piezo1 channel activity, including inactivation (Fig. 4C, D) or recovery from inactivation (Fig. 4E-G). Together, these results indicated that Pacsin3 binds Piezo1 through its SH3 domain to increase channel mechanosensitivity and to slow its inactivation in an F-BAR domain-dependent manner. The interaction between these two proteins was also evaluated in a microendothelial cell

model (HMEC) that expresses Piezo1 endogenously. A considerable colocalization of the heterologous expressed Pacsin3-CFP (no good anti-Pacsin3 antibodies are available) and endogenous Piezo1 was observed in the proximity of the PM, compared with the cytoplasmic region (Fig. 5A, B).

A predicted PRD domain in Piezo1 seems responsible for the interaction with the SH3 domain of Pacsin3.

Our next objective was to determine the region within Piezo1 responsible for the interaction with the SH3 of Pacsin3. As the SH3 domain is characterized by its capacity to bind the PRD of certain proteins, we investigated the sequence of Piezo1 in pursuit of PXXP motifs. We identified a total of 12 PXXP sequences distributed along the channel. After verifying the structure of Piezo1, we excluded sequences contained in transmembrane and extracellular regions that preclude the access of Pacsin3, ending up with 5 regions. Among these 5 PXXP motifs, one sequence was called to our attention because of its rich proline content (P1578/P1580/P1584/P1587) and because is located in a structurally unsolved region of the channel implicated in Piezo1 gating, between the latch and the TM29 (Fig. 5C, red dot), in close apposition to the beam (Fig. 5D, red molecular surface). We mutated the 4 prolines of this sequence to alanines (Piezo1-4PA) and we evaluated by electrophysiological experiments the mechanical response of the channel co-transfected with pcDNA3 or Pacsin3 (Fig. 5 E-G). We confirmed that whole-cell currents from the mutant Piezo1-4PA exhibited a similar response to poking than the WT channel. We reported similar maximal amplitude of currents (Imax)

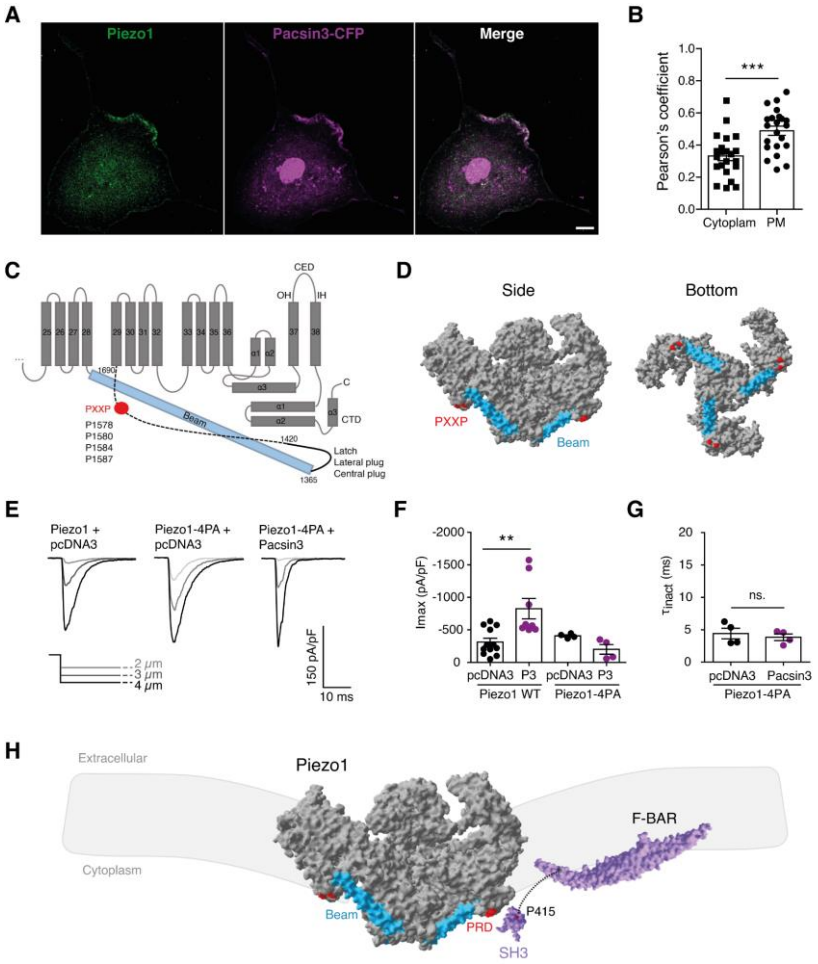

Fig. 5. Piezo1 has a predicted PRD domain responsible for the effect of Pacsin3. (A) Colocalization of Pacsin3-CFP and the endogenous Piezo1 from endothelial HMEC cells. Bar = 10 μm. (B) Pearson's coefficient quantification for Piezo1 and Pacsin3 localized either near the plasma membrane (PM) or in the cytoplasm. Analysis performed by calculation of the correlation intensity between the anti-Piezo1 signal and the CFP from Pacsin3. Mean ± S.E.M. of 22 cells (each dot represents an individual cell). Statistical significance was determined using a Student's unpaired t-test. (C) Partially Piezo1 structure based on the topological model from (Geng et al., 2020). The red dot indicates the proline-rich sequence (P1578/P1580/P1584/P1587) located in a structurally undefined region represented as a dashed line and proposed for interaction with the SH3 of Pacsin3. The beam is illustrated in blue. (D) Molecular surface

representation of the Piezo1 structure (left, side view; right, bottom view). In red, the structurally defined region flanking the predicted PRD domain. In blue, the beam is used as a visual reference for the pore location of the channel. (E) Representative whole-cell Piezo1 currents recorded at a holding potential of -80 mV in HEK293 cells stimulated by poking and overexpressing pcDNA3, Piezo1-WT, Piezo1-4PA, and Pacsin3 as indicated. (F) Mean of maximal whole-cell currents (Imax). (G) Mean inactivation time constant (τ) from whole-cell currents of the mutant Piezo1-4PA co-expressed with pcDNA3 or Pacsin3. Mean ± S.E.M. of 4 cells from each condition. Statistical significance was determined using a Student's unpaired t-test. (H) Model of the hypothetical interaction between Piezo1 (dark gray) and Pacsin3 (purple) in the PM (gray).

between the mutant and the WT channel (Fig. 5F), as well as no significant differences between inactivation kinetics ($\tau = 5.9 \pm 0.3$ ms for Piezo1 WT and $\tau = 4.4 \pm 0.8$ ms for Piezo1-4PA) (Fig. 5F). After proving that Piezo1-4PA displayed normal whole-cell currents, we co-transfected the mutant channel with Pacsin3. Piezo1-4PA currents stimulated with a poking pipette, were insensitive to the regulatory effect of Pacsin3 regarding Imax (Fig. 5F) and inactivation kinetics ($\tau = 3.8 \pm 0.5$ ms) (Fig. 5G). The loss of interaction between the mutant Piezo1-4PA channel and Pacsin3 has yet to be confirmed, in addition to the colocalization of those proteins in the PM. However, our results described a potential proline-rich sequence in Piezo1 in charge of Pacsin3-mediated increase of the mechanical response of the cell. Here, we presented a model in which the bowl-like shape imposed by Piezo1 on membranes is sensed by the F-BAR domain of Pacsin3, allowing the interaction of both proteins through the SH3 of Pacsin3 and a PRD in Piezo1 (Fig. 5H). One physiological relevance of this mechanical interplay will be presented in chapter 2.

Pacsin3 seems required for the correct localization of Piezo1 in the membrane.

Pacsin3 governs the subcellular localization of the mechanosensitive TRPV4 channel through direct interaction via its SH3 domain (Cuajungco et al., 2006). This blocks TRPV4 endocytosis and retains the channel in the PM. As Piezo1 seems to be another interactor of Pacsin3, we wondered if its PM localization was also affected by this interaction. To examine this possibility, we knockdown the endogenous Pacsin3 of HEK293 cells with a specific siRNA, reducing by more than a half its expression (Fig. 6A). Stimulating these cells by suction through the recording pipette in a cell-attached configuration, we noticed a significant fall in Piezo1 current density of cells expressing the siRNA of Pacsin3 (siPacsin3), compared to cells transfected with a scrambled sequence (siCtrl) (Fig. 6B, C). This can be incurred by channel inhibition or by the reduction of the channel content in the membrane. To study this subject, we quantified the PM content of the endogenous Piezo1 in HMEC cells transfected with siCtrl, siPacsin3, or overexpressing Pacsin3 (Fig. 6D) (siRNAs in this cell line are characterized in chapter 2). We used concanavalin A, a lectin that binds to glycoproteins and glycolipids from the cell surface, as a reference for membrane staining. We calculated the Pearson's coefficient between Piezo1 antibody signal and concanavalin A staining obtaining a ~42% reduction when depleting Pacsin3 from the cell (Fig. 6E). By contrast, overexpressing Pacsin3 did not affect Piezo1 localization in the PM. These results suggest that Pacsin3 participates in Piezo1 localization at the PM, thereby explaining the reduction in Piezo1 macrocurrents during mechanical stimulation. Unlike TRPV4-Pacsin3 interplay, Piezo1-Pacsin3 interaction seems more oriented to favour the trafficking of the channel to the PM than for its retention. However, further investigation is needed to study this second scenario.

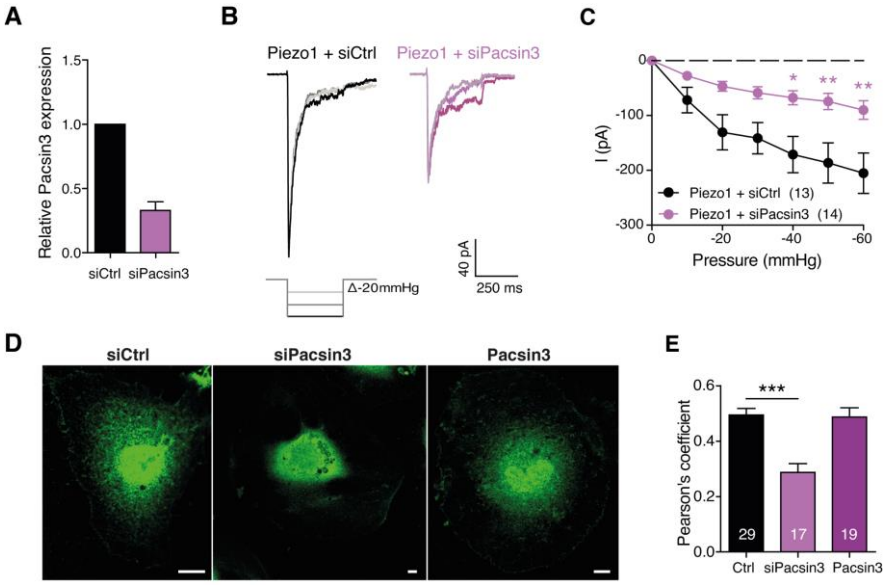

Fig. 6. Pacsin3 enriches Piezo1 localization in the membrane. (A) Quantitative PCR measurement of Pacsin3 mRNA transcript levels in HEK293 cells transfected with a control siRNA (siCtrl) or a siRNA for Pacsin3 (siPacsin3). (B) Representative cell-attached Piezo1 currents in HEK293 cells transfected with Piezo1 and siCtrl or siPacsin3. Piezo1 was stimulated with negative pressure pulses from -10 to -60 mmHg, with a step of -10 mmHg (only the traces corresponding to -20, -40, and -60 mmHg pulses are presented here). (C) Peak current density of cell-attached recordings in A. Mean ± S.E.M. of the number of cells indicated in the graph. Statistical significance was determined using an ANOVA followed by Bonferroni's post hoc test. (D) Immunofluorescence confocal microscopy images of endogenous Piezo1 in HMEC transfected with siCtrl, siPacsin3, or Pacsin3. Note a loss of Piezo1 signal reinforcement at the cell boundary in HMEC depleted in Pacsin3. Bar = 10 µm. (E) Pearson's coefficient quantification for endogenous Piezo1 and concanavalin A (not represented, used as a PM reference), in HMEC transfected with the indicated siRNA sequences or plasmid constructs. Mean ± S.E.M. of the number of cells indicated in each bar. Statistical significance was determined using an ANOVA followed by Bonferroni's post hoc test.

Chapter 2: The mechanosensitive Piezo1 channel controls endosome trafficking for an efficient cytokinetic abscission.

Title: The mechanosensitive Piezo1 channel controls endosome trafficking for an efficient cytokinetic abscission

Authors: Julia Carrillo-García, Víctor Herrera-Fernández, Selma A. Serra, Fanny Rubio-Moscardo, Marina Vogel-González, Pau Doñate-Macián and Miguel A. Valverde*

Affiliations:

Laboratory of Molecular Physiology, Department of Experimental and Health Sciences, Universitat Pompeu Fabra, 08003 Barcelona, Spain

*Correspondence to: miguel.valverde@upf.edu

Abstract: Mechanical forces are exerted throughout cytokinesis, the final step of cell division. Yet how forces are transduced and affect the signaling dynamics of cytokinetic proteins remain poorly characterized. We now show that the mechanosensitive Piezo1 channel is activated at the intercellular bridge (ICB) connecting daughter cells to regulate abscission. Piezo1 positioning at the ICB during cytokinesis depends on Pacsin3. Pharmacological and genetic inhibition of Piezo1 or Pacsin3 resulted in mislocation of ALIX-transporting Rab11-FIP3 endosomes and multinucleation. Furthermore, we identified FIP3 as the link between Piezo1-generated Ca^{2+} signals and ALIX delivery to the ICB, where ALIX recruits ESCRT-III components that promote abscission. These results provide a different view of how mechanical forces participate in cytokinesis and identify Piezo1 as a key modulator of endosome trafficking.

Short title: Mechanosensitive Piezo1 controls cytokinesis

One Sentence Summary: Piezo1 generates a Ca^{2+} signal at the intercellular bridge of dividing cells to control endosome trafficking and delivery of the ESCRT-III recruiting elements necessary for abscission.

Main Text: Cytokinetic abscission, the severing of the connecting intercellular bridge (ICB) between nascent daughter cells at the end of mitosis, is a sequential process that requires, among other events, the formation of the midbody at the ICB, delivery of Rab11-FIP3 endosomes to the ICB, cytoskeletal reorganization and, finally, the recruitment of the endosomal sorting complex required for transport–III (ESCRT-III) (*1–3*). Enrolment of the ESCRT-I subunit TSG101 and the ESCRT-III targeting factor ALIX at the midbody are prominent events initiated following the accumulation of the centrosomal protein Cep55 at the midbody. Both TSG101 and ALIX, through parallel pathways, recruit the ESCRT-III component charged multivesicular body protein 4B (CHMP4B) to direct abscission (*4, 5*). Successful cytokinesis also involves mechanical forces (*6–11*) and intracellular signals such as calcium (*12–14*), whose impact on the timely and spatially organized ESCRT-III components are unknown. Additional proteins able to bind to the membrane curvatures of the ICB, such as BIN-Amphiphysin-Rvs (BAR)-domain containing proteins, facilitate cytokinesis by means of anchoring key cytokinetic proteins at the correct location (*15–17*).

In this study, we aimed to identify how mechanical forces generated during cytokinesis are transduced to regulate the dynamics of key cytokinetic proteins, with a special focus on the activity of calcium permeable mechanosensitive ion channels. The presence of functional mechanosensitive TRPV4 (*18*), TRPM7 (*19*) and Piezo1 channels (*20*) was detected in human micro-endothelial cells (HMEC) (Fig. S1A-D). Piezo1 inhibition with GsMTx4 (*21*) or addition of the Ca^{2+} chelator BAPTA

significantly triggered the presence of multinucleated cells (Fig. 1A-B and the Fig. S2A), whereas inhibition of TRPM7 with FTY720 (*19*) or TRPV4 with HC067047 (*22*) did not induce significant multinucleation. GsMTx4 also prolonged the abscission time and the presence of daughter cells connected with elongated ICB (indicative of defective abscission), without affecting the time for mitotic rounding before metaphase (Fig. S2B-D). Transfection of HMEC with Piezo1 siRNA (Fig. S3A-B) also increased the number of nuclei per cell (Fig. 1C), verifying the involvement of Piezo1 in cytokinesis. Next, we evaluated Piezo1 localization and activity in both resting and dividing cells transfected with a genetically-encoded fluorescent Ca^{2+} reporter tagged to Piezo1 (GenEPI) (*23*). Resting cells showed plasma membrane GenEPI signal reinforcement (Fig. 1D), resembling the immunolocalization of native Piezo1 channel (Fig. S3A), while cells in late telophase showed increased GenEPI signal and colocalization with a-tubulin at the ICB (Fig. 1D). Time lapse imaging showed transient increases of GenEPI intensity at the ICB after release from cell cycle synchronization (Fig. 1E-F), indicating a predominant activation of Piezo1 at the ICB of mitotic cells. The use of the intracellular Ca^{2+} indicator Calbryte further confirmed that mitotic cells show a localized increase in intracellular Ca^{2+} concentration at the ICB (Fig. S3C).

Piezo1 is activated by changes in membrane curvature in response to mechanical stimulation (*24*). Membrane curvature is also sensed and influenced by BAR-domain proteins (*25*), of which Pacsin3, regulates trafficking and function of TRPV4 channel too (*26*, *27*). Therefore, we examined whether Pacsin3 may be responsible for Piezo1 localization at the ICB. In mitotic HMEC, Piezo1 and Pacsin3 signals colocalized with a-tubulin at the ICB (Fig. 1G and Fig. S4A). Knockdown of Piezo1 (Fig. S3A) with siRNA significantly decreased Piezo1 signal at the ICB and midbody (Fig. 1H-I). Similarly, siPacsin3 (Fig. S4B) reduced Piezo1

immunofluorescence at the ICB (Fig. 1H-I) without affecting Piezo1 expression (Fig. S4C). Knockdown of Pacsin3 also reduced mechanically stimulated and Piezo1-mediated Ca^{2+} signal whereas overexpression of Pacsin3 increased it (Fig. 1J). Coimmunoprecipitation experiments further confirmed the close interaction between endogenous (Fig. S4D) or overexpressed (Fig. S4E) Piezo1 and Pacsin3 proteins. Furthermore, and consistent with the Ca^{2+} imaging experiments in HMEC, we observed that HEK293 cells cotransfected with Piezo1 and Pacsin3, and mechanically stimulated with a blunt glass probe or by suction through the recording pipette presented larger whole-cell currents (Fig. 1K and Fig. S5A) and increased single-channel open probability (Fig. S5B-C) than cells overexpressing Piezo1 alone. Piezo1 inactivation, a crucial mechanism determining channel function, was also slowed (higher inactivation time constant t_{inact}) when co-expressed with Pacsin3 (Fig. 1L). Thus, Pacsin3 interaction with Piezo1 regulates both channel activity and location. Accordingly, siPacsin3 increased the number of nuclei/cell (Fig. 1C and Fig. S4F), an effect that was unaltered in the presence of GsMTx4. We also tested whether the effect of Pacsin3 knockdown on multinucleation could be overturned in the presence of the potent Piezo1 activator, Yoda1. We reasoned that Yoda1 may boost the activity of the Piezo1 channels remaining at the ICB of siPacsin3 treated cells. Indeed, exposure of cells depleted of Pacsin3 to Yoda1 reverted the presence of multinucleated cells (Fig. 1C). The percentage of multinucleated cells (Fig. S2A) and the length of the ICB (Fig. S2E) also increased with Piezo1 or Pacsin3 siRNA treatment. Furthermore, we identified a proline-rich domain in Piezo1 responsible for the interaction with Pacsin3 and the localization of Piezo1 to the ICB. Mutation of Pro1578, Pro1580, Pro1584 and Pro1587 to Ala (Piezo1-4PA) generated a functional channel that lost modulation by Pacsin3 (Fig. 1L and Fig. S5D). Rescue experiments overexpressing Piezo1-WT and Piezo1-4AP in HMEC depleted of endogenous Piezo1

using a siRNA directed against its 5'UTR showed that only Piezo1-WT localized to the cytokinetic bridge (Fig. 1M-N) and reverted the multinucleation phenotype (Fig. 1O). Together, these experiments suggested that both Pacsin3 and Piezo1 are in the same regulatory pathway required for efficient cytokinesis and that Pacsin3 modulates localization and activity of Piezo1 at the ICB of mitotic cells.

The presence of multinucleated cells and longer ICB following pharmacological or genetic inhibition of Piezo1 suggested a defect in abscission, the cutting of the narrow ICB, which depends on the ESCRT-III machinery (*1*). Consistent with the cytokinetic phenotype, endogenous CHMP4B was recruited to late cytokinetic bridges in control conditions but was absent in HMEC depleted of Piezo1, Pacsin3 or treated with GsMTx4, whereas pharmacological activation of Piezo1 with Yoda1 reverted the siPacsin3-induced mislocation of CHMP4B (Fig. 2A,D). The CHMP4B recruiting factor ALIX (Fig. 2B,E), and its upstream regulator Cep55 (Fig. 2 C,F) also disappeared from the ICB, indicating that Piezo1 modulates the recruitment of the ALIX-CHMP4B pathway to the midbody of late cytokinetic bridges. The role of Cep55 as a regulator of abscission has been recently disputed (*28*, *29*). To test the relevance of Cep55 in this process, we treated HMEC with siCep55 and observed a slight increase in the number of nuclei/cell (Fig. 2G), although less prominent than using siPiezo1 or siPacsin3 (Fig. 1C), that was reverted in the presence of Yoda1. Similarly, in Cep55-lacking human primary skin fibroblasts (Fig. 2H) siCep55, unlike siPiezo1, siPacsin3 or GsMTx4, did not modify the number of nuclei/cell (Fig. 2I), nor the effect of GsMTx4 on CHMP4B recruitment to the midbody (Fig. 2J). Together, these results indicate that Piezo1 involvement in cytokinetic abscission is independent of Cep55. To generalize our data showing a key role for Piezo1 in cytokinesis, we also examined human MDA-MB-231-BrM2 adenocarcinoma cells that express

several mechanosensitive ion channels (*30*). Akin to HMEC and fibroblasts, MDA-MB-231-BrM2 cells in which Piezo1 was knockdown (Fig. S6A-B) displayed a similar trend of increased percentage of multinucleated cells (Fig. S6C).

ALIX is a direct recruiter of CHMP4B and the formation of secondary ingression during late cytokinesis (*3*), and its midbody location is affected by genetic or pharmacological inhibition of Piezo1. Therefore, we focused on how Piezo1 may control the correct location of ALIX independently of Cep55. ALIX is present in endosomes (*31*) where can bind the ESCRT-III component CHMP4B (*32*). Thus, we tested the impact of Piezo1 on endosome trafficking and delivery of key molecules to the ICB. The small GTPase Rab11 and its effector FIP3 are present in endosomes and control endosome targeting to the ICB (*3*, *33*). Interference of Piezo1 or Pacsin3 reduced Rab11 presence at the ICB (Fig. 3A-B), consistent with the reduced ALIX signal. Piezo1 inhibition with GsMTx4 mimicked the effect of siPiezo1 whereas siPacsin3 effect was reverted with Yoda1 (Fig. 3A-B). To further explore the link between Rab11-containing endosomes and Piezo1 mediated signaling, we overexpressed wild-type (Rab11-WT), dominant negative (Rab11-S25N) and dominant positive (Rab11-Q70L) Rab11 and checked multinucleation (Fig. 3C-D) as well as ICB localization of CHMP4B (Fig. 3E,G) and ALIX (Fig. 3F,H). Overexpression of Rab11-WT did not alter the number of nuclei, the intensity of the CHMP4B and ALIX signals at the ICB or the effect of GsMTx4. Rab11-S25N overexpression significantly increased multinucleation, reduced CHMP4B and ALIX signals, effects that were not further increased in the presence of GsMTx4. On the other hand, Rab11-Q70L prevented the effect of GsMTx4 on any parameter tested, an effect not observed in cells overexpressing a dominant-positive Rab35 (*34*) (Fig. S7A-B). Other molecules relevant to cytokinesis and/or calcium signaling such as ALG-2 and Beclin-1 (*35*, *36*)

were tested and showed no changes in their location at the ICB (Fig. S8). Together, these results pointed to Rab11- and ALIX-containing endosomes as a target of Piezo1-mediated signaling during cytokinesis.

Next, we searched for the target of the Piezo1-mediated Ca^{2+} signal that controls the trafficking of Rab11 endosomes to the ICB. Rab11 has no Ca^{2+}-binding sites identified, whereas its effector, FIP3, presents two Ca^{2+} binding EF-hand domains (https://www.uniprot.org/uniprot/O75154). First, we localized FIP3 at the ICB and showed that FIP3 signal, like Rab11 signal, decreased in HMEC treated with GsMTx4, siPiezo1 or siPacsin3, but not in cells treated with siPacsin3 in the presence of Yoda1 (Fig. 4A-B). Second, we transfected HMEC with FIP3-WT or FIP3-4DA, in which four Asp (D215, D217, D219 and D247) present in the EF-hand domains that are required for Ca^{2+} binding were mutated to Ala, and we checked for the appearance of extra nuclei and CHMP4B at the ICB. Overexpression of FIP3-WT did not induce multinucleation or CHMP4B localization, nor altered the response to GsMTx4, whereas overexpression of FIP3-4DA significantly increased the number of nuclei and reduced the CHMP4B signal, effects that were not further modified in the presence of GsMTx4 (Fig. 4C-F). Similar effects to those obtained with FIP3-4DA were obtained when cells were transfected with a mutated FIP3 (FIP3-I738E) that does not interact with Rab11 (*37*) (Fig. S9).

The fact that mechanical forces are exerted throughout cytokinesis is generally accepted, although how these forces control cytokinesis is less clear. Activation of the mechanosensitive Piezo1 channel at the ICB generates local and transient increases in intracellular [Ca^{2+}] that are sensed by FIP3 to deliver Rab11-FIP3 endosomes containing ALIX to the ICB. This sequence of events ends with the ALIX-mediated recruitment of the ESCRT-III component CHMP4B, and the abscission of nascent daughter

cells. Together, our findings reveal that Piezo1-mediated transduction of mechanical forces (generated by cell crawling and elongation, cell interaction with extracellular matrix or by contraction of cytokinetic ring and protrusion of the cell poles) is key to the control of cytokinetic abscission, even under conditions of high cellular density and lower cell movement. The fact that a diffusible signal such as Ca^{2+} participates in the recruitment of abscission elements to the midbody may facilitate coordination of different cytokinetic events without the need of a physical/sequential interaction. A far reaching implication of our work is the role of force-induced Ca^{2+}-dependent regulation of the endosomal pathway and how it may affect other physiological functions that are under regulation by mechanical forces such as cargo targeting and release of exosomes (*32*, *38–40*).

References and Notes:

1. J. G. Carlton, J. Martin-Serrano, Parallels between cytokinesis and retroviral budding: A role for the ESCRT machinery. *Science.* **316**, 1908–1912 (2007).

2. R. A. Green, E. Paluch, K. Oegema, Cytokinesis in Animal Cells. *Annu. Rev. Cell Dev. Biol.* **28**, 29–58 (2012).

3. J. A. Schiel, G. C. Simon, C. Zaharris, J. Weisz, D. Castle, C. C. Wu, R. Prekeris, FIP3-endosome-dependent formation of the secondary ingression mediates ESCRT-III recruitment during cytokinesis. *Nat. Cell Biol.* **14**, 1068–1078 (2012).

4. E. Morita, V. Sandrin, H.-Y. Chung, S. G. Morham, S. P. Gygi, C. K. Rodesch, W. I. Sundquist, Human ESCRT and ALIX proteins interact with proteins of the midbody and function in cytokinesis. *EMBO J.* **26**, 4215–4227 (2007).

5. M. Vietri, M. Radulovic, H. Stenmark, The many functions of ESCRTs. *Nat. Rev. Mol. Cell Biol.* **21** (2020), pp. 25–42.

6. K. Burton, D. L. Taylor, Traction forces of cytokinesis measured with optically modified elastic substrata. *Nature*. **385**, 450–454 (1997).

7. J. Lafaurie-Janvore, P. Maiuri, I. Wang, M. Pinot, J.-B. Manneville, T. Betz, M. Balland, M. Piel, ESCRT-III Assembly and Cytokinetic Abscission Are Induced by Tension Release in the Intercellular Bridge. *Science.* **339**, 1625–1629 (2013).

8. D. K. Gupta, J. Du, S. A. Kamranvar, S. Johansson, Tension-induced cytokinetic abscission in human fibroblasts. *Oncotarget*. **9**, 8999–9009 (2018).

9. V. Srivastava, D. N. Robinson, Mechanical stress and network structure drive protein dynamics during cytokinesis. *Curr. Biol.* **25**, 663–670 (2015).

10. S. Nam, O. Chaudhuri, Mitotic cells generate protrusive extracellular forces to divide in three-dimensional microenvironments. *Nat. Phys.* **14**, 621–628 (2018).

11. M. Uroz, A. Garcia-Puig, I. Tekeli, A. Elosegui-Artola, J. F. Abenza, A. Marín-Llauradó, S. Pujals, V. Conte, L. Albertazzi, P. Roca-Cusachs, Á. Raya, X. Trepat, Traction forces at the cytokinetic ring regulate cell division and polyploidy in the migrating zebrafish epicardium. *Nat. Mater.* **18**, 1015–1023 (2019).

12. D. C. Chang, C. Meng, A localized elevation of cytosolic free calcium is associated with cytokinesis in the zebrafish embryo. *J. Cell Biol.* **131**, 1539–45 (1995).

13. E. Boucrot, T. Kirchhausen, Endosomal recycling controls plasma membrane area during mitosis. *Proc. Natl. Acad. Sci. U. S. A.* **104**, 7939–7944 (2007).

14. S. E. Webb, A. L. Miller, Calcium signalling and membrane dynamics during cytokinesis in animal cells. *Membr. Dyn. Calium signaling, Adv. Exp. Med. Biol.* **981**, 389–412 (2017).

15. C. M. Smith, M. Chircop, Clathrin-Mediated Endocytic Proteins are Involved in Regulating Mitotic Progression and Completion. *Traffic*. **13**, 1628–1641 (2012).

16. N. A. McDonald, C. W. Vander Kooi, M. D. Ohi, K. L. Gould, Oligomerization but Not Membrane Bending Underlies the Function of Certain F-BAR Proteins in Cell Motility and Cytokinesis. *Dev. Cell*. **35**, 725–736 (2015).

17. C. E. Snider, M. Chandra, N. A. McDonald, A. H. Willet, S. E. Collier, M. D. Ohi, L. P. Jackson, K. L. Gould, Opposite Surfaces of the Cdc15 F-BAR Domain Create a Membrane Platform That Coordinates Cytoskeletal and Signaling Components for Cytokinesis. *Cell Rep.* **33**, 108526 (2020).

18. J. Fernandes, I. M. Lorenzo, Y. N. Andrade, A. Garcia-Elias, S. a Serra, J. M. Fernandez-Fernandez, M. A. Valverde, IP3 sensitizes TRPV4 channel to the mechano- and osmotransducing messenger 5'-6'-epoxyeicosatrienoic acid. *J. Cell Biol.* **181**, 143–55 (2008).

19. R. Zhao, A. Afthinos, T. Zhu, P. Mistriotis, Y. Li, S. A. Serra, Y. Zhang, C. L. Yankaskas, S. He, M. A. Valverde, S. X. Sun, K. Konstantopoulos, Cell sensing and decision-making in confinement: The role of TRPM7 in a tug of war between hydraulic pressure and cross-sectional area. **5**, eaaw7243 (2019).

20. B. Coste, J. Mathur, M. Schmidt, T. J. Earley, S. Ranade, M. J. Petrus, A. E. Dubin, A. Patapoutian, Piezo1 and Piezo2 are essential components of distinct mechanically activated cation channels. *Science*. **330**, 55–60 (2010).

21. W. C. Hung, J. R. Yang, C. L. Yankaskas, B. S. Wong, P. H. Wu, C. Pardo-Pastor, S. A. Serra, M. J. Chiang, Z. Gu, D. Wirtz, M. A. Valverde, J. T. Yang, J. Zhang, K. Konstantopoulos, Confinement Sensing and Signal Optimization via Piezo1/PKA and Myosin II Pathways. *Cell Rep.* **15**, 1430–1441 (2016).

22. P. Doñate-Macian, Y. Duarte, F. Rubio-Moscardo, G. Pérez-Vilaró, J. Canan, J. Díez, F. González-Nilo, M. A. Valverde, *Br. J. Pharmacol.*, in press, doi:10.1111/bph.15267.

23. S. Yaganoglu, N. Helassa, B. M. Gaub, M. Welling, J. Shi, D. J. Müller, K. Török, P. Pantazis, GenEPi: Piezo1-based fluorescent reporter for visualizing mechanical stimuli with high spatiotemporal resolution. *bioRxiv* (2019), p. 702423.

24. Y. C. Lin, Y. R. Guo, A. Miyagi, J. Levring, R. MacKinnon, S. Scheuring, Force-induced conformational changes in PIEZO1. *Nature*. **573**, 230–234 (2019).

25. N. A. McDonald, K. L. Gould, Linking up at the BAR: Oligomerization and F-BAR protein function. *Cell Cycle*. **15** (2016), pp. 1977–1985.

26. M. P. Cuajungco, C. Grimm, K. Oshima, D. D'hoedt, B. Nilius, A. R. Mensenkamp, R. J. Bindels, M. Plomann, S. Heller, PACSINs bind to the TRPV4 cation channel. PACSIN 3 modulates the subcellular localization of TRPV4. *J.Biol.Chem.* **281**, 18753–18762 (2006).

27. A. Garcia-Elias, S. Mrkonjic, C. Pardo-Pastor, H. Inada, U. a Hellmich, F. Rubio-Moscardó, C. Plata, R. Gaudet, R. Vicente, M. a Valverde, Phosphatidylinositol-4,5-biphosphate-dependent rearrangement of TRPV4 cytosolic tails enables channel activation by physiological stimuli. *Proc. Natl. Acad. Sci. U. S. A.* **110**, 9553–8 (2013).

28. A. Lie-Jensen, K. Ivanauskiene, L. Malerød, A. Jain, K. W. Tan, J. K. Laerdahl, K. Liestøl, H. Stenmark, K. Haglund, Centralspindlin Recruits ALIX to the Midbody during Cytokinetic Abscission in Drosophila via a Mechanism Analogous to Virus Budding. *Curr. Biol.* **29**, 3538-3548.e7 (2019).

29. A. Tedeschi, J. Almagro, M. J. Renshaw, H. A. Messal, A. Behrens, M. Petronczki, Cep55 promotes cytokinesis of neural progenitors but is dispensable for most mammalian cell divisions. *Nat. Commun.* **11**, 1–16 (2020).

30. C. Pardo-Pastor, F. Rubio-Moscardo, M. Vogel-González, S. A. Serra, A. Afthinos, S. Mrkonjic, O. Destaing, J. F. Abenza, J. M. Fernández-Fernández, X. Trepat, C. Albiges-Rizo, K. Konstantopoulos, M. A. Valverde, Piezo2 channel regulates RhoA and actin cytoskeleton to promote cell mechanobiological responses. *Proc. Natl. Acad. Sci. U. S. A.* **115**, 1925–1930 (2018).

31. C. Bissig, M. Lenoir, M. C. Velluz, I. Kufareva, R. Abagyan, M. Overduin, J. Gruenberg, Viral Infection Controlled by a Calcium-Dependent Lipid-Binding Module in ALIX. *Dev. Cell*. **25**, 364–373 (2013).

32. J. Larios, V. Mercier, A. Roux, J. Gruenberg, ALIX- And ESCRT-III-dependent sorting of tetraspanins to exosomes. *J. Cell Biol.* **219** (2020), doi:10.1083/jcb.201904113.

33. C. P. Horgan, M. Walsh, T. H. Zurawski, M. W. McCaffrey, Rab11-FIP3 localises to a Rab11-positive pericentrosomal compartment during interphase and to the cleavage furrow during cytokinesis. *Biochem. Biophys. Res. Commun.* **319**, 83–94 (2004).

34. D. Dambournet, M. MacHicoane, L. Chesneau, M. Sachse, M. Rocancourt, A. El Marjou, E. Formstecher, R. Salomon, B. Goud, A. Echard, Rab35 GTPase and OCRL phosphatase remodel lipids and F-actin for successful cytokinesis. *Nat. Cell Biol.* **13**, 981–988 (2011).

35. L. L. Scheffer, S. C. handr. Sreetama, N. Sharma, S. Medikayala, K. J. Brown, A. Defour, J. K. Jaiswal, Mechanism of Ca^{2+}-triggered ESCRT assembly and regulation of cell membrane repair. *Nat. Commun.* **5**, 5646 (2014).

36. S. Y. You, Y. S. Park, H.-J. Jeon, D.-H. Cho, H. Bae Jeon, S. H. Kim, J. W. Chang, J.-S. Kim, & Jeong, S. Oh, Cell Cycle Beclin-1 knockdown shows abscission failure but not autophagy defect during oocyte meiotic maturation (2016), doi:10.1080/15384101.2016.1181235.

37. J. Bouchet, I. del Río-Iñiguez, E. Vázquez-Chávez, R. Lasserre, S. Agüera-González, C. Cuche, M. W. McCaffrey, V. Di Bartolo, A.

Alcover, Rab11-FIP3 Regulation of Lck Endosomal Traffic Controls TCR Signal Transduction. *J. Immunol.* **198**, 2967–2978 (2017).

38. M. Tytell, R. J. Lasek, H. Gainer, Axonal maintenance, glia, exosomes, and heat shock proteins. *F1000Research*. **5** (2016), p. 205.

39. Y. Wang, K. F. Goliwas, P. E. Severino, K. P. Hough, D. Van Vessem, H. Wang, S. Tousif, R. P. Koomullil, A. R. Frost, S. Ponnazhagan, J. L. Berry, J. S. Deshane, Mechanical strain induces phenotypic changes in breast cancer cells and promotes immunosuppression in the tumor microenvironment. *Lab. Investig.* **100**, 1503–1516 (2020).

40. A. Savina, C. M. Fader, M. T. Damiani, M. I. Colombo, Rab11 Promotes Docking and Fusion of Multivesicular Bodies in a Calcium-Dependent Manner. *Traffic*. **6**, 131–143 (2005).

41. M. Valiente, A. C. Obenauf, X. Jin, Q. Chen, X. H.-F. Zhang, D. J. Lee, J. E. Chaft, M. G. Kris, J. T. Huse, E. Brogi, J. Massagué, Serpins promote cancer cell survival and vascular co-option in brain metastasis. *Cell*. **156**, 1002–16 (2014).

42. R. Syeda, J. Xu, A. E. Dubin, B. Coste, J. Mathur, T. Huynh, J. Matzen, J. Lao, D. C. Tully, I. H. Engels, H. M. Petrassi, A. M. Schumacher, M. Montal, M. Bandell, A. Patapoutian, Chemical activation of the mechanotransduction channel Piezo1. *Elife*. **4**, e07369 (2015).

43. V. Venturini, F. Pezzano, F. C. Castro, H. M. Häkkinen, S. Jiménez-Delgado, M. Colomer-Rosell, M. Marro, Q. Tolosa-Ramon, S. Paz-López, M. A. Valverde, J. Weghuber, P. Loza-Alvarez, M. Krieg, S. Wieser, V. Ruprecht, The nucleus measures shape changes for cellular proprioception to control dynamic cell behavior. *Science (80-.).* **370** (2020), doi:10.1126/science.aba2644.

44. Bae, R. Gnanasambandam, C. Nicolai, F. Sachs, P. A. Gottlieb, Xerocytosis is caused by mutations that alter the kinetics of the mechanosensitive channel PIEZO1. *Proc.Natl.Acad.Sci.U.S.A.* **110**, E1162–E1168 (2013).

Acknowledgments: Members of the lab for insightful discussions.

Funding: the Spanish Ministry of Science, Education and Universities through grants RTI2018-099718-B-100 and an institutional “Maria de Maeztu" Programme for Units of Excellence in R&D and FEDER funds to M.A.V.; **Author contributions:** M.A.V. and J.C.-G. designed the research; J.G-C. performed electrophysiological, calcium imaging and confocal microscopy experiments; S.A.S., electrophysiological and immunoprecipitation experiments; F.R.-M., Calcium imaging, generation of cell lines and plasmids: V.H.-F., MDA231-BrM2 experiments; M.V.-G., PCR experiments, P.D.-M., Co-immunoprecipitation experiments; M.A.V., funding, supervision of the project and manuscript writing. All authors edited the manuscript; **Competing interests:** Authors declare no competing interests; and **Data and materials availability:** All data generated in this study is available in the main text or the supplementary materials.

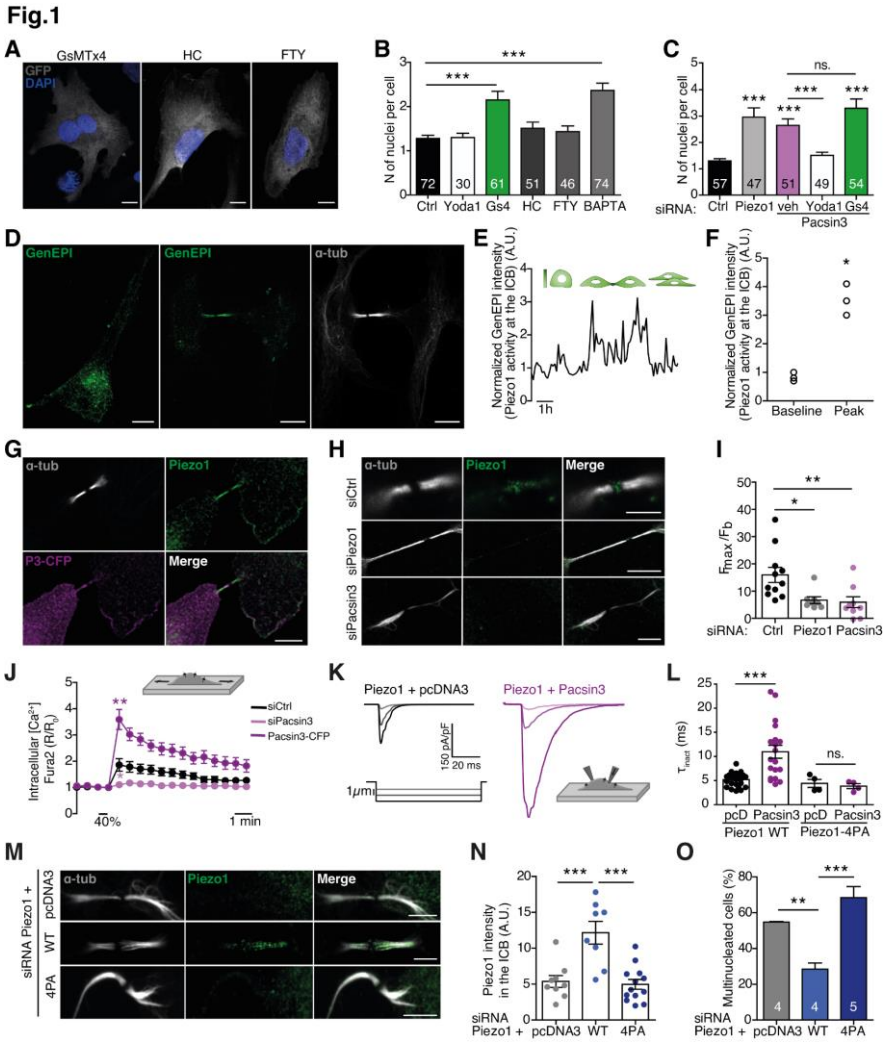

Fig. 1. Piezo1 localization and activity at the cytokinetic bridge. (A) Nuclear staining with DAPI in human microvascular endothelial cells (HMEC) expressing GFP and treated with GsMTx4 (1 μM), HC067047 (100 nM) or FTY720 (10 μM). Bar= 10 μm. (B and C) Number of nuclei/cell counted in HMEC exposed to the conditions indicated. Piezo1 activator Yoda1 (5 μM), BAPTA (1 μM). (D) Piezo1-GCamP6 (GenEPI) localization in interphase (left) and late mitosis (middle); anti-a-tubulin staining in late mitosis (right). Bar= 10 μm. (E) Piezo1-mediated Ca^{2+} signal, measured at the ICB in GenEPI-transfected HMEC, peaks around 2h after release from nocodazole synchronization. (F) Peak and baseline GenEPI fluorescence intensity at the ICB. (G) Colocalization of

overexpressed Pacsin3-CFP with endogenous Piezo1 and a-tubulin at the ICB. Bar= 5 µm. (H) Immunodetection of Piezo1 and a-tubulin in HMEC transfected with control siRNA, siPiezo1 or siPacsin3. Bar= 5 µm. (I) Quantification of Piezo1 signal at the ICB in HMEC transfected with siControl, siPiezo1 or siPacsin3. (J) Mean intracellular Ca^{2+} signals obtained from HMEC loaded with Fura-2-AM transfected with siControl (N=37), siPacsin3 (N=17) or overexpressing Pacsin3 (N=15) and exposed to uniaxial stretching (40% of the initial chamber length, inset illustration). (K) Whole-cell traces of mechanically activated Piezo1 currents recorded at a holding potential of −80 mV from HEK293 cells overexpressing Piezo1 (left) or Piezo1+Pacsin3 (right) following stimulation with a series of mechanical steps of 1 µm (Inset illustration). (L) Mean inactivation time constant (t) of whole-cell currents obtained in HEK293 cells overexpressing pcDNA3, Piezo1-WT, Piezo1-4PA and Pacsin3 as indicated. (M) Immunodetection of Piezo1 and a-tubulin in HMEC in which endogenous Piezo1 was knocked down with a siRNA directed against Piezo1 5'UTR and transfected with the indicated siRNA resistant Piezo constructs. Bar= 5 µm. (N) Quantification of Piezo1 signal at the ICB under the conditions indicated. (O) Percentage of multinucleated HMEC under the conditions indicated. Data are means ± S.E.M. Number of cells (or experimental repeats) indicated in each graph. Significance values are respect control condition as determined by Kruskal-Wallis followed by Dunn's post hoc, paired t test (F) or ANOVA followed by Bonferroni post hoc (L, N and O).

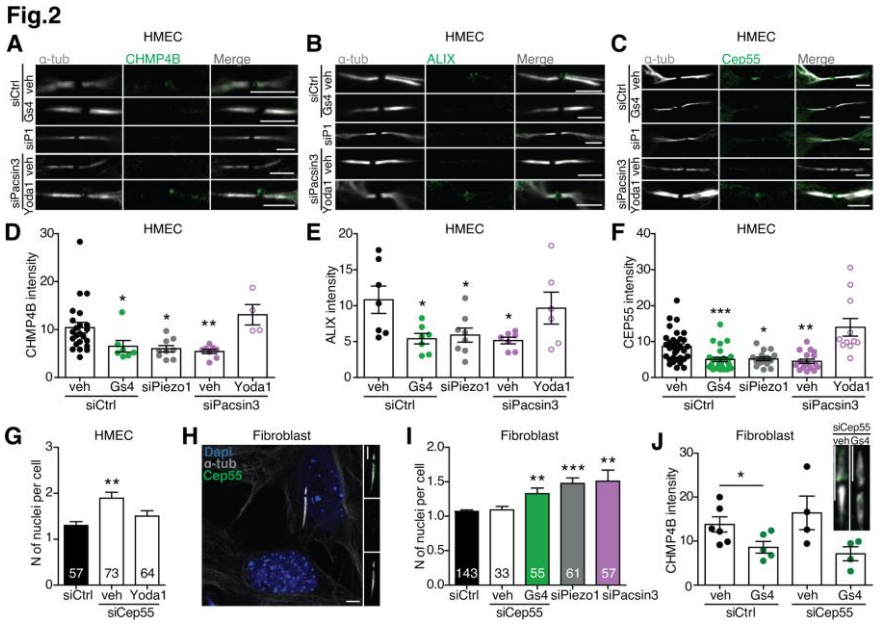

Fig. 2. Piezo1 regulates localization of ESCRT-III components to the late cytokinetic bridge. Immunolocalization of a-tubulin and CHMP4B (A), ALIX (B) and Cep55 (C) at the midbody of siControl, siPiezo1, GsMTx4, siPacsin3 and siPacsin3 + Yoda1 treated HMEC. Bar= 5 µm. Quantification of CHMP4B (D), ALIX (E) and Cep55 (F) immunofluorescence intensities at the midbody. (G) Quantification of the number of nuclei per cell in HMEC transfected with control siRNA or siCep55 in the presence/absence of Yoda1. (H) Immunolocalization of Cep55 and a-tubulin in primary human dermal fibroblasts. Nuclear staining with DAPI. Bar= 5 µm. (I) Quantification of the number of nuclei per cell in primary human dermal fibroblasts transfected with control siRNA, siCep55 in the presence/absence of GsMTx4, siPiezo1 or siPacsin3. (J) CHMP4B immunofluorescence intensities at the midbody of primary human dermal fibroblasts transfected with control siRNA or siCep55 in the presence or absence of GsMTx4. Bar= 5 µm. Data are means ± S.E.M. Number of cells (or experimental repeats) indicated in each graph. Significance values are respect control condition as determined by Kruskal-Wallis followed by Dunn's post hoc or ANOVA followed by Dunnett's post hoc test (E).

Fig.3

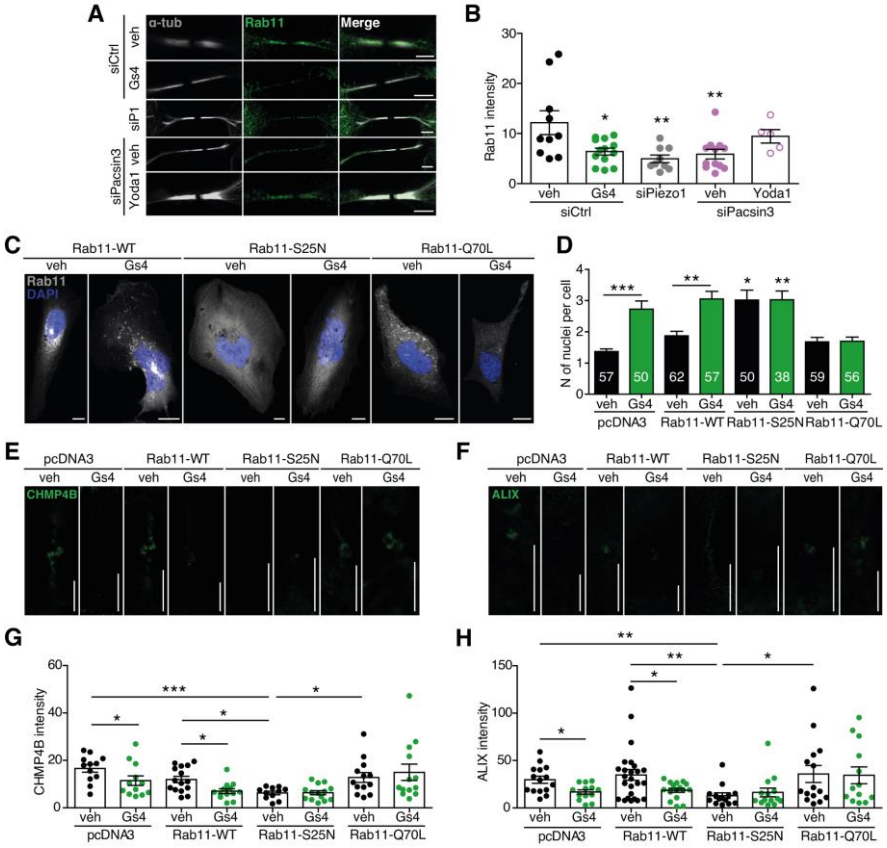

Fig. 3. Piezo1 controls delivery of Rab11-FIP3 endosomes to the cytokinetic ring. Immunolocalization of Rab11 at the midbody of siControl, siPiezo1, GsMTx4, siPacsin3 and siPacsin3 + Yoda1 treated HMEC. Immunolocalization of a-tubulin in white. Bar= 5 µm. (B) Quantification of Rab11 intensity at the ICB under the conditions shown in A. (C) Nuclear staining with DAPI (blue) in HMEC transfected with Rab11-WT, dominant-negative Rab11-S25N or dominant-positive Rab11-Q70L in the presence/absence of GsMTx4. Bar= 10 µm (D) Quantification of nuclei in HMEC overexpressing pcDNA3, Rab11-WT, Rab11-S25N or Rab11-Q70L in the presence or absence of GsMTx4. CHMP4B (E) and ALIX (F) immunofluorescence intensities at the midbody of HMEC overexpressing pcDNA3, Rab11-WT, Rab11-S25N and Rab11-Q70L in the presence or absence of GsMTx4. Quantification of CHMP4B (G) and ALIX (H) immunofluorescence intensities in HMEC under the conditions shown. Bar= 5 µm. Data are means ± S.E.M. Number of cells (or

experimental repeats) indicated in each graph. Significance values are respect control condition as determined by Kruskal-Wallis followed by Dunn's post hoc or ANOVA followed by Dunnett's post hoc test (B).

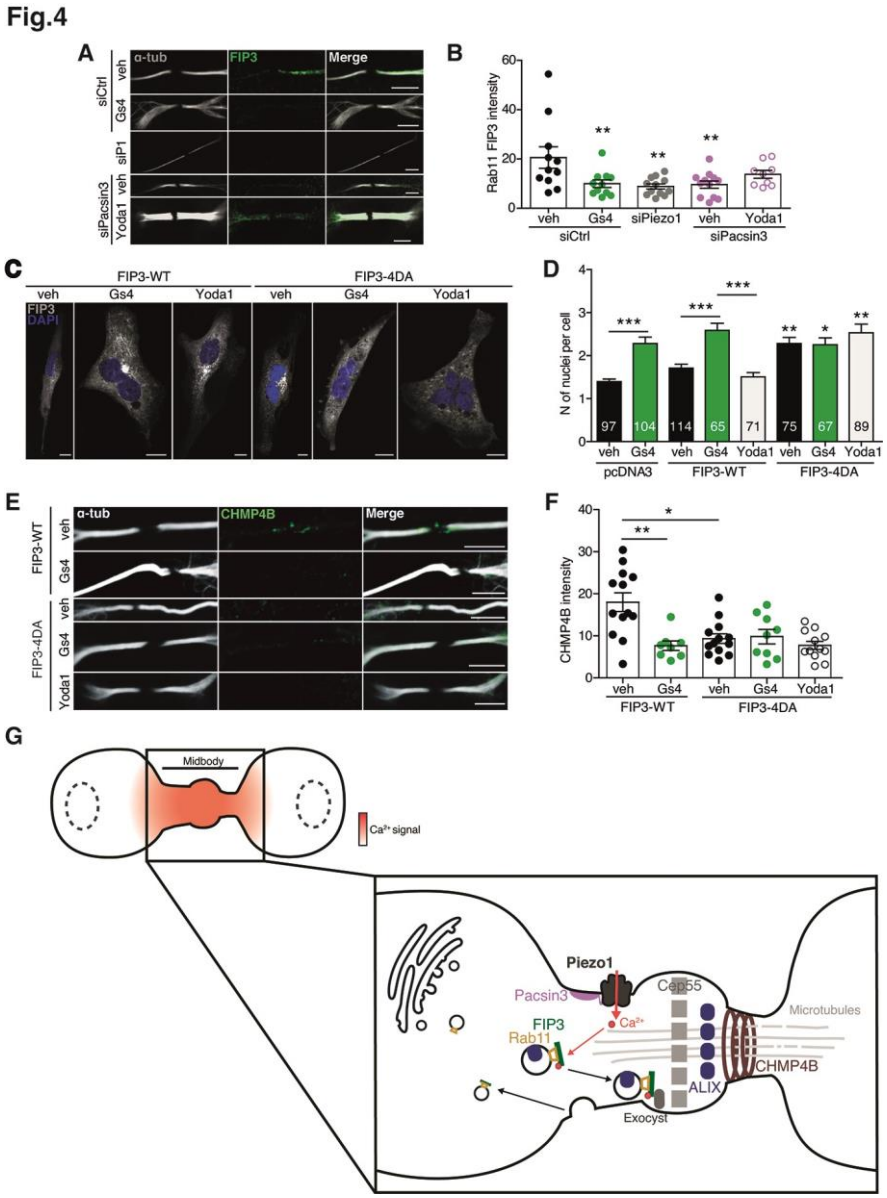

Fig. 4. FIP3 links Piezo1-generated Ca^{2+} signals to the recruitment of the abscission machinery. Immunolocalization of FIP3 at the midbody of siControl, siPiezo1, GsMTx4, siPacsin3 and siPacsin3 + Yoda1 treated HMEC. Immunolocalization of a-tubulin in white. Bar= 5 µm. (B) Quantification of FIP3 signal at the ICB under the conditions shown in A. (C) DAPI staining of the nuclei in HMEC overexpressing FIP3-WT and

FIP3-4DA in the presence and absence of GsMTx4 or Yoda1. Bar= 10 µm. (D) Quantification of nuclei in HMEC overexpressing FIP3-WT and FIP3-4DA in the presence and absence of GsMTx4 or Yoda1. (E) CHMP4B immunofluorescence of HMEC overexpressing FIP3-WT and FIP3-4DA in the presence and absence of GsMTx4 or Yoda1. Bar= 5 µm. (F) Quantification of CHMP4B immunofluorescence intensity in HMEC under the conditions shown. Data are means ± S.E.M. When required, number of cells (or experimental repeats) indicated in each graph. Significance values are respect control condition as determined by Kruskal-Wallis followed by Dunn's post hoc or ANOVA followed by Dunnett's post hoc test (B). (G) Overview of cytokinesis regulation by the Piezo1 channel. Mechanical forces exerted at the ICB activate Piezo1 channel generating a marked and localized increase in intracellular calcium (red shading). The increase in intracellular Ca^{2+} concentration is sensed by FIP3 to direct the transport of ALIX-containing Rab11-FIP3 endosomes to the ICB where ALIX recruits CHMP4B to complete abscission.

Supplementary Materials:

Materials and Methods

Materials

Drugs, antibodies, oligonucleotides and plasmids used are described in table S1.

Cell culture and transfection

HEK293 human kidney cells (catalog number 85120602) were purchased from the European Collection of Authenticated Cell Cultures. HEK293 cells were cultured in high glucose Dulbecco's modified Eagle's medium (DMEM) containing 10% Fetal Bovine Serum (Gibco, Life Technologies) and 1% Penicillin/Streptomycin (Gibco) at 5% CO2 and 37°C. Cells were transiently transfected with the Piezo1 plasmid plus pcDNA3 empty vector (for control condition) or Pacsin3 at a ratio 1:1, using polyethylenimine (PEI, Polysciences, 23966; ratio 5:1 PEI:DNA) and following manufacturer's protocol. Human microvascular endothelial cells (HMEC) from the American Type Culture Collection (ATCC®), was grown in MCDB-131 medium supplemented with 0.1 μg/mL hydrocortisone, 12 ng/mL EGF, 2 mM L-glutamine (G7513, Sigma), 1% Pen/Strep and 15% FBS at 5% CO2 and 37°C. Transient knockdown or overexpression in HMEC were performed using Lipofectamine RNAiMAX or 3000 (Thermo). A ratio of 1:1 LIPO:DNA diluted in Opti-MEM (Gibco) was used, following manufacturer's instructions. Experiments were conducted 1-3 days after transfection. For synchronization assays, HMEC cells were treated with 100 nM of nocodazole (Sigma) in complete medium for 16-20h and released with normal medium 2h before experiments. When specified, a drug treatment was added to the cells just after nocodazole release. Human dermal fibroblasts (GM05565) were purchased from the Coriell Institute (Camden) and grown in DMEM supplemented with 10%

v/v FBS and 1% v/v Pen/Strep (Gibco). All cells were plated in collagen type I (354236, Cultek, 10 µg/mL in 0.02 M acetic acid, 1h and 37ºC) coated chambers, coverslips or 35 mm MatTek glass bottom dishes.

MDA-MB-231-BrM2 cells (41) were kindly provided by Joan Massagué, Memorial Sloan Kettering Cancer Center, NY. MDA-MB-231-BrM2 cells were grown in DMEM + 10% FBS + 1% Pen/Strep + 1% GlutaMAX (Gibco). Knockdown of Piezo1 in MDA-MB-231BrM2 cells was obtained using lentivirus as previously described (30). In brief, HEK293 were transfected with 2 µg pMD2-G + 4 µg pSPAX2 and 5 µg pLKO.1-shPIEZO1 or pLKO.1-scramble (Table S1) using lipofectamine 3000 (Invitrogen). After collection, centrifugation, and titration, lentiviral supernatants were used to infect MDA-MB-231BrM2 cells. MDA-MB-231BrM2-shPIEZO1 and MB-231BrM2-scramble stable cell lines were generated by selection with 1 µg/mL puromycin. MDA-MB-231-BrM2 cells were synchronized with a double nocodazole block procedure (100 nM, 16h-8h-16h) and released with normal medium 2h before experiments were carried out.

Electrophysiological recordings

Stretch-activated currents were recorded on HEK293 cells 2 days after transfection. For whole-cell recordings, the bath solution contained (in mM) 140 NaCl, 2.5 KCl, 1.2 $CaCl_2$, 0.5 $MgCl_2$, 5 glucose and 10 HEPES (adjusted to pH 7.45 with NaOH). Borosilicate glass patch pipettes had a tip resistance of 1-5 MΩ and contained (in mM) 140 CsCl, 0.3 Na_3GTP, 4 Na_2ATP, 1 EGTA, 10 HEPES (adjusted to pH 7.3 with Tris). The membrane potential inside the patch was held at −80 mV using an Axopatch 200 A (Molecular Devices, U.S.A.). Piezo1 activity was assessed by applying a mechanical stimulation generated with a fire-polished glass

probe driven by a piezoelectric controller (E-665, Physik Instrumente). The probe had an upward motion consisting of 1 μm increment, 200 ms duration and a spaced interval of 10 s. Currents were sampled at 10 kHz and filtered at 1 kHz 20 using pClamp10.5 software (Axon Instruments).

For cell-attached configuration, borosilicate glass patch pipettes (2-3 MΩ) were filled with a solution containing (in mM) 130 NaCl, 5 KCl, 1 $CaCl_2$, 1 $MgCl_2$, 10 TEA-Cl, 10 HEPES (adjusted to pH 7.3 with NaOH). Piezo1 activity was also triggered under this recording condition using the Piezo activator Yoda (20 μM) (42), added to the pipette solution. The bath solution contained (in mM) 140 KCl, 1 $MgCl_2$, 10 glucose and 10 HEPES (adjusted to pH 7.3 with Tris). This extracellular potassium concentration was used to zero the membrane potential, allowing better control of the voltage (-80 mV) using an EPC10-USB patch-clamp amplifier (HEKA Elektronik). Stimulation of the Piezo1 channel was performed using a High-Speed Pressure Clamp (HSPC-1, ALA Scientific Instruments) applying a pre-pulse of -8 mmHg. Experiments were run at room temperature (22-26ºC). Data were analyzed using Igor Pro 8 (WaveMetrics) and MATLAB. Due to the biphasic kinetic of the currents, the time constant of inactivation τ_1 was obtained by fitting the results to a double exponential curve between the peak current and the end of the stimulus, according to the next equation:

$$I = I_0 + A_1 \exp\left(\frac{t - t_0}{\tau_1}\right) + A_2 \exp\left(\frac{t - t_0}{\tau_2}\right).$$

Cell Stretching and calcium imaging

To measure cytosolic calcium increases in response to stretch, cells were cultured in a silicone chamber (STB-CH-04, STRETX Inc.) to a 50% confluence and loaded with 4.5 μM fura 2-AM (Thermo) as previously described (18). Isotonic bath solutions contained 140 mM NaCl, 2.5 mM KCl, 1.2 mM $CaCl_2$, 0.5 mM $MgCl_2$, 5 mM glucose, and 10 mM HEPES

(adjusted to pH 7.3 with NaOH). For mechanical stimulation of Piezo1, two steps of 0.5 s uniaxial stretching (40% and 80% of the initial chamber length) were applied with a delay of 8 min, which is the time necessary to recover basal calcium levels after the first stimulus. The fluorescence ratio (F340/F380) was acquired with an imaging processing software (HCImage, Hamamatsu Photonics). Signals were normalized to the F340/F380 measured prior to cell stimulation. Intracellular [Ca^{2+}] was also measured in cells loaded with the single wavelength Ca^{2+} dye Calbryte (43). Signals were normalized to the fluorescence intensity measured before the application of different stimuli.

Immunofluorescence and time-lapse microscopy

HMEC and MDA-MB-231-BrM2 cells were washed with PBS and fixed in 4% PFA for 20 min at 37ºC. Cells were then permeabilized with 0.5% Triton X-100 (Sigma) in PBS for 5 min and blocked in 5% BSA in PBS for 1 h at room temperature. Primary antibodies (Table S1) were incubated overnight at 4ºC diluted in 1% BSA in PBS 1x. Secondary antibodies (Table S1) were diluted in PBS containing 1% BSA and incubated 1 h at room temperature. For the identification and quantification of nuclei, cells were incubated 10 min with DAPI (Table S1) diluted in PBS containing 1% BSA. To visualize cell plasma membrane, a pretreatment of 20 min with concanavalin A (1:50; in ice-cooled PBS) was carried out before cell fixation. Coverslips were mounted with Fluoromount (0100-01, Southern Biotech) and cells were examined with a Leica TCS-SP8 confocal microscope with a 63× 1.40 immersion oil objective and using maximal microscope resolution (95x95 nm). For time-lapse experiments using GenEPI, transfected HMEC plated in 35-mm glass-bottom dishes were synchronized inG2/M with 100 nM nocodazole in complete culture

medium for 16-20h and released 2h prior to image acquisition. Experiments were performed 48h post-transfection in a Leica TCS-SP8 confocal microscope with a 40× 1.40 immersion oil objective, using a resonant scanner and a HyD detector. For time-length measurements during cell cycle, HMEC at 70-90% confluence were synchronized in G2/M with 100 nM Nocodazole (Sigma) in complete culture medium for 16-20h. Following release from synchronization cells were exposed to either vehicle or the indicated drugs and image acquisition was started. Cytokinesis start time and the abscission time were manually calculated from the videos obtained. A time-lapse series was acquired using a fully motorized Zeiss Cell Observer HS microscope, 10× objective. Temperature was controlled at 37º C using the built-in microscope incubator providing a humidified atmosphere with 5% CO2. Imaging was performed for 24 h with a lapse time of 10- or 15-min. ImageJ software was used for image processing and immunofluorescence quantification at the ICB and midbody (Plot Profile tool).

Co-immunoprecipitation and western blot

Co-immunoprecipitation assay was performed as previously described (22). In brief, cell extracts were obtained by incubation in 1% Triton X-100 lysis buffer supplemented with 10% of protease inhibitor cocktail (Thermo) for 30 min at 4ºC. Cell lysates were centrifuged at 10.000g 5 min 4ºC and the soluble fraction was incubated with equilibrated GFP-Trap beads (gta-20, ChromoTek) for 2h at 4ºC. Complexes were centrifuged and washed four times with PBS buffer, denatured with SDS-PAGE sample buffer (NP0007, Invitrogen) for 10 min at 70 ºC and separated by SDS-PAGE in Tris-acetate 3-8% precast gels (EA0375BOX, Invitrogen). The immunoprecipitated proteins were analyzed by western blotting and soluble fractions from cell

lysis were used as input. Membranes were blocked by 5% non-fat-dry milk in TTBS and incubated in the same blocking buffer with anti-Myc and anti-GFP (Table S1) overnight at 4ºC. Secondary antibodies peroxidase-conjugated anti-rabbit IgG or anti-mouse IgG were used at a 1:2000 dilution in blocking buffer and incubated for 1h at RT. Detection was performed using the enhanced chemiluminescence (ECL) detection kit (1705061, Clarity Biorad). For co-immunoprecipitation of endogenous proteins in HMEC, cell extracts were centrifuged at 14.000g at 4ºC for 10 min to remove aggregates. Solubilized proteins were incubated overnight with an anti-Piezo1 antibody. Immuno-complexes were then incubated with 50 µL of protein G beads for 2 hours at 4ºC.

RT-PCR and plasmids

Total RNA was isolated from cells using NucleoSpin RNA isolation kit (740955, Macherey-Nagel) or NZY Total RNA Isolation kit (MB13402, NZYTech). SuperScript III reverse transcriptase system (18080044, Thermo) was used for cDNA synthesis. Quantitative real-time PCR was performed using SYBR Green (4367659, Applied Biosystems) in a QuantStudio 12K Flex system (Applied Biosystems) with the specific human primers shown in Table S1. GAPDH was used as a housekeeping gene for the quantification of relative gene expression using $2^{-\Delta\Delta Ct}$.

FIP3 Asp residues in EF-1 (D215/D217/D219) and EF-2 (D247) coordinating Ca2+ binding were mutated to Ala (FIP3-4DA) on the pEGFP-C1-FIP3 plasmid. Mutations were introduced by site-directed mutagenesis using the QuikChange kit (Stratagene). The primers used for mutagenesis are shown in Table S1.

Statistical analysis

All data are represented as mean ± S.E.M. Statistics and graphics were performed using GraphPad Prism. Prior to check statistical significance, a Shapiro-Wilk omnibus normality test was applied in all cases. For the data that followed normal distributions, a Student's unpaired t test was applied between two groups and one-way analysis of variance (ANOVA) followed by Bonferroni or Dunnett post hoc tests across multiple groups. For the data that did not assume Gaussian distributions, a Mann–Whitney's U test was used for comparing two groups, while Kruskal–Wallis followed by Dunn's post hoc test was applied for multiple groups. Significant difference was considered when a final value of $P < 0.05$ was reached (*). Values of $P<0.01$** and $P<0.001$***.

Fig. S1

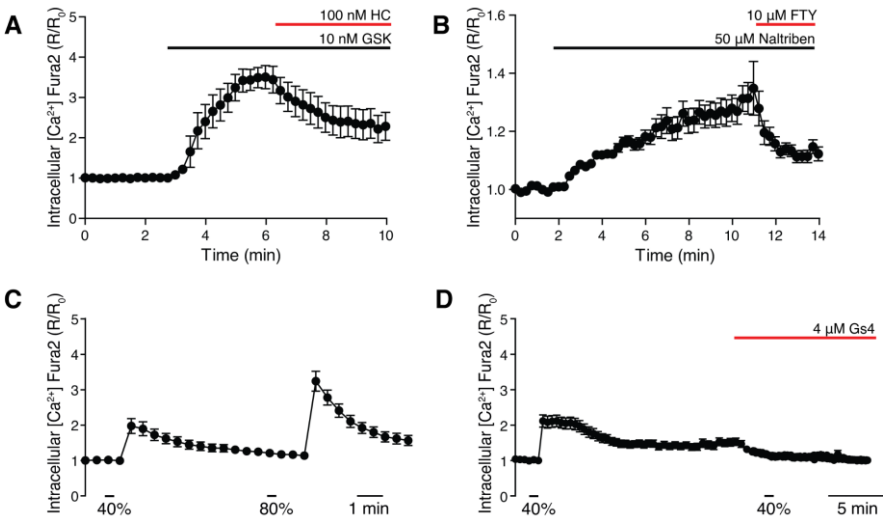

Fig. S1. Functional characterization of mechanosensitive ion channels in HMEC. (A) Changes in intracellular [Ca2+] (indicated by normalized fura-2 ratios) in HMEC after perfusion with the TRPV4 activator GSK1016790A follow by addition of the inhibitor HC067047 at the indicated concentrations (N=26). (B) Changes in intracellular [Ca2+] in HMEC after perfusion with the TRPM7 activator naltriben follow by addition of the inhibitor FTY720 at the indicated concentrations (N=29). (C) Changes in intracellular [Ca2+] in HMEC after application of two consecutive uniaxial stretching pulses of 40% and 80% of the initial chamber length (N=55). (D) Changes in intracellular [Ca2+] in HMEC after application of two consecutive uniaxial stretching pulses, the second after addition of 4 M GsMTx4 (N=38). Traces are means ± SEM.

Fig. S2

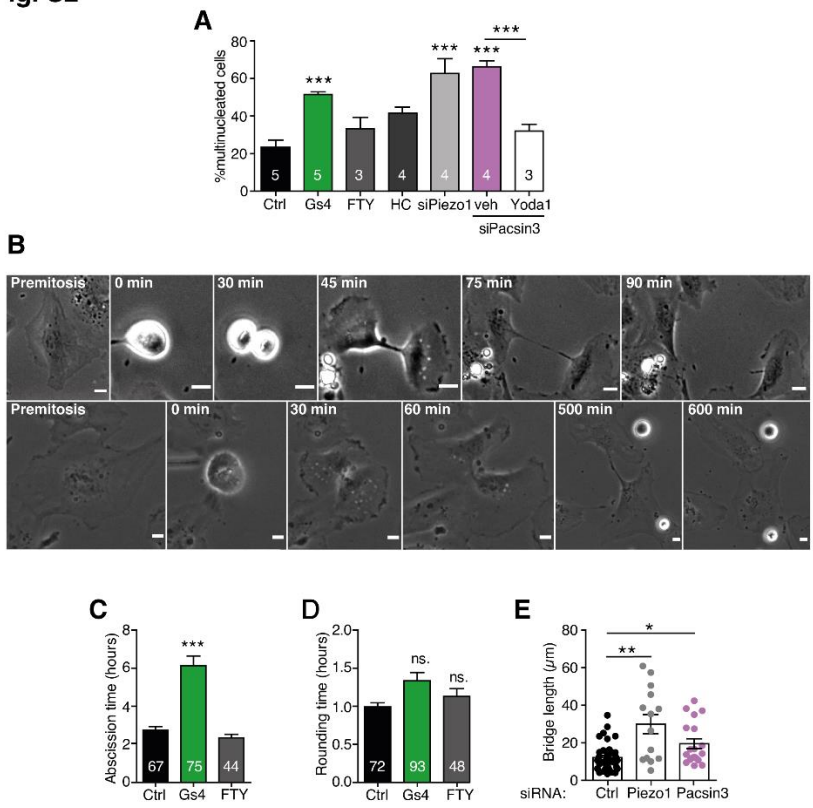

Fig. S2. Quantitative analysis of cytokinesis. (A) Multinucleation of HMEC transfected with the indicated siRNAs and/or treated with the Piezo1 inhibitor (GsMTx4, 1 M), TRPV4 inhibitor (HC067047, 100 nM) or TRPM7 inhibitor (FTY720, 1 M). Per sample, >30 cells were monitored for ≥ 2 nuclei (multinucleation). (B) Selected frames from time-lapse videos of HMEC exposed to vehicle (top) of GsMTx4 (bottom). (C) Quantification of abscission time, defined as the time from rounding (time=0) to the generation of two independent daughter cells. (D) Quantification of the time to enter mitosis (rounding time) following release from synchronization. At the time cell round up time is set to t=0. Bars represent mean ± S.E.M. of the number of cells indicated in each bar. (E) Quantification of the length of the ICB in HMEC transfected with control siRNA, siPiezo1 or siPacsin3. Statistical significance versus control was determined using Kruskal-Wallis followed by Dunn's post hoc (C,D,E) or ANOVA followed by Bonferroni's post hoc test (A). Scale bar, 15 μm.

Fig. S3

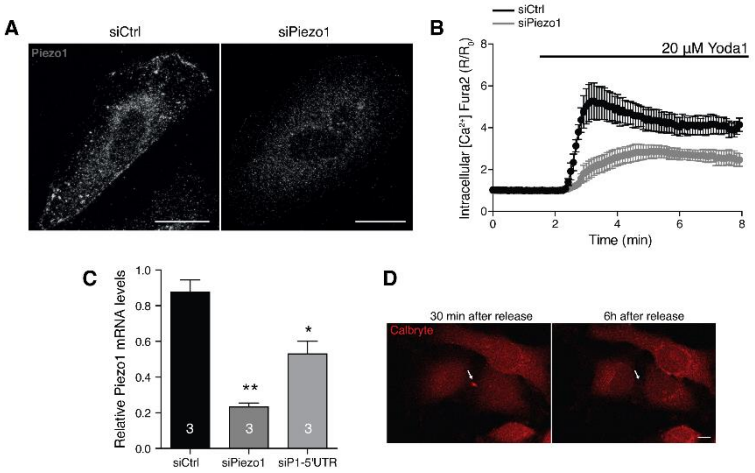

Fig. S3. Piezo1 expression and activity in HMEC. (A) Immunofluorescence confocal microscopy images of Piezo1 in HMEC. Note the strong reinforcement of Piezo1 signal at the cell boundary of control siRNA transfected cells and the absence of Piezo1 signal at the cell boundary in siPiezo1 transfected HMEC. Bar=10 μm. (B) Changes in intracellular [Ca2+] in HMEC transfected with siControl or siPiezo1 and exposed to the Piezo1 activator Yoda1 (20 M). Note the marked reduction in the response of siPiezo1 transfected cells. Data are mean ± S.E.M. of 43 siControl and 38 siPiezo1 transfected cells. (C) Quantitative real-time PCR of Piezo1 expression in siControl, siPiezo1 and siPiezo1 5'UTR in HMEC cells (n = 3). (D) Images of HeLa cells loaded with the Ca2+ indicator, CalbryteTM 630, taken at two different times after release from synchronization. Note the strong Calbryte signal at the intercellular bridge 30 min after release from synchronization. Scale bar, 10 μm.

Fig. S4

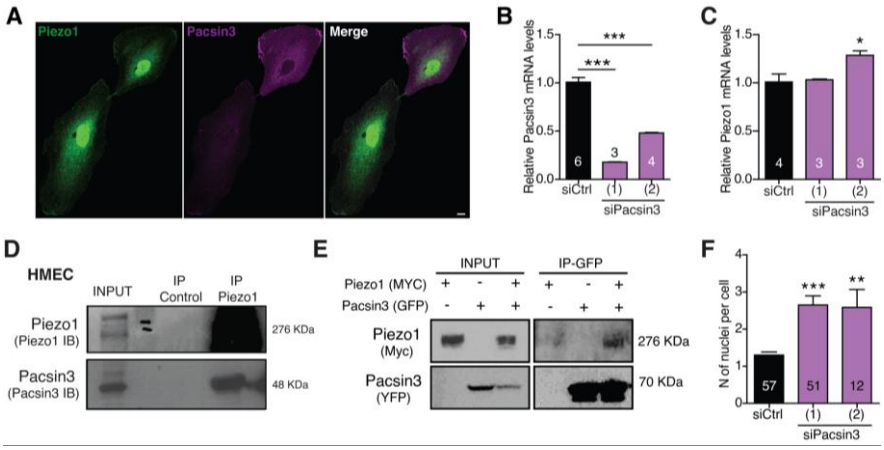

Fig. S4. Pacsin 3 interaction with Piezo1. (A) Colocalization of Pacsin3-CFP and endogenous Piezo1 in HMEC during mitosis. Note the clear presence of both Piezo1 and Pcsin3 at the intercellular bridge. Bar=5 μm. (B) Quantitative PCR measurements of Pacsin3 mRNA transcript levels in HMEC transfected with siControl or two different siPacsin3. (C) Quantitative real-time PCR measurements of Piezo1 mRNA transcript levels in HMEC transfected with siControl or two different siPacsin3. (D) Co-immunoprecipitation of endogenous Piezo1 and Pacsin3 in HMEC. (E) Co-immunoprecipitaion of Piezo1-myc and Pacsin3-CFP expressed in HEK293 cells. (F) Number of nuclei/cell counted in HMEC exposed to two different siRNAs generated against Pacsin3 (as shown in panel B). Mean ± S.E.M. of the number of cells (or replicas) indicated in each bar. Statistical significance was determined using an ANOVA followed by Dunnett's post hoc test (B,C) or Kruskal-Wallis followed by Dunn's post hoc (F).

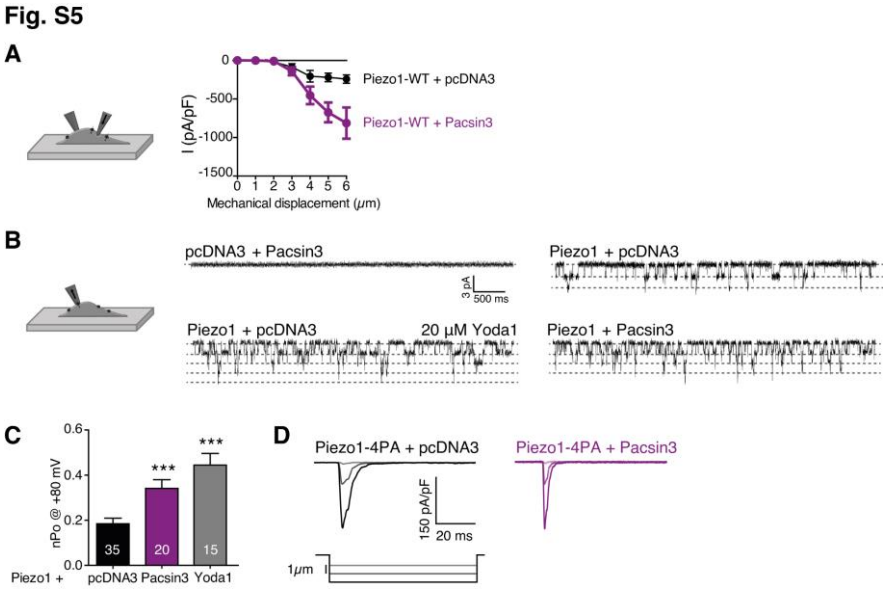

Fig. S5. Electrophysiological recordings of Piezo1 activity. (A) Peak current density of whole-cell current recordings of Piezo1 channels heterologously expressed in HEK293 cells with or without the coexpression of Pacsin3. Cells were mechanically stimulated with a blunt pipette under the control of a piezoelectric actuator in steps of 1 μm (Inset illustration). Mean ± S.E.M. of 18 cells transfected with Piezo1 and 15 cells transfected with Piezo1 plus Pacsin3. (B) Cell attached recordings obtained from HEK293 cells transfected with the indicated plasmids and exposed to a negative pressure pulses of -8 mm Hg for 10 sec (Inset illustration). Recordings were carried out immediately after removal of the pressure pulse and in the presence of the Piezo1 activator Yoda1 (bottom left). Note the absence of channel activity in the membrane patch obtained from HEK293 cells expressing Pacsin3 alone. (C) Mean open probability (NPo) calculated from cell-attach patches (as shown in B). Mean ± S.E.M. of NPo obtained from the number of patches indicated in each bar. Kruskal-Wallis followed by Dunn's post hoc. (D) Whole-cell recordings obtained from HEK293 cells transfected with Piezo1-WT or Piezo1-4PA expressed alone or co-expressed with Pacsin3 following stimulation with a series of mechanical steps of 1 μm.

Fig. S6

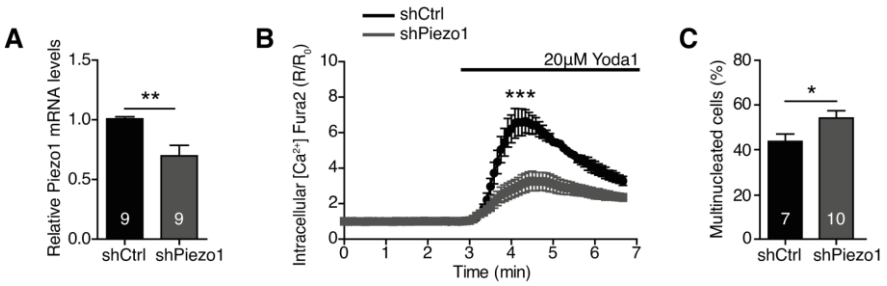

Fig. S6. Piezo1 knockdown induces multinucleation in breast cancer cells. (A) Quantitative real-time PCR of Piezo1 expression in shControl and shPiezo1 MDA-MB-231-BrM2 cells (n = 4). (B) Changes in intracellular [Ca2+] in shControl and shPiezo1 MDA-MB-231-BrM2 cells exposed to Yoda1 (20 M). Note the marked reduction in the response of shPiezo1 transfected cells. Data are means ± S.E.M. of N=4 shControl and N=4 shPiezo1 samples. Per sample, >20 cells were monitored. (C) Multinucleation of shControl and shPiezo1 MDA-MB-231-BrM2 cells. Per sample, >30 cells were monitored for ≥ 2 nuclei (multinucleation). Statistical significance was determined using a Student's unpaired t test.

Fig. S7

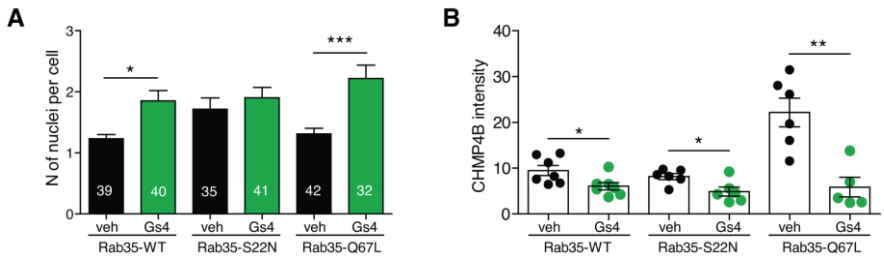

Fig. S7. Role of Rab small GTPases on Piezo1-mediated multinucleation and CHAMP4B localization. (A) Number of nuclei/cell counted in HMEC overexpressing Rab35-WT, Rab35-S22N or Rab35-Q67L in the presence or absence of GsMTx4. (B) Quantification of CHMP4B intensity at the ICB in HMEC under the conditions shown. Data are means ± S.E.M. Number of replicas indicated in each graph. Significance values versus control condition as determined by Kruskal-Wallis followed by Dunn's post hoc (A) or ANOVA followed by Bonferroni's post hoc test (B).

Fig. S8

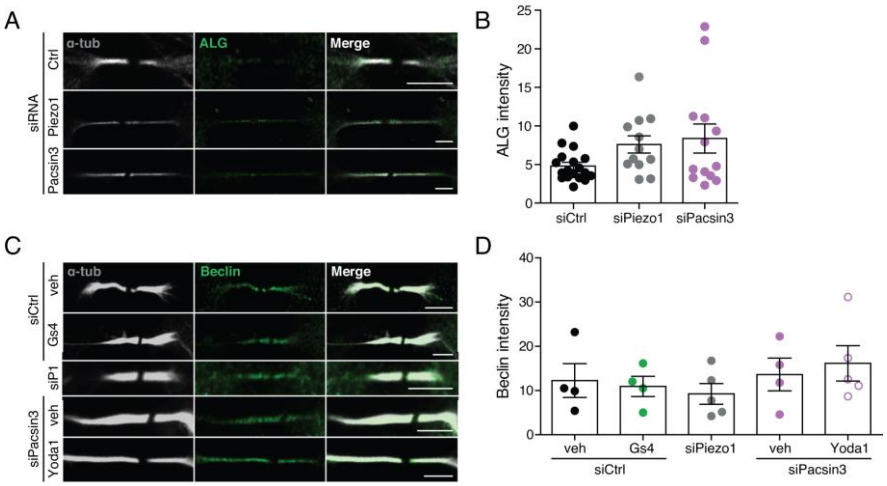

Fig. S8. Localization of ALG-2 and Beclin-1. Localization (A) and quantification (B) of ALG-2 signal at the ICB of HMEC under the conditions shown. Localization (C) and quantification (D) of Beclin-1 signal at the ICB of HMEC under the conditions shown. Data are means ± S.E.M. Number of replicas indicated in each graph. None of the conditions tested were significantly different to the siControl vehicle condition as determined by Kruskal-Wallis followed by Dunn's post hoc (B) or ANOVA followed by Dunnett's post hoc test (D). Scale bar, 5 μm.

Fig. S9

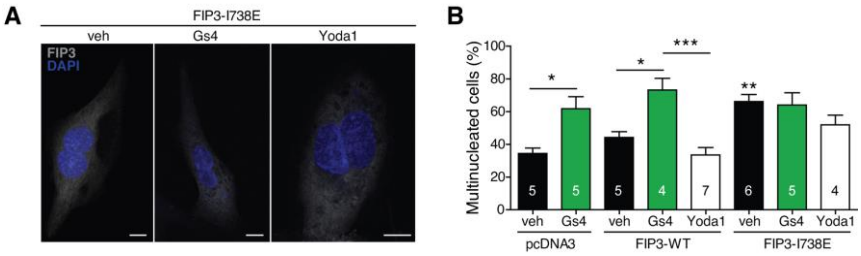

Fig. S9. Effect of FIP3 on HMEC multinucleation. (A) DAPI staining of the nuclei in HMEC overexpressing FIP3-I738E in the presence and absence of GsMTx4 or Yoda1. Bar= 10 μm. (B) Multinucleation of HMEC overexpressing pcDNA3, FIP3-WT or FIP3-I738E in the presence or absence of GsMTx4 or Yoda1. Data are means ± S.E.M. Number of replicas indicated in each graph. Significance values are versus pcDNA3 vehicle condition as determined by ANOVA and Bonferroni's post hoc test.

Table S1.

Drugs, antibodies, oligonucleotides, and plasmids used in this work

DRUG	SUPPLIER	TARGET	[µM]	INCUBATION	VEHICLE
GsMTx4	Alomone	Blocks Piezo1	4 1	Acute, Ca^{2+} imaging; 2h preincubation, time lapse/IF	H_2O
Yoda1	Tocris	Activates Piezo1	20 5	Acute, Ca^{2+} imaging; 2h preincubation, time lapse/IF	DMSO
HC067047	Tocris	Blocks TRPV4	0.1 0.01	Acute, Ca^{2+} imaging; 2h preincubation, time lapse/IF	DMSO
GSK1016790A	Sigma-Aldrich	Activates TRPV4	0.01	Acute, Ca^{2+} imaging;	DMSO
BAPTA-AM	Calbiochem	Ca^{2+} chelator	1	2h preincubation, time lapse/IF	DMSO
FTY720	Sigma-Aldrich	Blocks TRPM7	10 1	Acute, Ca^{2+} imaging; 2h preincubation, time lapse/IF	DMSO

Naltriben	Sigma-Aldrich	Activates TRPM7	50	Acute, Ca^{2+} imaging;	DMSO
Fura-2-AM	Life Technologies	Ratiometric Ca^{2+} indicator dye	4.5	30 min preincubation	DMSO
Calbryte^{TM} 630 AM red	Deltaclon	Ca^{2+} indicator dye	5	30 min preincubation	DMSO
DAPI	Thermo	DNA, nuclear staining		1:1000; 10 min preincubation	1% BSA in PBS
Fluoromount G	Southern Biotech	Storage of slide preparations	NA	NA	H_2O

ANTIBODIES		**REFERENCES**	**CONCENTRATION**
Rabbit polyclonal anti-Piezo1	Novus Biologicals	NBP1-78446	1:350 (1% BSA) for IF; 1:1000 for WB
Rabbit polyclonal. anti-ALG-2 (aka PDCD6)	Protein Tech	12303-1-AP	1:500 (1% BSA)
Rabbit polyclonal anti-CHMP4B	Sigma-Aldrich	HPA041401	1:300 (1% BSA)

Mouse Monoclonal Anti-αTubulin	Sigma-Aldrich	T6793	1:500 (1% BSA)
Mouse monoclonal anti-Pacsin3	Santa Cruz	sc-166923	1:1000 (1% BSA); 1:1000 (5% milk) for CoIP and WB
Goat anti-rabbit IgG AlexaFluor 647	Thermo-Fisher	A-21244	1:1000 (1% BSA)
Goat anti-mouse IgG AlexaFluor 555	ThermoFisher	A-21424	1:1000 (1% BSA)
Mouse monoclonal anti-α-Myc	Sigma-Aldrich	M4439	1:1000 (1% BSA) 1:1000 (5% milk) for CoIP and WB
Anti-GFP	Clontech	632380	1:1000 (5% milk)
Peroxidase-conjugated anti-rabbit IgG	GE Health-care	NA934	1:2000 (5% milk) 1:1000 (5% milk) for CoIP and WB
Secondary anti-mouse HRP	GE Health-care	NXA931	1:2000 (5% milk)
Rabbit polyclonal anti-ALIX	Cell signaling	992880	1:350 (1% BSA)
Rabbit polyclonal anti-Cep55	GeneTex	GTX112190	1:350 (1% BSA)
Rabbit polyclonal anti-Rab11	Abcam	ab3612	1:350 (1% BSA)
Rabbit polyclonal anti-FIP3	Sigma-Aldrich	HPA028631	1:350 (1% BSA)
Rabbit polyclonal anti-Beclin1	Abcam	ab62557	1:350 (1% BSA)

PLASMIDS	SUPPLIER	REFERENCE
Human Piezo1- pIres-GFP		Provided by Dr. Frederick Sachs (University of Buffalo, USA) (*8*)
Human Piezo1-P1578A/P1580A/P1584A/P1587A-Ires-GFP	Biomatik	
hPiezo1-WT-myc-IRES-GFP	Biomatik	
GenEPI		Dr. Periklis Pantazis, Imperial College London.
pcDNA3-Pacsin3-CFP	Own plasmid	Generated based on pcDNA3-myc-Pacsin3 provided by Markus Ploman (University of Cologne, Germany)
pCDNA3-Pacsin3-YFP	Own plasmid	Generated based on pcDNA3-myc-Pacsin3 provided by Markus Ploman (University of Cologne, Germany)
Rab11-WT-GFP	Addgene 12674	Dr. Ricardo Pagano (Mayo Clinic, Rochester, USA)
Rab11-Q70L-GFP	Addgene 49553	Dr. Marci Scidmore (University of Texas, USA)
Rab11-S25N-GFP	Addgene 12678	Dr. Ricardo Pagano (Mayo Clinic, Rochester, USA)
FIP3-GFP		Mary McCaffrey (University College Cork, Ireland)
FIP3-I738E-GFP		Mary McCaffrey (University College Cork, Ireland)
FIP3-4DA-GFP	Own plasmid	

EGFP-Rab35	Addgene 49552	Dr. Marci Scidmore (University of Texas, USA)
EGFP-Rab35- Q67L	Addgene 49612	Dr. Marci Scidmore (University of Texas, USA)
EGFP-Rab35-S22N	Addgene 49613	Dr. Marci Scidmore (University of Texas, USA)
mCherry-α-Tubulin	Addgene 49149	Dr. Michael W Davison (Florida State University, USA)

MOLECULAR BIOLOGY TOOLS	**SUPPLIER**	**TARGET SEQUENCE (5' to 3')**
Control siRNA	Thermo Scientific	AATTCTCCGAACGTGTCACGT
Piezo1 siRNA	Thermo scientific GENOME Human PIEZO1 (9780)	UCGCGGUGGUCGUCAAGUA
Piezo1 5'UTR siRNA	Horizon	CGAAGGAGAAGGAGGAAGA
Pacsin3 siRNA-1	Qiagen Pacsin3-6	CAGAGGACCATCAGCCGGCAAA
Pacsin3 siRNA-2	Dharmacon	GGACAUGGAACAGGCCUUU
PLKO.1-shRNA scramble	Dharmacon	Sense: TCCTAAGGTTAAGTTAAGTCGCCCTCG; Antisense: CGAGGGCGACTTAACCTTAGG

PLKO.1-shRNA-Piezo1	Dharmacon	Sense: ATGATTGTACTTCTTGGTGAG; Antisense: CTCACCAAGAAGTACAATCAT
Cep55 siRNA	Dharmacon	GTCCCAAGTGCAATATACAGTAT
OLIGONUCLEOTIDES	**SEQUENCE (5' to 3')**	
pEGFP-C1-FIP3-D215A/D217A/D219A/D247A (FIP3-4DA) Mutagenesis primers	Mutg1_Forward: GTCCGCATCGAGG**C**CTTCATCCAGTTTGC; Mutg1_Reverse: GCAAACTGGATGAAGGCCTCGATGCGGAC Mutg2_Forward: CTTAACTAAGTACTTGGCTCCCAGTGGGCTC Mutg2_Reverse: GAGCCCACTGGGAGCCAAGTACTTAGTTAAG	
Piezo1 SYBR green-based real time RT-PCR	Forward: TTCCTGCTGTACCAGTACCT Reverse: AGGTACAGCCACTTGATGAG	
Pacsin3 SYBR green-based real time RT-PCR	Forward: GGACCTGGTCAGCTGCTTC Reverse: GCCTTCTCCAGTGTGCCATA	
GAPDH SYBR green-based real time RT-PCR	Forward: CTCCTGCACCACCAACTGCT Reverse: GGGCCATCCACAGTCTTCTG	

41. M. Valiente, A. C. Obenauf, X. Jin, Q. Chen, X. H.-F. Zhang, D. J. Lee, J. E. Chaft, M. G. Kris, J. T. Huse, E. Brogi, J. Massagué, Serpins promote cancer cell survival and vascular co-option in brain metastasis. Cell. 156, 1002–16 (2014).

42. R. Syeda, J. Xu, A. E. Dubin, B. Coste, J. Mathur, T. Huynh, J. Matzen, J. Lao, D. C. Tully, I. H. Engels, H. M. Petrassi, A. M. Schumacher, M. Montal, M. Bandell, A. Patapoutian, Chemical activation of the mechanotransduction channel Piezo1. Elife. 4, e07369 (2015).

43. V. Venturini, F. Pezzano, F. C. Castro, H. M. Häkkinen, S. Jiménez-Delgado, M. Colomer-Rosell, M. Marro, Q. Tolosa-Ramon, S. Paz-López, M. A. Valverde, J. Weghuber, P. Loza-Alvarez, M. Krieg, S. Wieser, V. Ruprecht, The nucleus measures shape changes for cellular proprioception to control dynamic cell behavior. Science (80-.). 370 (2020), doi:10.1126/science.aba2644.

44. Bae, R. Gnanasambandam, C. Nicolai, F. Sachs, P. A. Gottlieb, Xerocytosis is caused by mutations that alter the kinetics of the mechanosensitive channel PIEZO1. Proc.Natl.Acad.Sci.U.S.A. 110, E1162–E1168 (2013).

5. Discussion

4.1 Concave BAR proteins Pacsin3 and Amphiphysin increase Piezo1 mechanical response

Since its discovery, Piezo1 response to membrane mechanics has been vastly studied revealing miscellaneous modes of activation. A large part of these studies was mainly focused on exploring how external mechano/osmotic forces modulate the response of the channel. Now we know that Piezo1 can be activated by virtually all types of physical inputs, including tension, compression, and shear stress. All these forces generate the same type of response: the instantaneous opening of the channel, followed by its inactivation and deactivation. Recently, the regulatory effect of force-transducing elements within the cell, such as the cytoskeleton, the ECM, or lipids, begins to be understood. Researchers have found that these elements mainly regulate Piezo1 mechanical sensitivity or inactivation. However, little is still known about the impact of surface binding proteins able to sense and modulate local membrane curvature on the mechanical response of the channel.

Here, we present a comprehensive study of the Pìezo1 channel employing different modes of mechanical stimulation (indentation, suction, and stretching) in order to investigate the effect of a group of membrane-shaping proteins: the BAR domain-containing proteins. To this end, Pacsin3 (F-BAR), Amphiphysin (N-BAR), and IRSp53 (I-BAR) were individually overexpressed in HEK293 cells together with Piezo1.

We have demonstrated that the F-BAR protein Pacsin3, can increase Piezo1 mechanotransduction by impairing the inactivated state of the channel. In consequence, the channel stays longer times in the open conformation, as reflected in the increase in Piezo1 open probability from cell-attached patch-clamp experiments of cells stimulated by suction.

These results shared a certain degree of similarity to the Yoda1 treatment, which also affects Piezo1 inactivation and open probability. This induced a more prolonged and marked intracellular Ca^{2+} load as shown in Ca^{2+} imaging experiments with cells stimulated by uniaxial stretching. Besides, the recovery from inactivation of Piezo1 currents was much faster when co-overexpressed with Pacsin3 in cell-attached patches stimulated by negative pressure. Therefore, the interplay of Pacsin3 and Piezo1 endow the cell with improved mechanotransduction and an upgraded ability to increase the frequency filtering of repetitive stimuli.

A large part of the modulation of Piezo1 kinetics by Pacsin3 was shared by Amphiphysin, another concave protein with an N-BAR domain. However, the IRSp53 protein, with a convex I-BAR domain, displayed no effects on Piezo1 currents under our experimental conditions. One may ask whether the type of BAR protein curvature determines channel regulation. Piezo1 is both activated by concave and convex cell-scale mechanically inflicted deformation (Lewis & Grandl, 2015). It is important to note that, as positive or negative pressure is applied to the cell, global curvature increases in the sense of force but, in both cases, regions of local curvature within the wrinkled cell surface end up being flattened (Bavi et al., 2016). This is an important mechanism to buffer small membrane tensions applied to resting membranes providing a certain degree of mechanoprotection to the cell. As the Piezo1 structure generates local curvature itself, when enough tension is applied, its surrounding membrane flattens pulling and gating the channel. Thus, under pressure, global curvature increase and local flattening of the membrane are responsible for Piezo1 activation. Interestingly, the type of concave membrane bending produced by the Piezo1 structure is likely to match with Pacsin3 and Amphiphysin shape, but not with that of IRSp53. This might hamper I-BAR to sense Piezo1 surrounding curvature. The importance of BAR shape preservation is

suggested by our Pacsin3 mutant lacking the F-BAR domain, which completely lost its ability to modulate Piezo1 current kinetics. However, so far we can not exclude the possibility that accessory domains present in BAR proteins are the real determinants of discrepancies on Piezo1 modulation among BAR types. In future experiments, Pacsin3-IRSp53 chimeras will better assess the importance of the BAR domain shape in the context of Piezo1 regulation.

Besides being directly gated by bilayer tension, the mechanical stimulation of Piezo1 can be modified by linkages to the extracellular matrix or to cytoskeletal proteins. Among the different patch-clamp configurations and Ca^{2+} measures, the influence of these force-transducing components varies (Cox et al., 2016; Gaub & Müller, 2017). We observed that cells cultured in a coating of collagen displayed a prolonged activation time under Pacsin3 both stretching the whole matrix underneath the adherent cell or applying local suction to membrane patches from the non-adhered above part of the cell. Also, electrophysiological experiments performed in inside-out patch-clamp configuration indicate that the cytoskeleton was not determining Piezo1 modulation by Pacsin3, as we obtained the same 2-fold increase in the time constant of inactivation as in whole-cell and cell-attached measures. Although more experimentation is needed in this respect, these results suggest that Pacsin3 can regulate the response of Piezo1 to mechanical stimulation operating independently from these cellular force-transducers.

A dysfunctional inactivation is the major hallmark of many Piezo1-related diseases (Fig. 1C). This is often associated with gain-of-function mutations critical for the proper operation of several organs, such as the vascular system. However, from a physiological point of view, the regulation of Piezo1 inactivation by internal cell pathways may represent an important tool for the local control of the mechanical response.

4.2 The SH3 of Pacsin3 and a proline-rich region of Piezo1 are essential for their interplay

Next, we have combined protein-protein interaction techniques, mutagenesis and *in silico* analysis with functional characterizations, to explore the mechanism of Piezo1 modulation by Pacsin3. As the SH3 is a domain that endows Pacsin3 with the ability to interact with other proteins, we examined Piezo1 as a possible new binding partner. In this respect, we have shown through coimmunoprecipitation and colocalization techniques with confocal microscopy that Pacsin3 has the ability to closely interact with Piezo1, either overexpressed in HEK293 cells or endogenously expressed in microendothelial HMEC cells. These results were supported by the P415L mutant of the SH3 domain of Pacsin3, which caused a complete loss of interaction and modulation of Piezo1. Amphiphysin and IRSp53 also contain SH3 domains, but only Amphiphysin seemed able to interact with Piezo1, returning to the question of the importance of BAR concavity.

The SH3 domain is an important interaction platform for proline-rich motif-containing proteins. We have identified a potential PRD within the structure of Piezo1 which seems responsible for its interaction with the SH3 domain of Pacsin3. The sequence prediction was supported by the electrophysiological characterization of the mutant Piezo1-4PA, which displayed whole-cell currents similar to the WT channel but was not affected by Pacsin3 regulation. This predicted PRD is located in a domain that Dr. Ward and collaborators called the “clasp” (Saotome et al., 2018) (Fig. 1). This region is one of the few that has not yet been structurally determined, suggesting the clasp as a dynamic part of the protein difficult to crystallize. Flexibility is a requirement for regions implicated in channel inactivation as it is a process that tends to demand rapid conformational

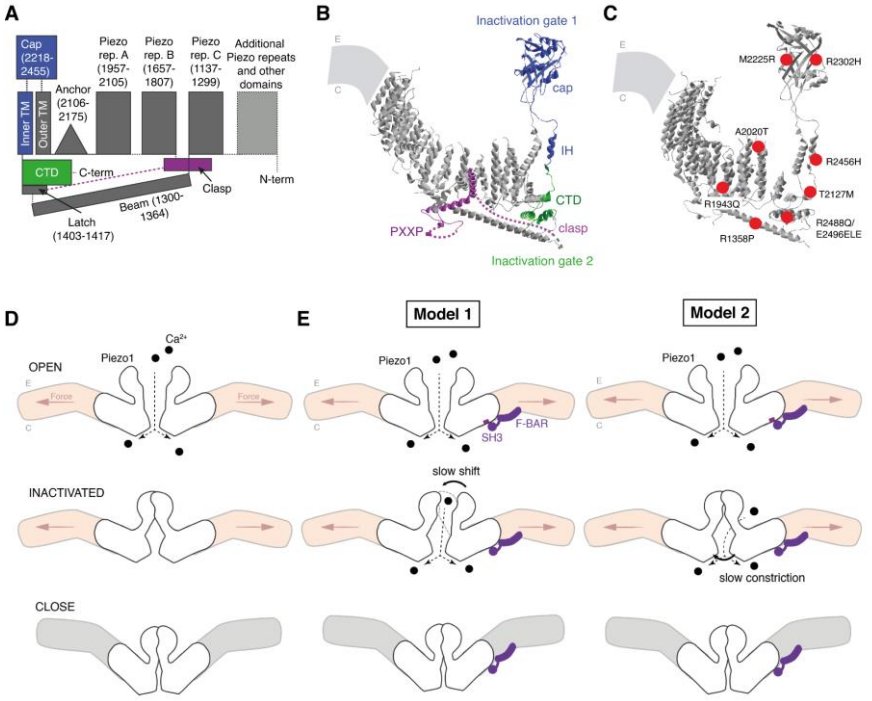

Fig. 1. **Piezo1 inactivation and its hypothetical regulation by Pacsin3 binding.** (A) Structural arrangement of Piezo1 core domains. Flexible regions not resolved are represented as dotted lines. Modified from (Saotome et al., 2018). (B) Cartoon representation of the two inactivation gates (blue, cap and IH; green, CTD) and the clasp (green). Dotted lines represent regions structurally unresolved. (C) Mapping disease-causing mutations in human PIEZO1. Red dots represent the disease-causing residues labeled in the figure. (D) Schematic representation of the three-state model (open, inactivated, and close) of Piezo1 in response to forces. Note the concave membrane curvature generated by the channel in resting condition (gray). (E) Proposed models of the influence of Pacsin3 (purple) binding in channel conformational changes from the open to the inactivated state. Model 1 represents an allosteric slowdown in motion of the inactivation gate 1 by Pacsin3 binding. Model 2 represents an allosteric modulation of the inactivation gate 2, restraining CTD mobility. Rectangular purple box represents the proline-rich region of Piezo1 suggested for Pacsin3 interaction. “E” extracellular, “C” cytoplasm.

changes. The clasp connects the blades directly to the CTD (Fig. 1 A,B). Point mutations in the latter region of the channel (M2493/F2494 and P2536/E2537) have shown to impair neck constriction enhancing by 1.5-2.7 fold the constant of inactivation of whole-cell Piezo1 currents stimulated by indentation (Zheng et al., 2019). These results are quite similar to Pacsin3 modulation, which might indicate a functional crosslink between the clasp and the CTD (Fig. 1B, D-E). Under this assumption, the intracellular clasp may represent an interesting binding region for regulatory proteins to reversibly modulate neck constriction at the CTD, increasing chemically and locally mechanotransduction.

Besides, researchers suggest that Piezo1 inactivation is also determined by another inactivation gate established by the cap-IH axis (Fig. 1B). Mutating residues from the pore-lining IH (L2475 and V2476) drastically prolong inactivation with an almost 10-fold increase in τ_{inact}, without altering channel sensitivity (Zheng et al., 2019). Also, the IH contains a lysine in 2479 responsible for voltage-dependent inactivation (Lewis & Grandl, 2020; Moroni et al., 2018; J. Wu et al., 2017). These studies suggest that the IH is directly coupled to the cap of the channel. Chimeric constructs exchanging Piezo1 and Piezo2 whole cap, or subdomains from the base of the cap, show drastic differences in current kinetics and voltage-dependence, inactivating similarly to the donor cap protein (Lewis & Grandl, 2020; J. Wu et al., 2017). Thus, Piezo1 inactivation seems determined by a primary gate within the cap and the IH dictating the majority of Piezo1 inactivation, and a secondary gate involving the CTD, which moderately controls Piezo1 inactivation (Fig. 1B). It is possible that Pacsin3 acts as an allosteric regulator of this cap-IH gate (Fig. 1E). However, the engagement of Pacsin3 in this primary inactivation gate appears unlikely, as one would expect a more pronounced effect on τ_{inact}.

It is important to consider that disease-causing Piezo1 mutations that slow inactivation kinetics are also found in the anchor, beam, and blades (Fig. 1C). This suggests that more regions of the channel are implicated in the process of inactivation by operating in one or both gates, or constituting themselves new inactivation gates. As two different modes of channel opening seem to coexist, one from the anticlockwise movement of the cap and the other from the clockwise movement of the blades, there is the possibility that the channel also undergoes two types of channel inactivation modes dictated by the same regions (Fig. 1E). Our present results can not discriminate whether the clasp causes structural rearrangements within one or both inactivation gates, or if it is implicated in a completely new inactivation mode. However, we present here a potential novel role for the clasp, a region whose relevance in channel function has been so far ignored.

Interestingly, the human Piezo2 structure has a unique insertion of a hundred amino acids located in its equivalent clasp structure, representing one of the most marked differences between both channel isoform sequences (Q. Zhao et al., 2018). Given that the major functional discrepancy between Piezo1 and Piezo2 is related to their inactivation, the clasp could be an important structural element dictating their distinctive cellular roles.

We must also note that as in the case of STOML3, which binds to cholesterol stiffening the membrane and sensitizing the mechanical response of Piezo1, BAR proteins could also affect membrane parameters, such as thickness or stiffness, explaining part or the whole of the effect on channel kinetics. BAR proteins act as a mold, forcing lipids to adopt a specific conformation. This could decrease the fluidity of the membrane surrounding Piezo1. A certain level of membrane fluidity may be required for the rapid transition of Piezo1 from the open to the inactivated state. Therefore, we can not exclude that Pacsin3 binding to Piezo1 changes

surrounding lipid architecture explaining channel modulation, instead of producing a direct conformational change on Piezo1 structure.

Deepening into membrane mechanics, the curvature generated by the arc-shaped arms of Piezo1 acts as the channel mechanosensitive modulus (Guo & MacKinnon, 2017). However, Pacsin3 did not affect Piezo1 sensitivity to mechanical stimuli, suggesting that it works alone sensing Piezo1 surrounding lipid shape, rather than clustering to induce curvature changes. Besides, mechanical forces have been shown to increase the binding of BAR proteins to the membrane but inhibit BAR oligomerization (Shi & Baumgart, 2015; Simunovic & Voth, 2015). Thus, Pacsin3 is unlikely to induce large curvature changes when bound to the Piezo1 channel.

The latter could explain why under Pacsin3 overexpression we have not observed a reduction in Piezo1 membrane localization as a result of channel endocytosis. By contrast, Pacsin3-Piezo1 interaction seems important to localize Piezo1 to specific PM regions. This was inferred by the depletion of Pacsin3 with specific siRNAs, which caused a reduction in the staining of the endogenously expressed Piezo1 in the PM of HMEC. This reduction was not only observed in the overall PM but also in specific regions such as the ICB connecting dividing cells, where we have demonstrated that both proteins colocalize. Also, patch-clamp experiments showed a decrease in the current density of Piezo1 in HEK293 cells under Pacsin3 RNA silencing. These results relate Pacsin3 to Piezo1 localization, similarly to its effect on TRPV4, whose localization is reinforced through its interaction with the SH3 domain of Pacsin3 (Cuajungco et al., 2006). However, Pacsin3 inhibits TRPV4 mechanotransduction by altering channel gating, while enhancing that of Piezo1. This might represent an important mechanism during membrane shape changes for the selection of MSCs for a concrete physiological task.

Thus, we have demonstrated that Pacsin3 binds to Piezo1 contributing to its PM localization and impairing channel inactivation. Whether the latter effect is determined by conformational impediments, membrane mechanic changes, or a combination, stills an interesting open question. Deepening our understanding of this relationship could enlighten the mechanism of some physiological processes.

4.3 Piezo1 and Pacsin3 participate in conjunction to regulate cytokinesis

During cytokinesis, the inward pinching of the membrane makes the ICB a region of high tension and deformability optimal for concave BAR domain binding and MSC activation. Besides, this process is accompanied by a transient increase in cytosolic Ca^{2+} concentration (Sarah E. Webb et al., 2008; Sarah E. Webb & Miller, 2017; Wong et al., 2005). However, the specific triggers and the role of this Ca^{2+} transient for the proper separation of the 2 daughter cells are still not well understood. We hypothesized that Pacsin3/Piezo1 interplay may be involved in sensing forces generated in the midbody, inducing a Ca^{2+} signaling necessary for the correct function of the abscission machinery. To address this theory, we study the process of cytokinesis mostly with a microendothelial HMEC cell line, but also in HELA cells, fibroblasts, and MDA-MB-231-BrM2 cells, performing mutagenesis experiments, knockdown strategies, drug treatments, and confocal microscopy to understand the contribution of these molecules in the completion of cell division.

According to the above-cited studies, we have observed that chelating Ca^{2+} with BAPTA-AM induced an increase in multinucleation in HMEC cells. Besides, the fluorescent Ca^{2+} indicator Calbryte displayed a strong

concentration of the signal at the ICB of HELA cells. This signal reinforcement was observed until the end of abscission. Our results are consistent with previous observations, which demonstrate that Ca^{2+} signaling is spatially and temporally correlated with the course of cytokinesis (Chang & Meng, 1995; X. Liu et al., 2011; S. E. Webb et al., 1997). Researchers conducted these studies in distinct somatic and germ eukaryotic cells, providing evidence of the extensive nature of this process. Most of these studies argue that the Ca^{2+} signal is released from internal stores, as blockers of the $InsP_3$ receptor in the endoplasmic reticulum impede cytokinesis (Chang & Meng, 1995; K. W. Lee et al., 2006). However, we must note that internal stores tend to be excellent amplifiers of responses originated in the PM. Thus, we proposed MSCs as sensors of cytokinetic forces upstream of this intra-store Ca^{2+} release.

Our candidates among MSCs were Piezo1, TRPV4, and TRPM7. The reason was their recent implication in cell cycle progression in mammalian cells (Gudipaty et al., 2017; Han et al., 2019; Nam et al., 2019; Yee et al., 2011). Therefore, we tested its activity in HMEC by Ca^{2+} imaging experiments, measuring its response to different drug agonists (Yoda1, GSK, and Naltriben) and antagonists (GsMTx4, HC, and FTY). We concluded that HMEC cells are endowed with functional Piezo1, TRPV4, and TRPM7. To study the engagement of these MSCs in cell division, we selectively blocked these channels with their respective antagonists concluding that only GsMTx4, the inhibitor of Piezo1 mechanotransduction, induced significant multinucleation, in addition to an almost 3-fold delay in the abscission time and elongated ICBs. All these features are characteristic signs of impaired abscission, revealing the importance of Piezo1 function during daughter cell separation. Besides, similar results were observed in fibroblasts and MDA-MB-231-BrM2 cells, where the knockdown of channel expression enhanced multinucleation.

Thus, Piezo1 implication in cytokinesis seems a process shared by different cell types. Among the mentioned MSCs, only Piezo1 has so far been related to cell division in normal tissues. In this regard, Rosenblatt's group has discovered that Piezo1 activation by mechanical stretching triggers rapid epithelial cell division (Gudipaty et al., 2017). They demonstrated that transient knockdown of *PIEZO1* or pharmacological inhibition with gadolinium, a non-specific MSC inhibitor, prevented Ca^{2+}-dependent phosphorylation of ERK1/2 and the successive accumulation of cyclin B during stretch-dependent cell division. They also observed a lower proliferation in unstretched control cells under Piezo1 depletion. The latter might be due to a similar reduction in cyclin B or to additional roles of the channel in cell division. Our results fit this second scenario in which Piezo1 is engaged beyond the mitotic entry, with a novel function in cytokinesis.

To delve into this finding, we investigated the importance of Piezo1 Ca^{2+} activity and localization during cell division. We overexpressed in HMEC the plasmid GenEPI consisting of a genetically encoded Ca^{2+}-indicator (GCaMP) fused to the C-terminus of Piezo1 (Yaganoglu et al., 2019). We observed a specific Piezo1-mediated Ca^{2+} increase in the midbody of dividing cells, extended until the end of cytokinesis. Also, confocal microscopy showed strong staining of the endogenous Piezo1 channel along the ICB of HMEC cells, compared to the rest of the PM. Previously, we have demonstrated that Piezo1 localization to the PM is mediated by Pacsin3 in interphase cells. In addition, some BAR proteins have shown to sense membrane curvature at the ICB, recruiting cytokinetic proteins (Martín-García et al., 2018; C. M. Smith & Chircop, 2012; Snider et al., 2020). Hence, we investigated whether Pacsin3 was mediating Piezo1 localization at the ICB. We observed that both proteins were strongly colocalized in this region. Genetically inhibition of Pacsin3 caused a reduction of Piezo1 staining in the midbody without impairing channel

expression, as well as multinucleation, and longer ICBs. Besides, blocking Piezo1 with GsMTx4 did not exacerbate the multinucleated phenotype in depleted Pacsin3 cells. By contrast, Yoda1 treatment was able to prevent cytokinetic failure in the siPacsin3 condition. These results supported that these proteins belong to the same regulatory pathway. Even if Piezo1 localization at the ICB was reduced because of the depletion of Pacsin3, Yoda1 may enhance the activity of the remaining channels, inducing enough Ca^{2+} entry to trigger the downstream signaling necessary for the completion of cytokinesis. Additionally, we were able to revert multinucleation in HMEC cells depleted of native Piezo1 by overexpressing a WT channel, but not the mutant Piezo1-4PA, which also failed to localize at the ICB. As Pacsin3 is a regulator of Piezo1 activity, we concluded that Pacsin3 recruits Piezo1 at the ICB increasing Ca^{2+} influx, necessary for the proper separation of the two daughter cells.

4.4 Piezo1/Pacsin3 mediate vesicle trafficking and the recruitment of the abscission machinery

To investigate which part of cytokinesis was mediated by the Piezo1/Pacsin3 interplay, we focused on two major events occurring during abscission, the remodeling of the ICB and the tune of the cytokinetic machinery, which often imply a Ca^{2+} signaling (Sarah E. Webb & Miller, 2017). Rab11- and Rab35-containing endosomes fusion to the ICB orchestrates these processes during the last steps of cell division. They are responsible for the secondary ingression of the ICB and the recruitment of important proteins and lipids mediating the final cut of the membrane (Fielding et al., 2005; Kouranti et al., 2006; Schiel et al., 2012). Thus, we aimed to study their relation to the Piezo1/Pacsin3 pathway.

We observed that depleting HMEC cells of Piezo1 or Pacsin3 using specific siRNAs or blocking the channel with GsMTx4, reduced the presence of Rab11 and its effector FIP3 at the ICB and increased multinucleation. Treating siPacsin3 cells with Yoda1 restored normal Rab11 and FIP3 levels at the ICB, confirming the interplay between Piezo1 and Pacsin3 in the modulation of Rab11-FIP3 vesicle localization. The delivery of vesicles to the ICB has already been associated with a Ca^{2+}-dependent process in zebrafish embryos (K. W. Lee et al., 2006; W. M. Li et al., 2008). To investigate this scenario, we overexpressed in parallel WT proteins, dominant-negative mutants, and constitutively active mutants of Rab11 and Rab35 in HMEC. In line with previous studies, the overexpression of dominant-negative mutants, Rab11-S25N or Rab35-S22N, induced an increase in the number of nuclei per cell, supporting the importance of the endosomal vesicle trafficking in cytokinesis (Kouranti et al., 2006; Wilson et al., 2005). Cells transfected with the WT version of Rab11 or Rab35 displayed normal cytokinesis. We observed that blocking Ca^{2+} influx through Piezo1 with GsMTx4 produced multinucleation in both WT conditions, according to the importance of Piezo1 in cytokinesis. However, only by overexpressing the dominant positive Rab11-Q70L, but not Rab35-Q67L, we were able to revert the multinucleation phenotype caused by GsMTx4. These results suggest that Piezo1-mediated Ca^{2+} signaling is upstream of Rab11-FIP3 vesicle function and supports its independent modulation from the Rab35 endocytic recycling pathway (Zerial & McBride, 2001).

Besides, Rab11-FIP3 endosome vesicles, but not Rab35-containing vesicles, participate in CHMP4B recruitment, responsible for the final cut of the ICB (Aoh et al., 2009). Therefore, we investigated the localization of the ESCRT-III machinery and its interacting partner ALIX (Morita et al., 2007). The ESCRT machinery is implicated not only in cytokinetic

abscission but also in cell membrane repair, viral budding, neuronal pruning, and nuclear membrane maintenance, among others (Vietri et al., 2020). Interestingly, ESCRT-II-III proteins participate in all these processes, however, the upstream targeting proteins (ALG-2, Cep55, GAG, HRS) are specific for a particular function. In addition, Cep55, the upstream regulator of ESCRT during cytokinesis, does not appear to be required in all cell types (Morita et al., 2007; Tedeschi et al., 2020; W.-M. Zhao et al., 2006). Accordingly, Cep55 was present at the midbody of HMEC cells but was missed in our fibroblast cell line. However, cytokinetic abscission in both cell lines was affected by the lack of Pacsin3 or Piezo1, increasing multinucleation. Thus, we decided to focus on the effect of our proteins in the downstream assembly of the ESCRT machinery, implicating ALIX and CHMP4B.

We observed that reducing functional Piezo1, Pacsin3, or Rab11 in the cell, led to a mislocalization of CHMP4B and ALIX from the midbody. According to our previous results, the positive-dominant Rab11-Q70L was able to restore CHMP4B and ALIX localization at the ICB, even under the blockade of Piezo1 by GsMTx4. Thus, these results demonstrate that Piezo1/Pacsin3 interplay modulate Rab11-FIP3 vesicles, which in turn not only contribute to CHMP4B recruitment, but also to its binding partner ALIX. Until now, Rab11-FIP3 was related to CHMP4B recruitment through the delivery of SCAMP3, an interactor of Tsg101 which in turn controls CHMP4B localization (Schiel et al., 2012). However, it was not well understood why depletion of Tsg101 induced milder effects on cytokinesis compared to the lack of ALIX or Rab11 and FIP3 proteins (Morita et al., 2007). We propose a possible explanation in which Rab11-FIP3 vesicles transport ALIX to the midbody, where it is delivered through Piezo1-mediated Ca^{2+} signaling, ending up in the recruitment of CHMP4B. However, we can not discard that Rab11-FIP3 endosomes deliver a lost

binding partner of ALIX or that SCAMP3 may also be responsible for ALIX recruitment.

These findings led us to investigate possible Ca^{2+} binding candidates regulated by Piezo1 activation and implicated in Rab11 vesicle delivery to the ICB. We observed that FIP3, the effector of Rab11, contains in its structure two Ca^{2+} binding EF-hand domains (https://www.uniprot.org /uniprot/O75154). As we have already mentioned, FIP3 localization at the ICB is modulated by Piezo1 and Pacsin3 similar to Rab11. Accordingly, FIP3-WT transfected cells developed normal cytokinesis, impaired under GsMTx4 treatment, where multinucleation and deficient CHMP4B at the midbody appeared. Through mutagenesis strategies, we mutate all asparagine residues from EF-hands to alanine (FIP3-4DA). Overexpressing the FIP3 mutant in HMEC caused multinucleation and a reduction of CHMP4B in the midbody. Neither GsMTx4 nor activation of Piezo1 by Yoda1 modified any of these parameters, persisting a similar failure in cytokinesis. Similar results were obtained with the mutant FIP3-I738E, unable to bind Rab11, which also was insensitive to Ca^{2+} signaling through Piezo1. Our results suggest that Piezo1 is activated by the tension generated at the ICB producing a transient Ca^{2+} increase necessary for FIP3 activation and the successive fusion of Rab11 vesicles to the midbody recruiting important proteins for the abscission machinery.

Alternatively, we also investigate the capacity of Pacsin3 and Piezo1 to regulate other pathways related to Ca^{2+} and the ESCRT machinery or cytokinesis. Our first candidate was ALG-2, a Ca^{2+}-binding protein responsible for trigger ESCRT assembly during cell membrane repair (Maki et al., 2011; Scheffer et al., 2014; S. Sun et al., 2015). This protein interacts with ALIX, promoting its accumulation in the injured cell membrane. We observed that the presence of ALG-2 in the midbody was minor and neither the genetic inhibition of Piezo1 nor Pacsin3 caused any

changes in its ICB localization. This was consistent with a previous study demonstrating that ALG-2 knockdown had no effect on cytokinetic abscission (S. Sun et al., 2015). Secondly, we investigate Beclin-1, a protein from the PI3K-III lipid-kinase complex which recruits abscission effectors and destabilizes actin filaments at the cleavage furrow (Raiborg et al., 2013; Schink et al., 2013). Its inhibition causes the arrest of cytokinesis, increasing the number of multinucleated cells (Thoresen et al., 2010; You et al., 2016). Reducing the expression of Pacsin3 and Piezo1, or inhibiting channel activity with GsMTx4, did not impair Beclin-1 localization at the ICB. Our results suggested that this pathway is not affected by Pacsin3/Piezo1 interplay. However, as in the case of Rab35-containing vesicles that increase PIP2 at the ICB, we can not discard the reverse regulation, as the Beclin-1-containing complex increases PtdIns(3)P content at the midbody, which could lead to changes in membrane mechanics sensed by Pacsin3 and/or Piezo1.

Our results shed light on the role of mechanical forces and intracellular Ca^{2+} signaling on the spatial organization of the ESCRT-III machinery through a Ca^{2+}-dependent protein in the endosomal pathway, FIP3, targeted by Piezo1 activity. As the secondary ingression site is a region in constant tension, a faster recovery from inactivation of Piezo1, induced by Pacsin3, could be an important mechanism to overcome possible channel desensitization in the course of abscission. We must also consider the promiscuous nature of Ca^{2+}, suggesting the possibility that Piezo1 has additional roles in cytokinetic events. In this regard, we have observed that the time needed by the mitotic cell to round out was not significantly altered by Piezo1 inhibition. This agrees with previous studies pointing that mitotic cell rounding implies low PM deformability and mechanotransduction (Maddox & Burridge, 2003; Matthews et al., 2012). However, we can not discard that Piezo1 is activated during furrow ingression by forces coming

from the actomyosin ring contraction, or even participate itself in the assembly of the actomyosin ring given its implication in RhoA activity (Hung et al., 2016). Besides, Rac1 is pointed to as a negative regulator of cytokinesis (Jordan & Canman, 2012). It is inactivated within the division plane, while active Rac1 is engaged in the cell poles. Interestingly, both Piezo1 and Pacsins concentrate at the ICB and are recognized as inactivators of Rac1 signaling (Hung et al., 2016; Kreuk et al., 2011). Thus, further research in this line is needed for a better understanding of cell division regulation. Furthermore, studying this new pathway in the context of other physiological processes that are under the regulation of membrane dynamics, such as membrane cell repair or viral infections, could contribute to our knowledge of these processes.

4.5 Physiological and pathophysiological implications

Cell division is a process with vast implications in developmental biology and in the pathogenesis of several diseases, including cancer. Focusing on organ development, the regulation of growth and division within different cell populations varies, however, the basic mechanisms are similar in the area of multicellular organisms. In this context, Piezo1 has been widely related to the proliferation and development of many organs with growing evidence (Choi et al., 2019; Del Mármol et al., 2018; Faucherre et al., 2020; Jiang et al., 2021; Pathak et al., 2014; Ranade et al., 2014; W. Sun et al., 2019; Velasco-Estevez et al., 2020).

The *in vitro* nature of our study and many of the cited researches may involve an alteration of the native behavior of Piezo1 and forces occurring during cell division in confined 3-D tissues. However, the fact that Piezo1 knockout is lethal at the embryonic stage hampers *in vivo* characterization, at the same time that highlights the importance of Piezo1 during

embryogenesis (Jing Li et al., 2014; Ranade et al., 2014; Woo et al., 2014). The generation of conditional knockouts of Piezo1 in mice and drosophila tissues (blood cells and vessels, gut, kidney, bones, sensory neurons) is expanding our understanding of channel function in 3D tissues (Cahalan et al., 2015; S. E. Kim et al., 2012; X. Li et al., 2019; Martins et al., 2016; Nonomura et al., 2018; Song et al., 2019; Sugisawa et al., 2020). Even so, cell cycle regulation is an intricate signaling network affected by the type and number of neighboring cells, their size, microenvironmental factors, and the stage of development. Many of these facts could be missing in conditional knockouts of Piezo1. An alternative is the knockdown of the channel in entire organisms using morpholinos or other RNA strategies (Faucherre et al., 2020; Gudipaty et al., 2017). This, together with the development of new mechanical devices and the current upgrading of microscopy and electrophysiology techniques, will facilitate the incoming research in the field of mechanobiology and developmental research.

The fact that Piezo1 seems to participate in the cytokinesis of tumor MDA-MD-231-BrM2 correlates to the widespread involvement of this MSC in cancer. Indeed, Piezo1 is crucial for the tumorigenesis of multiple solid cancers. Recent studies link Piezo1 to poor cancer prognosis, accelerating cell cycle and proliferation, or improving the metastatic capacity of tumoral cells (Han et al., 2019; Hung et al., 2016; Zhou et al., 2020). Thus, Piezo1 is more and more at the focus of cancer therapeutic strategy, boosting the importance of revealing channel regulatory pathways.

6. Conclusions

1. Piezo1 inactivation is difficulted by its interaction with Pacsin3 and Amphiphysin, but not by IRSp53, resulting in increased channel mechanotransduction.

2. Pacsin3 interacts with Piezo1 through its SH3 domain.

3. A proline-rich region in Piezo1, connecting the blades to the CTD, is responsible for Pacsin3-mediated modulation.

4. Pacsin3 localizes Piezo1 at the intercellular bridge of dividing cells where it generates a Ca^{2+} transient necessary for the completion of cytokinesis.

5. Piezo1/Pacsin3 mediate the delivery of Rab11-FIP3-containing vesicles to the intercellular bridge and the subsequent recruitment of ALIX and CHMP4B during abscission.

6. The Ca^{2+}-binding protein FIP3 is sensitive to the Ca^{2+} entry through Piezo1.

7. References

Abe, K., & Puertollano, R. (2011). Role of TRP channels in the regulation of the endosomal pathway. *Physiology* , *26*(1), 14–22.

Abou-Kheir, W., Isaac, B., Yamaguchi, H., & Cox, D. (2008). Membrane targeting of WAVE2 is not sufficient for WAVE2-dependent actin polymerization: a role for IRSp53 in mediating the interaction between Rac and WAVE2. *Journal of Cell Science*, *121*(Pt 3), 379–390.

Albarrán-Juárez, J., Iring, A., Wang, S., Joseph, S., Grimm, M., Strilic, B., Wettschureck, N., Althoff, T. F., & Offermanns, S. (2018). Piezo1 and Gq/G11 promote endothelial inflammation depending on flow pattern and integrin activation. *The Journal of Experimental Medicine*, *215*(10), 2655–2672.

Albuisson, J., Murthy, S. E., Bandell, M., Coste, B., Louis-Dit-Picard, H., Mathur, J., Fénéant-Thibault, M., Tertian, G., de Jaureguiberry, J.-P., Syfuss, P.-Y., Cahalan, S., Garçon, L., Toutain, F., Simon Rohrlich, P., Delaunay, J., Picard, V., Jeunemaitre, X., & Patapoutian, A. (2013). Dehydrated hereditary stomatocytosis linked to gain-of-function mutations in mechanically activated PIEZO1 ion channels. *Nature Communications*, *4*, 1884.

Alessandri-Haber, N., Dina, O. A., Joseph, E. K., Reichling, D. B., & Levine, J. D. (2008). Interaction of Transient Receptor Potential Vanilloid 4, Integrin, and Src Tyrosine Kinase in Mechanical Hyperalgesia. In *Journal of Neuroscience* (Vol. 28, Issue 5, pp. 1046–1057). https://doi.org/10.1523/jneurosci.4497-07.2008

Ambroso, M. R., Hegde, B. G., & Langen, R. (2014). Endophilin A1 induces different membrane shapes using a conformational switch that is regulated by phosphorylation. *Proceedings of the National Academy of Sciences of the United States of America*, *111*(19), 6982–6987.

Angers-Loustau, A., Côté, J. F., Charest, A., Dowbenko, D., Spencer, S., Lasky, L. A., & Tremblay, M. L. (1999). Protein tyrosine phosphatase-PEST regulates focal adhesion disassembly, migration, and cytokinesis in fibroblasts. *The Journal of Cell Biology*, *144*(5), 1019–1031.

Anggono, V., Smillie, K. J., Graham, M. E., Valova, V. A., Cousin, M. A., & Robinson, P. J. (2006). Syndapin I is the phosphorylation-regulated dynamin I partner in synaptic vesicle endocytosis. *Nature Neuroscience*, *9*(6), 752–760.

Aoh, Q. L., Castle, A. M., Hubbard, C. H., Katsumata, O., & Castle, J. D. (2009). SCAMP3 negatively regulates epidermal growth factor receptor degradation and promotes receptor recycling. *Molecular Biology of the Cell*, *20*(6), 1816–1832.

Atilla-Gokcumen, G. E., Muro, E., Relat-Goberna, J., Sasse, S., Bedigian, A., Coughlin, M. L., Garcia-Manyes, S., & Eggert, U. S. (2014). Dividing cells regulate their lipid composition and localization. *Cell*, *156*(3), 428–439.

Ayee, M. A. A., & Levitan, I. (2018). Membrane Stiffening in Osmotic Swelling: Analysis of Membrane Tension and Elastic Modulus. *Current Topics in Membranes*, *81*, 97–123.

Bae, C., Gnanasambandam, R., Nicolai, C., Sachs, F., & Gottlieb, P. A. (2013). Xerocytosis is caused by mutations that alter the kinetics of the mechanosensitive channel PIEZO1. In *Proceedings of the National Academy of Sciences* (Vol. 110, Issue 12, pp. E1162–E1168). https://doi.org/10.1073/pnas.1219777110

Bae, C., Sachs, F., & Gottlieb, P. A. (2011). The mechanosensitive ion channel Piezo1 is inhibited by the peptide GsMTx4. *Biochemistry*, *50*(29), 6295–6300.

Bae, C., Sachs, F., & Gottlieb, P. A. (2015). Protonation of the human PIEZO1 ion channel stabilizes inactivation. *The Journal of Biological Chemistry*, *290*(8), 5167–5173.

Bai, X., Meng, G., Luo, M., & Zheng, X. (2012). Rigidity of wedge loop in PACSIN 3 protein is a key factor in dictating diameters of tubules. *The Journal of Biological Chemistry*, *287*(26), 22387–22396.

Bauerfeind, R., Takei, K., & De Camilli, P. (1997). Amphiphysin I is associated with coated endocytic intermediates and undergoes stimulation-dependent dephosphorylation in nerve terminals. *The Journal of Biological Chemistry*, *272*(49), 30984–30992.

Bavi, O., Cox, C. D., Vossoughi, M., Naghdabadi, R., Jamali, Y., & Martinac, B. (2016). Influence of Global and Local Membrane Curvature on Mechanosensitive Ion Channels: A Finite Element Approach. *Membranes*, *6*(1). https://doi.org/10.3390/membranes6010014

Bavi, Navid, Yury A. Nikolaev, Omid Bavi, Pietro Ridone, Adam D. Martinac, Yoshitaka Nakayama, Charles D. Cox, and Boris

Martinac. 2017. “Principles of Mechanosensing at the Membrane Interface.” In *Springer Series in Biophysics*, 85–119. Springer Series in Biophysics. Singapore: Springer Singapore.

Benaud, C., Le Dez, G., Mironov, S., Galli, F., Reboutier, D., & Prigent, C. (2015). Annexin A2 is required for the early steps of cytokinesis. *EMBO Reports*, *16*(4), 481–489.

Berna-Erro, A., Izquierdo-Serra, M., Sepúlveda, R. V., Rubio-Moscardo, F., Doñate-Macián, P., Serra, S. A., Carrillo-Garcia, J., Perálvarez-Marín, A., González-Nilo, F., Fernández-Fernández, J. M., & Valverde, M. A. (2017). Structural determinants of 5′,6′-epoxyeicosatrienoic acid binding to and activation of TRPV4 channel. In *Scientific Reports* (Vol. 7, Issue 1). https://doi.org/10.1038/s41598-017-11274-1

Blaser, H., Reichman-Fried, M., Castanon, I., Dumstrei, K., Marlow, F. L., Kawakami, K., Solnica-Krezel, L., Heisenberg, C.-P., & Raz, E. (2006). Migration of zebrafish primordial germ cells: a role for myosin contraction and cytoplasmic flow. *Developmental Cell*, *11*(5), 613–627.

Borbiro, I., Badheka, D., & Rohacs, T. (2015). Activation of TRPV1 channels inhibits mechanosensitive Piezo channel activity by depleting membrane phosphoinositides. *Science Signaling*, *8*(363), ra15.

Bos, J. L., Rehmann, H., & Wittinghofer, A. (2007). GEFs and GAPs: critical elements in the control of small G proteins. *Cell*, *129*(5), 865–877.

Botello-Smith, W. M., Jiang, W., Zhang, H., Ozkan, A. D., Lin, Y.-C., Pham, C. N., Lacroix, J. J., & Luo, Y. (2019). A mechanism for the activation of the mechanosensitive Piezo1 channel by the small molecule Yoda1. *Nature Communications*, *10*(1), 4503.

Boucrot, E., Ferreira, A. P. A., Almeida-Souza, L., Debard, S., Vallis, Y., Howard, G., Bertot, L., Sauvonnet, N., & McMahon, H. T. (2015). Endophilin marks and controls a clathrin-independent endocytic pathway. *Nature*, *517*(7535), 460–465.

Brehm, P., Kullberg, R., & Moody-Corbett, F. (1984). Properties of non-junctional acetylcholine receptor channels on innervated muscle of Xenopus laevis. *The Journal of Physiology*, *350*, 631–648.

Brohawn, S. G., Su, Z., & MacKinnon, R. (2014). Mechanosensitivity is mediated directly by the lipid membrane in TRAAK and TREK1 K+ channels. *Proceedings of the National Academy of Sciences of the United States of America*, *111*(9), 3614–3619.

Burton, K., & Taylor, D. L. (1997). Traction forces of cytokinesis measured with optically modified elastic substrata. *Nature*, *385*(6615), 450–454.

Buyan, A., Cox, C. D., Rae, J., Barnoud, J., Li, J., Cvetovska, J., Bastiani, M., Chan, H. S. M., Hodson, M. P., Martinac, B., Parton, R. G., Marrink, S. J., & Corry, B. (2019). Piezo1 Induces Local Curvature in a Mammalian Membrane and Forms Specific Protein-Lipid Interactions. In *bioRxiv* (p. 787531). https://doi.org/10.1101/787531

Cahalan, S. M., Lukacs, V., Ranade, S. S., Chien, S., Bandell, M., & Patapoutian, A. (2015). Piezo1 links mechanical forces to red blood cell volume. *eLife*, *4*. https://doi.org/10.7554/eLife.07370

Cao, L., Yonis, A., Vaghela, M., Barriga, E. H., Chugh, P., Smith, M. B., Maufront, J., Lavoie, G., Méant, A., Ferber, E., Bovellan, M., Alberts, A., Bertin, A., Mayor, R., Paluch, E. K., Roux, P. P., Jégou, A., Romet-Lemonne, G., & Charras, G. (2020). SPIN90 associates with mDia1 and the Arp2/3 complex to regulate cortical actin organization. *Nature Cell Biology*, *22*(7), 803–814.

Carattino, M. D., & Montalbetti, N. (2020). Acid-sensing ion channels in sensory signaling. *American Journal of Physiology. Renal Physiology*, *318*(3), F531–F543.

Carlton, J. G., & Martin-Serrano, J. (2007). Parallels between cytokinesis and retroviral budding: a role for the ESCRT machinery. *Science*, *316*(5833), 1908–1912.

Carman, Peter J., and Roberto Dominguez. 2018. “BAR Domain Proteins-a Linkage between Cellular Membranes, Signaling Pathways, and the Actin Cytoskeleton.” *Biophysical Reviews* 10 (6): 1587–1604.

Chang, D. C., & Meng, C. (1995). A localized elevation of cytosolic free calcium is associated with cytokinesis in the zebrafish embryo. *The Journal of Cell Biology*, *131*(6 Pt 1), 1539–1545.

Chen, A., Ulloa Severino, L., Panagiotou, T. C., Moraes, T. F., Yuen, D. A., Lavoie, B. D., & Wilde, A. (2021). Inhibition of polar actin assembly by astral microtubules is required for cytokinesis. *Nature*

Communications, *12*(1), 2409.

Chen, C.-K., Hsu, P.-Y., Wang, T.-M., Miao, Z.-F., Lin, R.-T., & Juo, S.-H. H. (2018). TRPV4 Activation Contributes Functional Recovery from Ischemic Stroke via Angiogenesis and Neurogenesis. *Molecular Neurobiology*, *55*(5), 4127–4135.

Chen, X., Wanggou, S., Bodalia, A., Zhu, M., Dong, W., Fan, J. J., Yin, W. C., Min, H.-K., Hu, M., Draghici, D., Dou, W., Li, F., Coutinho, F. J., Whetstone, H., Kushida, M. M., Dirks, P. B., Song, Y., Hui, C.-C., Sun, Y., … Huang, X. (2018). A Feedforward Mechanism Mediated by Mechanosensitive Ion Channel PIEZO1 and Tissue Mechanics Promotes Glioma Aggression. *Neuron*, *100*(4), 799–815.e7.

Chen, Z., Shi, Z., & Baumgart, T. (2015). Regulation of membrane-shape transitions induced by I-BAR domains. *Biophysical Journal*, *109*(2), 298–307.

Chircop, M., Malladi, C. S., Lian, A. T., Page, S. L., Zavortink, M., Gordon, C. P., McCluskey, A., & Robinson, P. J. (2010). Calcineurin activity is required for the completion of cytokinesis. *Cellular and Molecular Life Sciences: CMLS*, *67*(21), 3725–3737.

Chircop, M., Sarcevic, B., Larsen, M. R., Malladi, C. S., Chau, N., Zavortink, M., Smith, C. M., Quan, A., Anggono, V., Hains, P. G., Graham, M. E., & Robinson, P. J. (2011). Phosphorylation of dynamin II at serine-764 is associated with cytokinesis. *Biochimica et Biophysica Acta*, *1813*(10), 1689–1699.

Choi, D., Park, E., Jung, E., Cha, B., Lee, S., Yu, J., Kim, P. M., Lee, S., Hong, Y. J., Koh, C. J., Cho, C.-W., Wu, Y., Li Jeon, N., Wong, A. K., Shin, L., Kumar, S. R., Bermejo-Moreno, I., Srinivasan, R. S., Cho, I.-T., & Hong, Y.-K. (2019). Piezo1 incorporates mechanical force signals into the genetic program that governs lymphatic valve development and maintenance. *JCI Insight*, *4*(5). https://doi.org/10.1172/jci.insight.125068

Chong, J., De Vecchis, D., Hyman, A. J., Povstyan, O. V., & Shi, J. (2019). Computational reconstruction of the complete Piezo1 structure reveals a unique footprint and specific lipid interactions. *BioRxiv*. https://www.biorxiv.org/content/10.1101/783753v1.abstract

Chong, Jiehan, Dario De Vecchis, Adam J. Hyman, Oleksandr V. Povstyan, Melanie J. Ludlow, Jian Shi, David J. Beech, and

Antreas C. Kalli. 2021. “Modeling of Full-Length Piezo1 Suggests Importance of the Proximal N-Terminus for Dome Structure.” *Biophysical Journal* 120 (8): 1343–56.

Christ, L., Wenzel, E. M., Liestøl, K., Raiborg, C., Campsteijn, C., & Stenmark, H. (2016). ALIX and ESCRT-I/II function as parallel ESCRT-III recruiters in cytokinetic abscission. *The Journal of Cell Biology*, *212*(5), 499–513.

Ciardo, M. G., & Ferrer-Montiel, A. (2017). Lipids as central modulators of sensory TRP channels. *Biochimica et Biophysica Acta, Biomembranes*, *1859*(9 Pt B), 1615–1628.

Cinar, E., Zhou, S., DeCourcey, J., Wang, Y., Waugh, R. E., & Wan, J. (2015). Piezo1 regulates mechanotransductive release of ATP from human RBCs. *Proceedings of the National Academy of Sciences of the United States of America*, *112*(38), 11783–11788.

Collins, C., Guilluy, C., Welch, C., O’Brien, E. T., Hahn, K., Superfine, R., Burridge, K., & Tzima, E. (2012). Localized tensional forces on PECAM-1 elicit a global mechanotransduction response via the integrin-RhoA pathway. *Current Biology: CB*, *22*(22), 2087–2094.

Corradi, V., Mendez-Villuendas, E., Ingólfsson, H. I., Gu, R.-X., Siuda, I., Melo, M. N., Moussatova, A., DeGagné, L. J., Sejdiu, B. I., Singh, G., Wassenaar, T. A., Delgado Magnero, K., Marrink, S. J., & Tieleman, D. P. (2018). Lipid-Protein Interactions Are Unique Fingerprints for Membrane Proteins. *ACS Central Science*, *4*(6), 709–717.

Coste, B., Mathur, J., Schmidt, M., Earley, T. J., Ranade, S., Petrus, M. J., Dubin, A. E., & Patapoutian, A. (2010). Piezo1 and Piezo2 are essential components of distinct mechanically activated cation channels. *Science*, *330*(6000), 55–60.

Coste, B., Murthy, S. E., Mathur, J., Schmidt, M., Mechioukhi, Y., Delmas, P., & Patapoutian, A. (2015). Piezo1 ion channel pore properties are dictated by C-terminal region. *Nature Communications*, *6*, 7223.

Cox, C. D., Bae, C., Ziegler, L., Hartley, S., Nikolova-Krstevski, V., Rohde, P. R., Ng, C.-A., Sachs, F., Gottlieb, P. A., & Martinac, B. (2016). Removal of the mechanoprotective influence of the cytoskeleton reveals PIEZO1 is gated by bilayer tension. In *Nature Communications* (Vol. 7, Issue 1).

https://doi.org/10.1038/ncomms10366

Cox, C. D., & Gottlieb, P. A. (2019). Amphipathic molecules modulate PIEZO1 activity. *Biochemical Society Transactions*, *47*(6), 1833–1842.

Cox, C. D., N. Bavi, and B. Martinac. 2017. "Origin of the Force: The Force-from-Lipids Principle Applied to Piezo Channels." *Current Topics in Membranes* 79: 59–96.

Craig, A. W. B. (2012). FES/FER kinase signaling in hematopoietic cells and leukemias. *Frontiers in Bioscience* , *17*, 861–875.

Cuajungco, M. P., Grimm, C., Oshima, K., D'hoedt, D., Nilius, B., Mensenkamp, A. R., Bindels, R. J. M., Plomann, M., & Heller, S. (2006). PACSINs bind to the TRPV4 cation channel. PACSIN 3 modulates the subcellular localization of TRPV4. *The Journal of Biological Chemistry*, *281*(27), 18753–18762.

Cui, H., Mim, C., Vázquez, F. X., Lyman, E., Unger, V. M., & Voth, G. A. (2013). Understanding the role of amphipathic helices in N-BAR domain driven membrane remodeling. *Biophysical Journal*, *104*(2), 404–411.

Dao, V. T., Dupuy, A. G., Gavet, O., Caron, E., & de Gunzburg, J. (2009). Dynamic changes in Rap1 activity are required for cell retraction and spreading during mitosis. *Journal of Cell Science*, *122*(Pt 16), 2996–3004.

Daum, B., Auerswald, A., Gruber, T., Hause, G., Balbach, J., Kühlbrandt, W., & Meister, A. (2016). Supramolecular organization of the human N-BAR domain in shaping the sarcolemma membrane. *Journal of Structural Biology*, *194*(3), 375–382.

Della Pietra, A., Mikhailov, N., & Giniatullin, R. (2020). The Emerging Role of Mechanosensitive Piezo Channels in Migraine Pain. *International Journal of Molecular Sciences*, *21*(3). https://doi.org/10.3390/ijms21030696

Delle Vedove, A., Storbeck, M., Heller, R., Hölker, I., Hebbar, M., Shukla, A., Magnusson, O., Cirak, S., Girisha, K. M., O'Driscoll, M., Loeys, B., & Wirth, B. (2016). Biallelic Loss of Proprioception-Related PIEZO2 Causes Muscular Atrophy with Perinatal Respiratory Distress, Arthrogryposis, and Scoliosis. *American Journal of Human Genetics*, *99*(6), 1406–1408.

Del Mármol, J. I., Touhara, K. K., Croft, G., & MacKinnon, R. (2018). Piezo1 forms a slowly-inactivating mechanosensory channel in mouse embryonic stem cells. *eLife, 7*. https://doi.org/10.7554/eLife.33149

D'hoedt, D., Owsianik, G., Prenen, J., Cuajungco, M. P., Grimm, C., Heller, S., Voets, T., & Nilius, B. (2008). Stimulus-specific modulation of the cation channel TRPV4 by PACSIN 3. *The Journal of Biological Chemistry*, *283*(10), 6272–6280.

Discher, D. E., Janmey, P., & Wang, Y.-L. (2005). Tissue cells feel and respond to the stiffness of their substrate. *Science*, *310*(5751), 1139–1143.

Dislich, B., Than, M. E., & Lichtenthaler, S. F. (2011). Specific amino acids in the BAR domain allow homodimerization and prevent heterodimerization of sorting nexin 33. *Biochemical Journal*, *433*(1), 75–83.

Dix, C. L., Matthews, H. K., Uroz, M., McLaren, S., Wolf, L., Heatley, N., Win, Z., Almada, P., Henriques, R., Boutros, M., Trepat, X., & Baum, B. (2018). The Role of Mitotic Cell-Substrate Adhesion Remodeling in Animal Cell Division. *Developmental Cell*, *45*(1), 132–145.e3.

Diz-Muñoz, A., Krieg, M., Bergert, M., Ibarlucea-Benitez, I., Muller, D. J., Paluch, E., & Heisenberg, C.-P. (2010). Control of directed cell migration in vivo by membrane-to-cortex attachment. *PLoS Biology*, *8*(11), e1000544.

Doñate-Macian, P., Duarte, Y., Rubio-Moscardo, F., Pérez-Vilaró, G., Canan, J., Díez, J., González-Nilo, F., & Valverde, M. A. (2020). Structural determinants of TRPV4 inhibition and identification of new antagonists with antiviral activity. *British Journal of Pharmacology*. https://doi.org/10.1111/bph.15267

Douglas, M. E., & Mishima, M. (2010). Still entangled: assembly of the central spindle by multiple microtubule modulators. *Seminars in Cell & Developmental Biology*, *21*(9), 899–908.

Echard, A. (2012). Phosphoinositides and cytokinesis: the "PIP" of the iceberg. *Cytoskeleton* , *69*(11), 893–912.

Echard, Arnaud. 2012. "Connecting Membrane Traffic to ESCRT and the Final Cut." *Nature Cell Biology* 14 (10): 983–85.

Eisenhoffer, G. T., Loftus, P. D., Yoshigi, M., Otsuna, H., Chien, C.-B., Morcos, P. A., & Rosenblatt, J. (2012). Crowding induces live cell extrusion to maintain homeostatic cell numbers in epithelia. In *Nature* (Vol. 484, Issue 7395, pp. 546–549). https://doi.org/10.1038/nature10999

Ellefsen, K. L., Holt, J. R., Chang, A. C., Nourse, J. L., Arulmoli, J., Mekhdjian, A. H., Abuwarda, H., Tombola, F., Flanagan, L. A., Dunn, A. R., Parker, I., & Pathak, M. M. (2019). Myosin-II mediated traction forces evoke localized Piezo1-dependent Ca 2+ flickers. *Communications Biology*, *2*(1), 1–13.

Elosegui-Artola, A., Bazellières, E., Allen, M. D., Andreu, I., Oria, R., Sunyer, R., Gomm, J. J., Marshall, J. F., Jones, J. L., Trepat, X., & Roca-Cusachs, P. (2014). Rigidity sensing and adaptation through regulation of integrin types. *Nature Materials*, *13*(6), 631–637.

Emoto, K., Inadome, H., Kanaho, Y., Narumiya, S., & Umeda, M. (2005). Local change in phospholipid composition at the cleavage furrow is essential for completion of cytokinesis. *The Journal of Biological Chemistry*, *280*(45), 37901–37907.

Errico, A., Ballabio, A., & Rugarli, E. I. (2002). Spastin, the protein mutated in autosomal dominant hereditary spastic paraplegia, is involved in microtubule dynamics. *Human Molecular Genetics*, *11*(2), 153–163.

Evans, E. L., Cuthbertson, K., Endesh, N., Rode, B., Blythe, N. M., Hyman, A. J., Hall, S. J., Gaunt, H. J., Ludlow, M. J., Foster, R., & Beech, D. J. (2018). Yoda1 analogue (Dooku1) which antagonizes Yoda1-evoked activation of Piezo1 and aortic relaxation. *British Journal of Pharmacology*, *175*(10), 1744–1759.

Faucherre, A., Moha Ou Maati, H., Nasr, N., Pinard, A., Theron, A., Odelin, G., Desvignes, J.-P., Salgado, D., Collod-Béroud, G., Avierinos, J.-F., Lebon, G., Zaffran, S., & Jopling, C. (2020). Piezo1 is required for outflow tract and aortic valve development. *Journal of Molecular and Cellular Cardiology*, *143*, 51–62.

Fernandes, J., Lorenzo, I. M., Andrade, Y. N., Garcia-Elias, A., Serra, S. A., Fernández-Fernández, J. M., & Valverde, M. A. (2008). IP3 sensitizes TRPV4 channel to the mechano- and osmotransducing messenger 5'-6'-epoxyeicosatrienoic acid. *The Journal of Cell Biology*, *181*(1), 143–155.

Fielding, A. B., Schonteich, E., Matheson, J., Wilson, G., Yu, X., Hickson, G. R. X., Srivastava, S., Baldwin, S. A., Prekeris, R., & Gould, G. W. (2005). Rab11-FIP3 and FIP4 interact with Arf6 and the Exocyst to control membrane traffic in cytokinesis. In *The EMBO Journal* (Vol. 24, Issue 19, pp. 3389–3399). https://doi.org/10.1038/sj.emboj.7600803

Fink, J., Carpi, N., Betz, T., Bétard, A., Chebah, M., Azioune, A., Bornens, M., Sykes, C., Fetler, L., Cuvelier, D., & Piel, M. (2011). External forces control mitotic spindle positioning. *Nature Cell Biology*, *13*(7), 771–778.

Fischer-Friedrich, E., Hyman, A. A., Jülicher, F., Müller, D. J., & Helenius, J. (2014). Quantification of surface tension and internal pressure generated by single mitotic cells. *Scientific Reports*, *4*, 6213.

Floyd, S. R., Porro, E. B., Slepnev, V. I., Ochoa, G. C., Tsai, L. H., & De Camilli, P. (2001). Amphiphysin 1 binds the cyclin-dependent kinase (cdk) 5 regulatory subunit p35 and is phosphorylated by cdk5 and cdc2. *The Journal of Biological Chemistry*, *276*(11), 8104–8110.

Fotiou, E., Martin-Almedina, S., Simpson, M. A., Lin, S., Gordon, K., Brice, G., Atton, G., Jeffery, I., Rees, D. C., Mignot, C., Vogt, J., Homfray, T., Snyder, M. P., Rockson, S. G., Jeffery, S., Mortimer, P. S., Mansour, S., & Ostergaard, P. (2015). Novel mutations in PIEZO1 cause an autosomal recessive generalized lymphatic dysplasia with non-immune hydrops fetalis. *Nature Communications*, *6*, 8085.

Frost, A., Perera, R., Roux, A., Spasov, K., Destaing, O., Egelman, E. H., De Camilli, P., & Unger, V. M. (2008). Structural basis of membrane invagination by F-BAR domains. *Cell*, *132*(5), 807–817.

Frost, A., Unger, V. M., & De Camilli, P. (2009). The BAR domain superfamily: membrane-molding macromolecules. *Cell*, *137*(2), 191–196.

Garcia-Elias, A., Mrkonjić, S., Pardo-Pastor, C., Inada, H., Hellmich, U. A., Rubio-Moscardó, F., Plata, C., Gaudet, R., Vicente, R., & Valverde, M. A. (2013). Phosphatidylinositol-4,5-biphosphate-dependent rearrangement of TRPV4 cytosolic tails enables channel activation by physiological stimuli. In *Proceedings of the National Academy of Sciences* (Vol. 110, Issue 23, pp. 9553–9558). https://doi.org/10.1073/pnas.1220231110

Gaub, B. M., & Müller, D. J. (2017). Mechanical Stimulation of Piezo1 Receptors Depends on Extracellular Matrix Proteins and Directionality of Force. *Nano Letters*, *17*(3), 2064–2072.

Ge, J., Li, W., Zhao, Q., Li, N., Chen, M., Zhi, P., Li, R., Gao, N., Xiao, B., & Yang, M. (2015). Architecture of the mammalian mechanosensitive Piezo1 channel. *Nature*, *527*(7576), 64–69.

Geng, J., Liu, W., Zhou, H., Zhang, T., Wang, L., Zhang, M., Li, Y., Shen, B., Li, X., & Xiao, B. (2020). A Plug-and-Latch Mechanism for Gating the Mechanosensitive Piezo Channel. *Neuron*, *106*(3), 438–451.e6.

Geng, Jie, Wenhao Liu, Heng Zhou, Tingxin Zhang, Li Wang, Mingmin Zhang, Yiran Li, Bo Shen, Xueming Li, and Bailong Xiao. 2020. "A Plug-and-Latch Mechanism for Gating the Mechanosensitive Piezo Channel." *Neuron* 106 (3): 438-451.e6.

Gnanasambandam, R., Ghatak, C., Yasmann, A., Nishizawa, K., Sachs, F., Ladokhin, A. S., Sukharev, S. I., & Suchyna, T. M. (2017). GsMTx4: Mechanism of Inhibiting Mechanosensitive Ion Channels. *Biophysical Journal*, *112*(1), 31–45.

Goretzki, Benedikt, Nina A. Glogowski, Erika Diehl, Elke Duchardt-Ferner, Carolin Hacker, Rachelle Gaudet, and Ute A. Hellmich. 2018. "Structural Basis of TRPV4 N Terminus Interaction with Syndapin/PACSIN1-3 and PIP2." *Structure (London, England: 1993)* 26 (12): 1583-1593.e5.

Gortat, A., San-Roman, M. J., Vannier, C., & Schmidt, A. A. (2012). Single point mutation in Bin/Amphiphysin/Rvs (BAR) sequence of endophilin impairs dimerization, membrane shaping, and Src homology 3 domain-mediated partnership. *The Journal of Biological Chemistry*, *287*(6), 4232–4247.

Gottlieb, P. A., Bae, C., & Sachs, F. (2012). Gating the mechanical channel Piezo1: a comparison between whole-cell and patch recording. *Channels* , *6*(4), 282–289.

Gottlieb, P. A., Maneshi, M. M., Sachs, F., & Hua, S. Z. (2019). Enantiomeric Aβ Peptides Inhibit the Fluid Shear Stress Response of PIEZO1. In *Biophysical Journal* (Vol. 116, Issue 3, p. 460a). https://doi.org/10.1016/j.bpj.2018.11.2483

Gromley, A., Yeaman, C., Rosa, J., Redick, S., Chen, C.-T., Mirabelle, S.,

Guha, M., Sillibourne, J., & Doxsey, S. J. (2005). Centriolin anchoring of exocyst and SNARE complexes at the midbody is required for secretory-vesicle-mediated abscission. *Cell*, *123*(1), 75–87.

Gudipaty, S. A., Lindblom, J., Loftus, P. D., Redd, M. J., Edes, K., Davey, C. F., Krishnegowda, V., & Rosenblatt, J. (2017). Mechanical stretch triggers rapid epithelial cell division through Piezo1. *Nature*, *543*(7643), 118–121.

Guerrier, S., Coutinho-Budd, J., Sassa, T., Gresset, A., Jordan, N. V., Chen, K., Jin, W.-L., Frost, A., & Polleux, F. (2009). The F-BAR domain of srGAP2 induces membrane protrusions required for neuronal migration and morphogenesis. *Cell*, *138*(5), 990–1004.

Guharay, F., & Sachs, F. (1984). Stretch-activated single ion channel currents in tissue-cultured embryonic chick skeletal muscle. *The Journal of Physiology*, *352*, 685–701.

Guilherme, A., Soriano, N. A., Bose, S., Holik, J., Bose, A., Pomerleau, D. P., Furcinitti, P., Leszyk, J., Corvera, S., & Czech, M. P. (2004). EHD2 and the novel EH domain binding protein EHBP1 couple endocytosis to the actin cytoskeleton. *The Journal of Biological Chemistry*, *279*(11), 10593–10605.

Güler, A. D., Lee, H., Iida, T., Shimizu, I., Tominaga, M., & Caterina, M. (2002). Heat-evoked activation of the ion channel, TRPV4. *The Journal of Neuroscience: The Official Journal of the Society for Neuroscience*, *22*(15), 6408–6414.

Guo, Y. R., & MacKinnon, R. (2017). Structure-based membrane dome mechanism for Piezo mechanosensitivity. *eLife*, *6*. https://doi.org/10.7554/eLife.33660

Haliloglu, G., Becker, K., Temucin, C., Talim, B., Küçükşahin, N., Pergande, M., Motameny, S., Nürnberg, P., Aydingoz, U., Topaloglu, H., & Cirak, S. (2017). Recessive PIEZO2 stop mutation causes distal arthrogryposis with distal muscle weakness, scoliosis and proprioception defects. *Journal of Human Genetics*, *62*(4), 497–501.

Hamill, O. P. (1983). Potassium and Chloride Channels in Red Blood Cells. *Single-Channel Recording*.

Han, Y., Liu, C., Zhang, D., Men, H., Huo, L., Geng, Q., Wang, S., Gao,

Y., Zhang, W., Zhang, Y., & Jia, Z. (2019). Mechanosensitive ion channel Piezo1 promotes prostate cancer development through the activation of the Akt/mTOR pathway and acceleration of cell cycle. *International Journal of Oncology*, *55*(3), 629–644.

Haselwandter, C. A., & MacKinnon, R. (2018). Piezo's membrane footprint and its contribution to mechanosensitivity. In *eLife* (Vol. 7). https://doi.org/10.7554/elife.41968

Hatzakis, N. S., Bhatia, V. K., Larsen, J., Madsen, K. L., Bolinger, P.-Y., Kunding, A. H., Castillo, J., Gether, U., Hedegård, P., & Stamou, D. (2009). How curved membranes recruit amphipathic helices and protein anchoring motifs. *Nature Chemical Biology*, *5*(11), 835–841.

Henne, W. M., Kent, H. M., Ford, M. G. J., Hegde, B. G., Daumke, O., Butler, P. J. G., Mittal, R., Langen, R., Evans, P. R., & McMahon, H. T. (2007). Structure and analysis of FCHo2 F-BAR domain: a dimerizing and membrane recruitment module that effects membrane curvature. *Structure* , *15*(7), 839–852.

Hinz, B. (2015). The extracellular matrix and transforming growth factor-β1: Tale of a strained relationship. *Matrix Biology: Journal of the International Society for Matrix Biology*, *47*, 54–65.

Hung, W.-C., Chen, S.-H., Paul, C. D., Stroka, K. M., Lo, Y.-C., Yang, J. T., & Konstantopoulos, K. (2013). Distinct signaling mechanisms regulate migration in unconfined versus confined spaces. *The Journal of Cell Biology*, *202*(5), 807–824.

Hung, W.-C., Yang, J. R., Yankaskas, C. L., Wong, B. S., Wu, P.-H., Pardo-Pastor, C., Serra, S. A., Chiang, M.-J., Gu, Z., Wirtz, D., Valverde, M. A., Yang, J. T., Zhang, J., & Konstantopoulos, K. (2016). Confinement Sensing and Signal Optimization via Piezo1/PKA and Myosin II Pathways. *Cell Reports*, *15*(7), 1430–1441.

Hutterer, A., Glotzer, M., & Mishima, M. (2009). Clustering of centralspindlin is essential for its accumulation to the central spindle and the midbody. *Current Biology: CB*, *19*(23), 2043–2049.

Itoh, T., Erdmann, K. S., Roux, A., Habermann, B., Werner, H., & De Camilli, P. (2005). Dynamin and the actin cytoskeleton cooperatively regulate plasma membrane invagination by BAR and F-BAR proteins. *Developmental Cell*, *9*(6), 791–804.

Jetta, D., Bahrani Fard, M. R., Sachs, F., Munechika, K., & Hua, S. Z. (2021). Adherent cell remodeling on micropatterns is modulated by Piezo1 channels. *Scientific Reports*, *11*(1), 5088.

Jiang, F., Yin, K., Wu, K., Zhang, M., Wang, S., Cheng, H., Zhou, Z., & Xiao, B. (2021). The mechanosensitive Piezo1 channel mediates heart mechano-chemo transduction. *Nature Communications*, *12*(1), 869.

Johannes, Ludger, Christian Wunder, and Patricia Bassereau. 2014. "Bending 'on the Rocks'--a Cocktail of Biophysical Modules to Build Endocytic Pathways." *Cold Spring Harbor Perspectives in Biology* 6 (1): a016741–a016741.

Jordan, S. N., & Canman, J. C. (2012). Rho GTPases in animal cell cytokinesis: an occupation by the one percent. *Cytoskeleton* , *69*(11), 919–930.

Joshi, S., Perera, S., Gilbert, J., Smith, C. M., Mariana, A., Gordon, C. P., Sakoff, J. A., McCluskey, A., Robinson, P. J., Braithwaite, A. W., & Chircop, M. (2010). The dynamin inhibitors MiTMAB and OcTMAB induce cytokinesis failure and inhibit cell proliferation in human cancer cells. *Molecular Cancer Therapeutics*, *9*(7), 1995–2006.

Kamaraju, K., Gottlieb, P. A., Sachs, F., & Sukharev, S. (2010). Effects of GsMTx4 on Bacterial Mechanosensitive Channels in Inside-Out Patches from Giant Spheroplasts. In *Biophysical Journal* (Vol. 99, Issue 9, pp. 2870–2878). https://doi.org/10.1016/j.bpj.2010.09.022

Kanada, M., Nagasaki, A., & Uyeda, T. Q. P. (2005). Adhesion-dependent and contractile ring-independent equatorial furrowing during cytokinesis in mammalian cells. *Molecular Biology of the Cell*, *16*(8), 3865–3872.

Kang, H., Hong, Z., Zhong, M., Klomp, J., Bayless, K. J., Mehta, D., Karginov, A. V., Hu, G., & Malik, A. B. (2019). Piezo1 mediates angiogenesis through activation of MT1-MMP signaling. *American Journal of Physiology. Cell Physiology*, *316*(1), C92–C103.

Kast, D. J., & Dominguez, R. (2019). IRSp53 coordinates AMPK and 14-3-3 signaling to regulate filopodia dynamics and directed cell migration. *Molecular Biology of the Cell*, *30*(11), 1285–1297.

Katz, B. (1950). Action potentials from a sensory nerve ending. *The*

Journal of Physiology, *111*(3-4), 248–260.

Kelkar, M., Bohec, P., & Charras, G. (2020). Mechanics of the cellular actin cortex: From signalling to shape change. *Current Opinion in Cell Biology*, *66*, 69–78.

Kelley, C. F., Messelaar, E. M., Eskin, T. L., Wang, S., Song, K., Vishnia, K., Becalska, A. N., Shupliakov, O., Hagan, M. F., Danino, D., Sokolova, O. S., Nicastro, D., & Rodal, A. A. (2015). Membrane Charge Directs the Outcome of F-BAR Domain Lipid Binding and Autoregulation. *Cell Reports*, *13*(11), 2597–2609.

Kessels, M. M., & Qualmann, B. (2004). The syndapin protein family: linking membrane trafficking with the cytoskeleton. *Journal of Cell Science*, *117*(Pt 15), 3077–3086.

Khatibzadeh, N., Spector, A. A., Brownell, W. E., & Anvari, B. (2013). Effects of plasma membrane cholesterol level and cytoskeleton F-actin on cell protrusion mechanics. *PloS One*, *8*(2), e57147.

Kim, C., Ye, F., & Ginsberg, M. H. (2011). Regulation of integrin activation. *Annual Review of Cell and Developmental Biology*, *27*, 321–345.

Kim, S. E., Coste, B., Chadha, A., Cook, B., & Patapoutian, A. (2012). The role of Drosophila Piezo in mechanical nociception. *Nature*, *483*(7388), 209–212.

Koser, D. E., Thompson, A. J., Foster, S. K., Dwivedy, A., Pillai, E. K., Sheridan, G. K., Svoboda, H., Viana, M., Costa, L. da F., Guck, J., Holt, C. E., & Franze, K. (2016). Mechanosensing is critical for axon growth in the developing brain. *Nature Neuroscience*, *19*(12), 1592–1598.

Kouranti, I., Sachse, M., Arouche, N., Goud, B., & Echard, A. (2006). Rab35 regulates an endocytic recycling pathway essential for the terminal steps of cytokinesis. *Current Biology: CB*, *16*(17), 1719–1725.

Koyama, H., Umeda, T., Nakamura, K., Higuchi, T., & Kimura, A. (2012). A high-resolution shape fitting and simulation demonstrated equatorial cell surface softening during cytokinesis and its promotive role in cytokinesis. *PloS One*, *7*(2), e31607.

Kreuk, B.-J. de, de Kreuk, B.-J., Nethe, M., Fernandez-Borja, M.,

Anthony, E. C., Hensbergen, P. J., Deelder, A. M., Plomann, M., & Hordijk, P. L. (2011). The F-BAR domain protein PACSIN2 associates with Rac1 and regulates cell spreading and migration. In *Journal of Cell Science* (Vol. 124, Issue 14, pp. 2375–2388). https://doi.org/10.1242/jcs.080630

Kunda, P., Pelling, A. E., Liu, T., & Baum, B. (2008). Moesin controls cortical rigidity, cell rounding, and spindle morphogenesis during mitosis. *Current Biology: CB*, *18*(2), 91–101.

Lacroix, B., & Maddox, A. S. (2012). Cytokinesis, ploidy and aneuploidy. *The Journal of Pathology*, *226*(2), 338–351.

Lancaster, O. M., Le Berre, M., Dimitracopoulos, A., Bonazzi, D., Zlotek-Zlotkiewicz, E., Picone, R., Duke, T., Piel, M., & Baum, B. (2013). Mitotic rounding alters cell geometry to ensure efficient bipolar spindle formation. *Developmental Cell*, *25*(3), 270–283.

Lee, H. H., Elia, N., Ghirlando, R., Lippincott-Schwartz, J., & Hurley, J. H. (2008). *Midbody targeting of the ESCRT machinery by a non-canonical coiled-coil in CEP55*. Worldwide Protein Data Bank. https://doi.org/10.2210/pdb3e1r/pdb

Lee, K. W., Webb, S. E., & Miller, A. L. (2006). Requirement for a localized, IP3R-generated Ca2+ transient during the furrow positioning process in zebrafish zygotes. *Zygote* , *14*(2), 143–155.

Lee, K.-Y., Esmaeili, B., Zealley, B., & Mishima, M. (2015). Direct interaction between centralspindlin and PRC1 reinforces mechanical resilience of the central spindle. *Nature Communications*, *6*, 7290.

Lee, W., Leddy, H. A., Chen, Y., Lee, S. H., Zelenski, N. A., McNulty, A. L., Wu, J., Beicker, K. N., Coles, J., Zauscher, S., Grandl, J., Sachs, F., Guilak, F., & Liedtke, W. B. (2014). Synergy between Piezo1 and Piezo2 channels confers high-strain mechanosensitivity to articular cartilage. *Proceedings of the National Academy of Sciences of the United States of America*, *111*(47), E5114–E5122.

Lekomtsev, S., Su, K.-C., Pye, V. E., Blight, K., Sundaramoorthy, S., Takaki, T., Collinson, L. M., Cherepanov, P., Divecha, N., & Petronczki, M. (2012). Centralspindlin links the mitotic spindle to the plasma membrane during cytokinesis. *Nature*, *492*(7428), 276–279.

Lewis, A. H., & Grandl, J. (2015). Mechanical sensitivity of Piezo1 ion channels can be tuned by cellular membrane tension. *eLife*, *4*.

https://doi.org/10.7554/eLife.12088

Lewis, A. H., & Grandl, J. (2020). Inactivation Kinetics and Mechanical Gating of Piezo1 Ion Channels Depend on Subdomains within the Cap. *Cell Reports*, *30*(3), 870–880.e2.

Liang, X., & Howard, J. (2018). Structural Biology: Piezo Senses Tension through Curvature. *Current Biology: CB*, *28*(8), R357–R359.

Li, C. J., Heim, R., Lu, P., Pu, Y., Tsien, R. Y., & Chang, D. C. (1999). Dynamic redistribution of calmodulin in HeLa cells during cell division as revealed by a GFP-calmodulin fusion protein technique. *Journal of Cell Science*, *112 (Pt 10)*, 1567–1577.

Lie-Jensen, A., Ivanauskiene, K., Malerød, L., Jain, A., Tan, K. W., Laerdahl, J. K., Liestøl, K., Stenmark, H., & Haglund, K. (2019). Centralspindlin Recruits ALIX to the Midbody during Cytokinetic Abscission in Drosophila via a Mechanism Analogous to Virus Budding. *Current Biology: CB*, *29*(20), 3538–3548.e7.

Li, J., Hou, B., Tumova, S., Muraki, K., Bruns, A., Ludlow, M. J., Sedo, A., Hyman, A. J., McKeown, L., Young, R. S., Yuldasheva, N. Y., Majeed, Y., Wilson, L. A., Rode, B., Bailey, M. A., Kim, H. R., Fu, Z., Carter, D. A., Bilton, J., … Beech, D. J. (2014). Piezo1 integration of vascular architecture with physiological force. *Nature*, *515*(7526), 279–282.

Li, J., Ng, C. A., Cheng, D., & Cox, C. D. (2021). Modified N-Linked Glycosylation Status Predicts Trafficking Defective Piezo1 Channel Mutations. In *Biophysical Journal* (Vol. 120, Issue 3, p. 236a – 237a). https://doi.org/10.1016/j.bpj.2020.11.1562

Lim, C.-G., Jang, J., & Kim, C. (2018). Cellular machinery for sensing mechanical force. *BMB Reports*, *51*(12), 623–629.

Lim, K. B., Bu, W., Goh, W. I., Koh, E., Ong, S. H., Pawson, T., Sudhaharan, T., & Ahmed, S. (2008). The Cdc42 effector IRSp53 generates filopodia by coupling membrane protrusion with actin dynamics. *The Journal of Biological Chemistry*, *283*(29), 20454–20472.

Lin, Y.-C., Guo, Y. R., Miyagi, A., Levring, J., MacKinnon, R., & Scheuring, S. (2019). Force-induced conformational changes in PIEZO1. *Nature*, *573*(7773), 230–234.

Liu, J., Gao, H.-Y., & Wang, X.-F. (2015). The role of the Rho/ROCK signaling pathway in inhibiting axonal regeneration in the central nervous system. *Neural Regeneration Research*, *10*(11), 1892–1896.

Liu, X., Wang, P., Fu, J., Lv, D., Chen, D., & Li, Y. (2011). Two-photon fluorescence real-time imaging on the development of early mouse embryo by stages. *Journal of*. https://onlinelibrary.wiley.com/doi/abs/10.1111/j.1365-2818.2010.03426.x?casa_token=HtYZ4-Up2h4AAAAA:rZ1CSLDE9nA2aMqcJAdbUngwmh3JVLK-l2TDcJVk7CIPPd2jBhsuO5rtOzzIefckhDT7jiah6-iFsjs

Liu, Y.-J., Le Berre, M., Lautenschlaeger, F., Maiuri, P., Callan-Jones, A., Heuzé, M., Takaki, T., Voituriez, R., & Piel, M. (2015). Confinement and low adhesion induce fast amoeboid migration of slow mesenchymal cells. *Cell*, *160*(4), 659–672.

Li, W. M., Webb, S. E., Chan, C. M., & Miller, A. L. (2008). Multiple roles of the furrow deepening Ca2+ transient during cytokinesis in zebrafish embryos. *Developmental Biology*, *316*(2), 228–248.

Li, X., Han, L., Nookaew, I., Mannen, E., Silva, M. J., Almeida, M., & Xiong, J. (2019). Stimulation of Piezo1 by mechanical signals promotes bone anabolism. *eLife*, *8*. https://doi.org/10.7554/eLife.49631

Loewenstein, W. R. (1959). The generation of electric activity in a nerve ending. *Annals of the New York Academy of Sciences*, *81*, 367–387.

Lolignier, S., Eijkelkamp, N., & Wood, J. N. (2015). Mechanical allodynia. *Pflugers Archiv: European Journal of Physiology*, *467*(1), 133–139.

Lukacs, V., Mathur, J., Mao, R., Bayrak-Toydemir, P., Procter, M., Cahalan, S. M., Kim, H. J., Bandell, M., Longo, N., Day, R. W., Stevenson, D. A., Patapoutian, A., & Krock, B. L. (2015). Impaired PIEZO1 function in patients with a novel autosomal recessive congenital lymphatic dysplasia. *Nature Communications*, *6*, 8329.

Lyon, R. C., Zanella, F., Omens, J. H., & Sheikh, F. (2015). Mechanotransduction in cardiac hypertrophy and failure. *Circulation Research*, *116*(8), 1462–1476.

Maddox, A. S., & Burridge, K. (2003). RhoA is required for cortical retraction and rigidity during mitotic cell rounding. *The Journal of*

Cell Biology, *160*(2), 255–265.

Maki, M., Suzuki, H., & Shibata, H. (2011). Structure and function of ALG-2, a penta-EF-hand calcium-dependent adaptor protein. *Science China. Life Sciences*, *54*(8), 770–779.

Mammoto, T., Mammoto, A., & Ingber, D. E. (2013). Mechanobiology and developmental control. *Annual Review of Cell and Developmental Biology*, *29*, 27–61.

Martinac, B., & Cox, C. D. (2017). Mechanosensory Transduction: Focus on Ion Channels ☆. In *Reference Module in Life Sciences*. Elsevier.

Martín-García, R., Arribas, V., Coll, P. M., Pinar, M., Viana, R. A., Rincón, S. A., Correa-Bordes, J., Ribas, J. C., & Pérez, P. (2018). Paxillin-Mediated Recruitment of Calcineurin to the Contractile Ring Is Required for the Correct Progression of Cytokinesis in Fission Yeast. *Cell Reports*, *25*(3), 772–783.e4.

Martins, J. R., Penton, D., Peyronnet, R., Arhatte, M., Moro, C., Picard, N., Kurt, B., Patel, A., Honoré, E., & Demolombe, S. (2016). Piezo1-dependent regulation of urinary osmolarity. *Pflugers Archiv: European Journal of Physiology*, *468*(7), 1197–1206.

Masingue, M., Fauré, J., Solé, G., Stojkovic, T., & Léonard-Louis, S. (2019). A novel nonsense PIEZO2 mutation in a family with scoliosis and proprioceptive defect. *Neuromuscular Disorders: NMD*, *29*(1), 75–79.

Masuda, M., & Mochizuki, N. (2010). Structural characteristics of BAR domain superfamily to sculpt the membrane. *Seminars in Cell & Developmental Biology*, *21*(4), 391–398.

Matthews, H. K., Delabre, U., Rohn, J. L., Guck, J., Kunda, P., & Baum, B. (2012). Changes in Ect2 localization couple actomyosin-dependent cell shape changes to mitotic progression. *Developmental Cell*, *23*(2), 371–383.

Matzke, R., Jacobson, K., & Radmacher, M. (2001). Direct, high-resolution measurement of furrow stiffening during division of adherent cells. *Nature Cell Biology*, *3*(6), 607–610.

McHugh, B. J., Buttery, R., Lad, Y., Banks, S., Haslett, C., & Sethi, T. (2010). Integrin activation by Fam38A uses a novel mechanism of R-Ras targeting to the endoplasmic reticulum. *Journal of Cell Science*,

123(Pt 1), 51–61.

Meinecke, M., Boucrot, E., Camdere, G., Hon, W.-C., Mittal, R., & McMahon, H. T. (2013). Cooperative recruitment of dynamin and BIN/amphiphysin/Rvs (BAR) domain-containing proteins leads to GTP-dependent membrane scission. *The Journal of Biological Chemistry*, *288*(9), 6651–6661.

Mierzwa, B. E., Chiaruttini, N., Redondo-Morata, L., von Filseck, J. M., König, J., Larios, J., Poser, I., Müller-Reichert, T., Scheuring, S., Roux, A., & Gerlich, D. W. (2017). Dynamic subunit turnover in ESCRT-III assemblies is regulated by Vps4 to mediate membrane remodelling during cytokinesis. *Nature Cell Biology*, *19*(7), 787–798.

Miki, H., Yamaguchi, H., Suetsugu, S., & Takenawa, T. (2000). IRSp53 is an essential intermediate between Rac and WAVE in the regulation of membrane ruffling. In *Nature* (Vol. 408, Issue 6813, pp. 732–735). https://doi.org/10.1038/35047107

Mim, C., Cui, H., Gawronski-Salerno, J. A., Frost, A., Lyman, E., Voth, G. A., & Unger, V. M. (2012). Structural basis of membrane bending by the N-BAR protein endophilin. *Cell*, *149*(1), 137–145.

Modregger, J., Ritter, B., Witter, B., Paulsson, M., & Plomann, M. (2000). All three PACSIN isoforms bind to endocytic proteins and inhibit endocytosis. *Journal of Cell Science*, *113 Pt 24*, 4511–4521.

Moravcevic, K., Alvarado, D., Schmitz, K. R., Kenniston, J. A., Mendrola, J. M., Ferguson, K. M., & Lemmon, M. A. (2015). Comparison of Saccharomyces cerevisiae F-BAR domain structures reveals a conserved inositol phosphate binding site. *Structure* , *23*(2), 352–363.

Morita, E., Sandrin, V., Chung, H.-Y., Morham, S. G., Gygi, S. P., Rodesch, C. K., & Sundquist, W. I. (2007). Human ESCRT and ALIX proteins interact with proteins of the midbody and function in cytokinesis. *The EMBO Journal*, *26*(19), 4215–4227.

Moroni, M., Servin-Vences, M. R., Fleischer, R., Sánchez-Carranza, O., & Lewin, G. R. (2018). Voltage gating of mechanosensitive PIEZO channels. *Nature Communications*, *9*(1), 1096.

Morris, C. E., & Homann, U. (2001). Cell surface area regulation and membrane tension. *The Journal of Membrane Biology*, *179*(2), 79–

102.

Myers, K. M., & Elad, D. (2017). Biomechanics of the human uterus. *Wiley Interdisciplinary Reviews. Systems Biology and Medicine*, *9*(5). https://doi.org/10.1002/wsbm.1388

Nagasaki, A., Kanada, M., & Uyeda, T. Q. (2009). Cell adhesion molecules regulate contractile ring-independent cytokinesis in Dictyostelium discoideum. *Cell Research*, *19*(2), 236–246.

Nam, S., Gupta, V. K., Lee, H.-P., Lee, J. Y., Wisdom, K. M., Varma, S., Flaum, E. M., Davis, C., West, R. B., & Chaudhuri, O. (2019). Cell cycle progression in confining microenvironments is regulated by a growth-responsive TRPV4-PI3K/Akt-p27Kip1 signaling axis. *Science Advances*, *5*(8), eaaw6171.

Neef, R., Gruneberg, U., Kopajtich, R., Li, X., Nigg, E. A., Sillje, H., & Barr, F. A. (2007). Choice of Plk1 docking partners during mitosis and cytokinesis is controlled by the activation state of Cdk1. *Nature Cell Biology*, *9*(4), 436–444.

Nepal, B., Sepehri, A., & Lazaridis, T. (2020). Mechanism of negative membrane curvature generation by the IRSP53 I-BAR domain. *bioRxiv*. https://www.biorxiv.org/content/10.1101/2020.08.19.256925v1.abstract

Newell-Litwa, K. A., & Horwitz, A. R. (2011). Cell migration: PKA and RhoA set the pace. *Current Biology: CB*, *21*(15), R596–R598.

Nikolaev, Y. A., Cox, C. D., Ridone, P., Rohde, P. R., Cordero-Morales, J. F., Vásquez, V., Laver, D. R., & Martinac, B. (2019). Mammalian TRP ion channels are insensitive to membrane stretch. *Journal of Cell Science*, *132*(23). https://doi.org/10.1242/jcs.238360

Nilius, B., Watanabe, H., & Vriens, J. (2003). The TRPV4 channel: structure-function relationship and promiscuous gating behaviour. *Pflugers Archiv: European Journal of Physiology*, *446*(3), 298–303.

Nishimura, T., Morone, N., & Suetsugu, S. (2018). Membrane re-modelling by BAR domain superfamily proteins via molecular and non-molecular factors. *Biochemical Society Transactions*, *46*(2), 379–389.

Nishimura, Y., & Yonemura, S. (2006). Centralspindlin regulates ECT2

and RhoA accumulation at the equatorial cortex during cytokinesis. *Journal of Cell Science*, *119*(Pt 1), 104–114.

Nonomura, K., Lukacs, V., Sweet, D. T., Goddard, L. M., Kanie, A., Whitwam, T., Ranade, S. S., Fujimori, T., Kahn, M. L., & Patapoutian, A. (2018). Mechanically activated ion channel PIEZO1 is required for lymphatic valve formation. *Proceedings of the National Academy of Sciences of the United States of America*, *115*(50), 12817–12822.

Northey, J. J., Przybyla, L., & Weaver, V. M. (2017). Tissue Force Programs Cell Fate and Tumor Aggression. *Cancer Discovery*, *7*(11), 1224–1237.

Nourse, Jamison L., and Medha M. Pathak. 2017. "How Cells Channel Their Stress: Interplay between Piezo1 and the Cytoskeleton." *Seminars in Cell & Developmental Biology* 71 (November): 3–12.

O'Connor, K. L., & Mercurio, A. M. (2001). Protein kinase A regulates Rac and is required for the growth factor-stimulated migration of carcinoma cells. *The Journal of Biological Chemistry*, *276*(51), 47895–47900.

Ou, G., Stuurman, N., D'Ambrosio, M., & Vale, R. D. (2010). Polarized myosin produces unequal-size daughters during asymmetric cell division. *Science*, *330*(6004), 677–680.

Ou-Yang, Q., Li, B., Xu, M., & Liang, H. (2018). TRPV4 promotes the migration and invasion of glioma cells via AKT/Rac1 signaling. *Biochemical and Biophysical Research Communications*, *503*(2), 876–881.

Pakshir, P., Alizadehgiashi, M., Wong, B., Coelho, N. M., Chen, X., Gong, Z., Shenoy, V. B., McCulloch, C. A., & Hinz, B. (2019). Dynamic fibroblast contractions attract remote macrophages in fibrillar collagen matrix. *Nature Communications*, *10*(1), 1850.

Pan, J., Tristram-Nagle, S., & Nagle, J. F. (2009). Effect of cholesterol on structural and mechanical properties of membranes depends on lipid chain saturation. *Physical Review. E, Statistical, Nonlinear, and Soft Matter Physics*, *80*(2 Pt 1), 021931.

Pardo-Pastor, C., Rubio-Moscardo, F., Vogel-González, M., Serra, S. A., Afthinos, A., Mrkonjic, S., Destaing, O., Abenza, J. F., Fernández-Fernández, J. M., Trepat, X., Albiges-Rizo, C., Konstantopoulos, K.,

& Valverde, M. A. (2018). Piezo2 channel regulates RhoA and actin cytoskeleton to promote cell mechanobiological responses. *Proceedings of the National Academy of Sciences of the United States of America*, *115*(8), 1925–1930.

Pasapera, A. M., Plotnikov, S. V., Fischer, R. S., Case, L. B., Egelhoff, T. T., & Waterman, C. M. (2015). Rac1-dependent phosphorylation and focal adhesion recruitment of myosin IIA regulates migration and mechanosensing. *Current Biology: CB*, *25*(2), 175–186.

Pathak, M. M., Nourse, J. L., Tran, T., Hwe, J., Arulmoli, J., Le, D. T. T., Bernardis, E., Flanagan, L. A., & Tombola, F. (2014). Stretch-activated ion channel Piezo1 directs lineage choice in human neural stem cells. *Proceedings of the National Academy of Sciences of the United States of America*, *111*(45), 16148–16153.

Petsalaki, E., & Zachos, G. (2016). Clks 1, 2 and 4 prevent chromatin breakage by regulating the Aurora B-dependent abscission checkpoint. *Nature Communications*, *7*, 11451.

Phillips, D. A., Zacharoff, L. A., Hampton, C. M., & Chong, G. W. (2020). A Prokaryotic Membrane Sculpting BAR Domain Protein. *bioRxiv*. https://www.biorxiv.org/content/10.1101/2020.01.30.926147v1.abstract

Phillips, R., Ursell, T., Wiggins, P., & Sens, P. (2009). Emerging roles for lipids in shaping membrane-protein function. *Nature*, *459*(7245), 379–385.

Piekny, A. J., & Glotzer, M. (2008). Anillin is a scaffold protein that links RhoA, actin, and myosin during cytokinesis. *Current Biology: CB*, *18*(1), 30–36.

Poirier, C. C., Ng, W. P., Robinson, D. N., & Iglesias, P. A. (2012). Deconvolution of the cellular force-generating subsystems that govern cytokinesis furrow ingression. *PLoS Computational Biology*, *8*(4), e1002467.

Poole, K., Herget, R., Lapatsina, L., Ngo, H.-D., & Lewin, G. R. (2014). Tuning Piezo ion channels to detect molecular-scale movements relevant for fine touch. *Nature Communications*, *5*, 3520.

Qi, Y., Andolfi, L., Frattini, F., Mayer, F., Lazzarino, M., & Hu, J. (2015). Membrane stiffening by STOML3 facilitates mechanosensation in

sensory neurons. *Nature Communications*, *6*, 8512.

Raghavan, V., & Weisz, O. A. (2016). Discerning the role of mechanosensors in regulating proximal tubule function. *American Journal of Physiology. Renal Physiology*, *310*(1), F1–F5.

Raiborg, C., Schink, K. O., & Stenmark, H. (2013). Class III phosphatidylinositol 3-kinase and its catalytic product PtdIns3P in regulation of endocytic membrane traffic. *The FEBS Journal*, *280*(12), 2730–2742.

Ramanathan, S. P., Helenius, J., Stewart, M. P., Cattin, C. J., Hyman, A. A., & Muller, D. J. (2015). Cdk1-dependent mitotic enrichment of cortical myosin II promotes cell rounding against confinement. *Nature Cell Biology*, *17*(2), 148–159.

Ranade, S. S., Qiu, Z., Woo, S.-H., Hur, S. S., Murthy, S. E., Cahalan, S. M., Xu, J., Mathur, J., Bandell, M., Coste, B., Li, Y.-S. J., Chien, S., & Patapoutian, A. (2014). Piezo1, a mechanically activated ion channel, is required for vascular development in mice. *Proceedings of the National Academy of Sciences of the United States of America*, *111*(28), 10347–10352.

Rao, Y., Ma, Q., Vahedi-Faridi, A., Sundborger, A., Pechstein, A., Puchkov, D., Luo, L., Shupliakov, O., Saenger, W., & Haucke, V. (2010). Molecular basis for SH3 domain regulation of F-BAR-mediated membrane deformation. *Proceedings of the National Academy of Sciences of the United States of America*, *107*(18), 8213–8218.

Reichl, E. M., Ren, Y., Morphew, M. K., Delannoy, M., Effler, J. C., Girard, K. D., Divi, S., Iglesias, P. A., Kuo, S. C., & Robinson, D. N. (2008). Interactions between myosin and actin crosslinkers control cytokinesis contractility dynamics and mechanics. *Current Biology: CB*, *18*(7), 471–480.

Retailleau, K., Duprat, F., Arhatte, M., Ranade, S. S., Peyronnet, R., Martins, J. R., Jodar, M., Moro, C., Offermanns, S., Feng, Y., Demolombe, S., Patel, A., & Honoré, E. (2015). Piezo1 in Smooth Muscle Cells Is Involved in Hypertension-Dependent Arterial Remodeling. *Cell Reports*, *13*(6), 1161–1171.

Ridone, P., Grage, S. L., Patkunarajah, A., Battle, A. R., Ulrich, A. S., & Martinac, B. (2018). “Force-from-lipids” gating of mechanosensitive channels modulated by PUFAs. *Journal of the Mechanical Behavior*

of Biomedical Materials, *79*, 158–167.

Ridone, P., Pandzic, E., Vassalli, M., Cox, C. D., & Macmillan, A. (2019). Disruption of membrane cholesterol organization impairs the concerted activity of PIEZO1 channel clusters. *BioRxiv*. https://www.biorxiv.org/content/10.1101/604488v1.abstract

Ritter, B., Modregger, J., Paulsson, M., & Plomann, M. (1999). PACSIN 2, a novel member of the PACSIN family of cytoplasmic adapter proteins. *FEBS Letters*, *454*(3), 356–362.

Robens, J. M., Yeow-Fong, L., Ng, E., Hall, C., & Manser, E. (2010). Regulation of IRSp53-dependent filopodial dynamics by antagonism between 14-3-3 binding and SH3-mediated localization. *Molecular and Cellular Biology*, *30*(3), 829–844.

Romero, L. O., Massey, A. E., Mata-Daboin, A. D., Sierra-Valdez, F. J., Chauhan, S. C., Cordero-Morales, J. F., & Vásquez, V. (2019). Dietary fatty acids fine-tune Piezo1 mechanical response. In *Nature Communications* (Vol. 10, Issue 1). https://doi.org/10.1038/s41467-019-09055-7

Rotin, D., Bar-Sagi, D., O'Brodovich, H., Merilainen, J., Lehto, V. P., Canessa, C. M., Rossier, B. C., & Downey, G. P. (1994). An SH3 binding region in the epithelial Na+ channel (alpha rENaC) mediates its localization at the apical membrane. *The EMBO Journal*, *13*(19), 4440–4450.

Roubinet, C., Decelle, B., Chicanne, G., Dorn, J. F., Payrastre, B., Payre, F., & Carreno, S. (2011). Molecular networks linked by Moesin drive remodeling of the cell cortex during mitosis. *The Journal of Cell Biology*, *195*(1), 99–112.

Saarikangas, J., Zhao, H., Pykäläinen, A., Laurinmäki, P., Mattila, P. K., Kinnunen, P. K. J., Butcher, S. J., & Lappalainen, P. (2009). Molecular mechanisms of membrane deformation by I-BAR domain proteins. *Current Biology: CB*, *19*(2), 95–107.

Sandquist, J. C., Swenson, K. I., Demali, K. A., Burridge, K., & Means, A. R. (2006). Rho kinase differentially regulates phosphorylation of nonmuscle myosin II isoforms A and B during cell rounding and migration. *The Journal of Biological Chemistry*, *281*(47), 35873–35883.

Saotome, K., Murthy, S. E., Kefauver, J. M., Whitwam, T., Patapoutian,

A., & Ward, A. B. (2018). Structure of the mechanically activated ion channel Piezo1. In *Nature* (Vol. 554, Issue 7693, pp. 481–486). https://doi.org/10.1038/nature25453

Saotome, Kei, Swetha E. Murthy, Jennifer M. Kefauver, Tess Whitwam, Ardem Patapoutian, and Andrew B. Ward. 2018. "Structure of the Mechanically Activated Ion Channel Piezo1." *Nature*. https://doi.org/10.1038/nature25453.

Sathe, M., Muthukrishnan, G., Rae, J., Disanza, A., Thattai, M., Scita, G., Parton, R. G., & Mayor, S. (2018). Small GTPases and BAR domain proteins regulate branched actin polymerisation for clathrin and dynamin-independent endocytosis. *Nature Communications*, *9*(1), 1835.

Saurin, A. T., Durgan, J., Cameron, A. J., Faisal, A., Marber, M. S., & Parker, P. J. (2008). The regulated assembly of a PKCε complex controls the completion of cytokinesis. *Nature Cell Biology*, *10*(8), 891–901.

Scheffer, L. L., Sreetama, S. C., Sharma, N., Medikayala, S., Brown, K. J., Defour, A., & Jaiswal, J. K. (2014). Mechanism of Ca2 -triggered ESCRT assembly and regulation of cell membrane repair. In *Nature Communications* (Vol. 5, Issue 1). https://doi.org/10.1038/ncomms6646

Schiel, J. A., Park, K., Morphew, M. K., Reid, E., Hoenger, A., & Prekeris, R. (2011). Endocytic membrane fusion and buckling-induced microtubule severing mediate cell abscission. *Journal of Cell Science*, *124*(Pt 9), 1411–1424.

Schiel, J. A., Simon, G. C., Zaharris, C., Weisz, J., Castle, D., Wu, C. C., & Prekeris, R. (2012). FIP3-endosome-dependent formation of the secondary ingression mediates ESCRT-III recruitment during cytokinesis. *Nature Cell Biology*, *14*(10), 1068–1078.

Schink, K. O., Raiborg, C., & Stenmark, H. (2013). Phosphatidylinositol 3-phosphate, a lipid that regulates membrane dynamics, protein sorting and cell signalling. *BioEssays: News and Reviews in Molecular, Cellular and Developmental Biology*, *35*(10), 900–912.

Schlunck, G., Damke, H., Kiosses, W. B., Rusk, N., Symons, M. H., Waterman-Storer, C. M., Schmid, S. L., & Schwartz, M. A. (2004). Modulation of Rac localization and function by dynamin. *Molecular Biology of the Cell*, *15*(1), 256–267.

Schöneberg, J., Lehmann, M., Ullrich, A., Posor, Y., Lo, W.-T., Lichtner, G., Schmoranzer, J., Haucke, V., & Noé, F. (2017). Lipid-mediated PX-BAR domain recruitment couples local membrane constriction to endocytic vesicle fission. *Nature Communications*, *8*, 15873.

Schwartz, M. A. (2010). Integrins and extracellular matrix in mechanotransduction. *Cold Spring Harbor Perspectives in Biology*, *2*(12), a005066.

Schwingshackl, A., Lopez, B., Teng, B., Luellen, C., Lesage, F., Belperio, J., Olcese, R., & Waters, C. M. (2017). Hyperoxia treatment of TREK-1/TREK-2/TRAAK-deficient mice is associated with a reduction in surfactant proteins. *American Journal of Physiology. Lung Cellular and Molecular Physiology*, *313*(6), L1030–L1046.

Seddiki, R., Narayana, G. H. N. S., Strale, P.-O., Balcioglu, H. E., Peyret, G., Yao, M., Le, A. P., Teck Lim, C., Yan, J., Ladoux, B., & Mège, R. M. (2018). Force-dependent binding of vinculin to α-catenin regulates cell-cell contact stability and collective cell behavior. *Molecular Biology of the Cell*, *29*(4), 380–388.

Sedzinski, J., Biro, M., Oswald, A., Tinevez, J.-Y., Salbreux, G., & Paluch, E. (2011). Polar actomyosin contractility destabilizes the position of the cytokinetic furrow. *Nature*, *476*(7361), 462–466.

Senju, Y., Rosenbaum, E., Shah, C., Hamada-Nakahara, S., Itoh, Y., Yamamoto, K., Hanawa-Suetsugu, K., Daumke, O., & Suetsugu, S. (2015). Phosphorylation of PACSIN2 by protein kinase C triggers the removal of caveolae from the plasma membrane. *Journal of Cell Science*, *128*(15), 2766–2780.

Sherratt, S. C. R., & Preston Mason, R. (2018). Eicosapentaenoic acid and docosahexaenoic acid have distinct membrane locations and lipid interactions as determined by X-ray diffraction. In *Chemistry and Physics of Lipids* (Vol. 212, pp. 73–79). https://doi.org/10.1016/j.chemphyslip.2018.01.002

Shimada, A., Niwa, H., Tsujita, K., Suetsugu, S., Nitta, K., Hanawa-Suetsugu, K., Akasaka, R., Nishino, Y., Toyama, M., Chen, L., Liu, Z.-J., Wang, B.-C., Yamamoto, M., Terada, T., Miyazawa, A., Tanaka, A., Sugano, S., Shirouzu, M., Nagayama, K., … Yokoyama, S. (2007). Curved EFC/F-BAR-domain dimers are joined end to end into a filament for membrane invagination in endocytosis. *Cell*, *129*(4), 761–772.

Shi, Z., & Baumgart, T. (2015). Membrane tension and peripheral protein density mediate membrane shape transitions. *Nature Communications*, *6*, 5974.

Simpson, F., Hussain, N. K., Qualmann, B., Kelly, R. B., Kay, B. K., McPherson, P. S., & Schmid, S. L. (1999). SH3-domain-containing proteins function at distinct steps in clathrin-coated vesicle formation. *Nature Cell Biology*, *1*(2), 119–124.

Simunovic, M., & Voth, G. A. (2015). Membrane tension controls the assembly of curvature-generating proteins. *Nature Communications*, *6*, 7219.

Simunovic, Mijo, Gregory A. Voth, Andrew Callan-Jones, and Patricia Bassereau. 2015. "When Physics Takes over: BAR Proteins and Membrane Curvature." *Trends in Cell Biology* 25 (12): 780–92.

Skop, A. R., Liu, H., Yates, J., 3rd, Meyer, B. J., & Heald, R. (2004). Dissection of the mammalian midbody proteome reveals conserved cytokinesis mechanisms. *Science*, *305*(5680), 61–66.

Smith, C. M., & Chircop, M. (2012). Clathrin-Mediated Endocytic Proteins are Involved in Regulating Mitotic Progression and Completion. In *Traffic* (Vol. 13, Issue 12, pp. 1628–1641). https://doi.org/10.1111/tra.12001

Smith, L. R., Cho, S., & Discher, D. E. (2018). Stem Cell Differentiation is Regulated by Extracellular Matrix Mechanics. *Physiology* , *33*(1), 16–25.

Snider, C. E., Chandra, M., McDonald, N. A., Willet, A. H., Collier, S. E., Ohi, M. D., Jackson, L. P., & Gould, K. L. (2020). Opposite Surfaces of the Cdc15 F-BAR Domain Create a Membrane Platform That Coordinates Cytoskeletal and Signaling Components for Cytokinesis. *Cell Reports*, *33*(12), 108526.

Snyder, J. L., McBeath, E., Thomas, T. N., Chiu, Y. J., Clark, R. L., & Fujiwara, K. (2017). Mechanotransduction properties of the cytoplasmic tail of PECAM-1. *Biology of the Cell / under the Auspices of the European Cell Biology Organization*, *109*(8), 312–321.

Somers, W. G., & Saint, R. (2003). A RhoGEF and Rho family GTPase-activating protein complex links the contractile ring to cortical microtubules at the onset of cytokinesis. *Developmental Cell*, *4*(1),

29–39.

Song, Y., Li, D., Farrelly, O., Miles, L., Li, F., Kim, S. E., Lo, T. Y., Wang, F., Li, T., Thompson-Peer, K. L., Gong, J., Murthy, S. E., Coste, B., Yakubovich, N., Patapoutian, A., Xiang, Y., Rompolas, P., Jan, L. Y., & Jan, Y. N. (2019). The Mechanosensitive Ion Channel Piezo Inhibits Axon Regeneration. *Neuron*, *102*(2), 373–389.e6.

Son, S., Kang, J. H., Oh, S., Kirschner, M. W., Mitchison, T. J., & Manalis, S. (2015). Resonant microchannel volume and mass measurements show that suspended cells swell during mitosis. *The Journal of Cell Biology*, *211*(4), 757–763.

Spencer, S., Dowbenko, D., Cheng, J., Li, W., Brush, J., Utzig, S., Simanis, V., & Lasky, L. A. (1997). PSTPIP: A Tyrosine Phosphorylated Cleavage Furrow–associated Protein that Is a Substrate for a PEST Tyrosine Phosphatase. *The Journal of Cell Biology*, *138*(4), 845–860.

Spindler, V., Schlegel, N., & Waschke, J. (2010). Role of GTPases in control of microvascular permeability. *Cardiovascular Research*, *87*(2), 243–253.

Srivastava, N., Traynor, D., Piel, M., Kabla, A. J., & Kay, R. R. (2020). Pressure sensing through Piezo channels controls whether cells migrate with blebs or pseudopods. *Proceedings of the National Academy of Sciences of the United States of America*, *117*(5), 2506–2512.

Stewart, M. P., Helenius, J., Toyoda, Y., Ramanathan, S. P., Muller, D. J., & Hyman, A. A. (2011). Hydrostatic pressure and the actomyosin cortex drive mitotic cell rounding. *Nature*, *469*(7329), 226–230.

Suchyna, T. M. (2017). Piezo channels and GsMTx4: Two milestones in our understanding of excitatory mechanosensitive channels and their role in pathology. *Progress in Biophysics and Molecular Biology*, *130*(Pt B), 244–253.

Suchyna, T. M., Markin, V. S., & Sachs, F. (2009). Biophysics and structure of the patch and the gigaseal. *Biophysical Journal*, *97*(3), 738–747.

Suchyna, T. M., Tape, S. E., Koeppe, R. E., 2nd, Andersen, O. S., Sachs, F., & Gottlieb, P. A. (2004). Bilayer-dependent inhibition of mechanosensitive channels by neuroactive peptide enantiomers.

Nature, *430*(6996), 235–240.

Sugimoto, A., Miyazaki, A., Kawarabayashi, K., Shono, M., Akazawa, Y., Hasegawa, T., Ueda-Yamaguchi, K., Kitamura, T., Yoshizaki, K., Fukumoto, S., & Iwamoto, T. (2017). Piezo type mechanosensitive ion channel component 1 functions as a regulator of the cell fate determination of mesenchymal stem cells. *Scientific Reports*, *7*(1), 17696.

Sugisawa, E., Takayama, Y., Takemura, N., Kondo, T., Hatakeyama, S., Kumagai, Y., Sunagawa, M., Tominaga, M., & Maruyama, K. (2020). RNA Sensing by Gut Piezo1 Is Essential for Systemic Serotonin Synthesis. *Cell*, *182*(3), 609–624.e21.

Su, K.-C., Takaki, T., & Petronczki, M. (2011). Targeting of the RhoGEF Ect2 to the equatorial membrane controls cleavage furrow formation during cytokinesis. *Developmental Cell*, *21*(6), 1104–1115.

Sukharev, S., Betanzos, M., Chiang, C. S., & Guy, H. R. (2001). The gating mechanism of the large mechanosensitive channel MscL. *Nature*, *409*(6821), 720–724.

Sukharev, S. I., Blount, P., Martinac, B., Blattner, F. R., & Kung, C. (1994). A large-conductance mechanosensitive channel in E. coli encoded by mscL alone. *Nature*, *368*(6468), 265–268.

Sumoy, L., Pluvinet, R., Andreu, N., Estivill, X., & Escarceller, M. (2001). PACSIN 3 is a novel SH3 domain cytoplasmic adapter protein of the pacsin-syndapin-FAP52 gene family. *Gene*, *262*(1-2), 199–205.

Sun, S., Zhou, X., Corvera, J., Gallick, G. E., Lin, S.-H., & Kuang, J. (2015). ALG-2 activates the MVB sorting function of ALIX through relieving its intramolecular interaction. *Cell Discovery*, *1*, 15018.

Sun, W., Chi, S., Li, Y., Ling, S., Tan, Y., Xu, Y., Jiang, F., Li, J., Liu, C., Zhong, G., Cao, D., Jin, X., Zhao, D., Gao, X., Liu, Z., Xiao, B., & Li, Y. (2019). The mechanosensitive Piezo1 channel is required for bone formation. *eLife*, *8*. https://doi.org/10.7554/eLife.47454

Suzuki, A., Badger, B. L., Haase, J., Ohashi, T., Erickson, H. P., Salmon, E. D., & Bloom, K. (2016). How the kinetochore couples microtubule force and centromere stretch to move chromosomes. *Nature Cell Biology*, *18*(4), 382–392.

Syeda, R., Florendo, M. N., Cox, C. D., Kefauver, J. M., Santos, J. S., Martinac, B., & Patapoutian, A. (2016). Piezo1 Channels Are Inherently Mechanosensitive. *Cell Reports*, *17*(7), 1739–1746.

Syeda, R., Xu, J., Dubin, A. E., Coste, B., Mathur, J., Huynh, T., Matzen, J., Lao, J., Tully, D. C., Engels, I. H., Petrassi, H. M., Schumacher, A. M., Montal, M., Bandell, M., & Patapoutian, A. (2015). Chemical activation of the mechanotransduction channel Piezo1. *eLife*, *4*. https://doi.org/10.7554/eLife.07369

Takeda, T., Robinson, I. M., Savoian, M. M., Griffiths, J. R., Whetton, A. D., McMahon, H. T., & Glover, D. M. (2013). Drosophila F-BAR protein Syndapin contributes to coupling the plasma membrane and contractile ring in cytokinesis. *Open Biology*, *3*(8), 130081.

Takenawa, Tadaomi, and Shiro Suetsugu. 2007. "The WASP-WAVE Protein Network: Connecting the Membrane to the Cytoskeleton." *Nature Reviews. Molecular Cell Biology* 8 (1): 37–48.

Taneja, N., Bersi, M. R., Baillargeon, S. M., Fenix, A. M., Cooper, J. A., Ohi, R., Gama, V., Merryman, W. D., & Burnette, D. T. (2020). Precise Tuning of Cortical Contractility Regulates Cell Shape during Cytokinesis. *Cell Reports*, *31*(1), 107477.

Taneja, N., Fenix, A. M., Rathbun, L., Millis, B. A., Tyska, M. J., Hehnly, H., & Burnette, D. T. (2016). Focal adhesions control cleavage furrow shape and spindle tilt during mitosis. *Scientific Reports*, *6*, 29846.

Tedeschi, A., Almagro, J., Renshaw, M. J., Messal, H. A., Behrens, A., & Petronczki, M. (2020). Cep55 promotes cytokinesis of neural progenitors but is dispensable for most mammalian cell divisions. *Nature Communications*, *11*(1), 1746.

Thompson, H. M., Cao, H., Chen, J., Euteneuer, U., & McNiven, M. A. (2004). Dynamin 2 binds gamma-tubulin and participates in centrosome cohesion. *Nature Cell Biology*, *6*(4), 335–342.

Thompson, H. M., Skop, A. R., Euteneuer, U., Meyer, B. J., & McNiven, M. A. (2002). The large GTPase dynamin associates with the spindle midzone and is required for cytokinesis. *Current Biology: CB*, *12*(24), 2111–2117.

Thoresen, S. B., Pedersen, N. M., Liestøl, K., & Stenmark, H. (2010). A phosphatidylinositol 3-kinase class III sub-complex containing

VPS15, VPS34, Beclin 1, UVRAG and BIF-1 regulates cytokinesis and degradative endocytic traffic. *Experimental Cell Research*, *316*(20), 3368–3378.

Toyoda, Y., Cattin, C. J., Stewart, M. P., Poser, I., Theis, M., Kurzchalia, T. V., Buchholz, F., Hyman, A. A., & Müller, D. J. (2017). Genome-scale single-cell mechanical phenotyping reveals disease-related genes involved in mitotic rounding. *Nature Communications*, *8*(1), 1266.

Tsai, F.-C., Bertin, A., Bousquet, H., Manzi, J., Senju, Y., Tsai, M.-C., Picas, L., Miserey-Lenkei, S., Lappalainen, P., Lemichez, E., Coudrier, E., & Bassereau, P. (2018). Ezrin enrichment on curved membranes requires a specific conformation or interaction with a curvature-sensitive partner. *eLife*, *7*. https://doi.org/10.7554/eLife.37262

Turk, H. F., & Chapkin, R. S. (2013). Membrane lipid raft organization is uniquely modified by n-3 polyunsaturated fatty acids. *Prostaglandins, Leukotrienes, and Essential Fatty Acids*, *88*(1), 43–47.

Uroz, M., Garcia-Puig, A., Tekeli, I., Elosegui-Artola, A., Abenza, J. F., Marín-Llauradó, A., Pujals, S., Conte, V., Albertazzi, L., Roca-Cusachs, P., Raya, Á., & Trepat, X. (2019). Traction forces at the cytokinetic ring regulate cell division and polyploidy in the migrating zebrafish epicardium. *Nature Materials*, *18*(9), 1015–1023.

van Oostende Triplet, C., Jaramillo Garcia, M., Haji Bik, H., Beaudet, D., & Piekny, A. (2014). Anillin interacts with microtubules and is part of the astral pathway that defines cortical domains. *Journal of Cell Science*, *127*(Pt 17), 3699–3710.

Velasco-Estevez, M., Gadalla, K. K. E., Liñan-Barba, N., Cobb, S., Dev, K. K., & Sheridan, G. K. (2020). Inhibition of Piezo1 attenuates demyelination in the central nervous system. *Glia*, *68*(2), 356–375.

Venturini, V., Pezzano, F., Català Castro, F., Häkkinen, H.-M., Jiménez-Delgado, S., Colomer-Rosell, M., Marro, M., Tolosa-Ramon, Q., Paz-López, S., Valverde, M. A., Weghuber, J., Loza-Alvarez, P., Krieg, M., Wieser, S., & Ruprecht, V. (2020). The nucleus measures shape changes for cellular proprioception to control dynamic cell behavior. *Science*, *370*(6514). https://doi.org/10.1126/science.aba2644

Vietri, M., Radulovic, M., & Stenmark, H. (2020). The many functions of ESCRTs. *Nature Reviews. Molecular Cell Biology*, *21*(1), 25–42.

Vukušić, K., Buđa, R., Bosilj, A., Milas, A., Pavin, N., & Tolić, I. M. (2017). Microtubule Sliding within the Bridging Fiber Pushes Kinetochore Fibers Apart to Segregate Chromosomes. *Developmental Cell*, *43*(1), 11–23.e6.

Wallin, E., & Von Heijne, G. (1998). Genome-wide analysis of integral membrane proteins from eubacterial, archaean, and eukaryotic organisms. In *Protein Science* (Vol. 7, Issue 4, pp. 1029–1038). https://doi.org/10.1002/pro.5560070420

Wang, L., You, X., Lotinun, S., Zhang, L., Wu, N., & Zou, W. (2020). Mechanical sensing protein PIEZO1 regulates bone homeostasis via osteoblast-osteoclast crosstalk. *Nature Communications*, *11*(1), 282.

Wang, L., Zhou, H., Zhang, M., Liu, W., Deng, T., Zhao, Q., Li, Y., Lei, J., Li, X., & Xiao, B. (2019). Structure and mechanogating of the mammalian tactile channel PIEZO2. In *Nature* (Vol. 573, Issue 7773, pp. 225–229). https://doi.org/10.1038/s41586-019-1505-8

Wang, Q., Navarro, M. V. A. S., Peng, G., Molinelli, E., Goh, S. L., Judson, B. L., Rajashankar, K. R., & Sondermann, H. (2009). Molecular mechanism of membrane constriction and tubulation mediated by the F-BAR protein Pacsin/Syndapin. *Proceedings of the National Academy of Sciences of the United States of America*, *106*(31), 12700–12705.

Wang, S., Chennupati, R., Kaur, H., Iring, A., Wettschureck, N., & Offermanns, S. (2016). Endothelial cation channel PIEZO1 controls blood pressure by mediating flow-induced ATP release. *The Journal of Clinical Investigation*, *126*(12), 4527–4536.

Wang, Y., Chi, S., Guo, H., Li, G., Wang, L., Zhao, Q., Rao, Y., Zu, L., He, W., & Xiao, B. (2018). A lever-like transduction pathway for long-distance chemical- and mechano-gating of the mechanosensitive Piezo1 channel. *Nature Communications*, *9*(1), 1300.

Wang, Y., & Xiao, B. (2018). The mechanosensitive Piezo1 channel: structural features and molecular bases underlying its ion permeation and mechanotransduction. *The Journal of Physiology*, *596*(6), 969–978.

Webb, S. E., Lee, K. W., Karplus, E., & Miller, A. L. (1997). Localized

calcium transients accompany furrow positioning, propagation, and deepening during the early cleavage period of zebrafish embryos. *Developmental Biology*, *192*(1), 78–92.

Webb, S. E., Li, W. M., & Miller, A. L. (2008). Calcium signalling during the cleavage period of zebrafish development. *Philosophical Transactions of the Royal Society of London. Series B, Biological Sciences*, *363*(1495), 1363–1369.

Webb, S. E., & Miller, A. L. (2017). Ca2 Signalling and Membrane Dynamics During Cytokinesis in Animal Cells. In *Advances in Experimental Medicine and Biology* (pp. 389–412). https://doi.org/10.1007/978-3-319-55858-5_15

Werner, M., Munro, E., & Glotzer, M. (2007). Astral signals spatially bias cortical myosin recruitment to break symmetry and promote cytokinesis. *Current Biology: CB*, *17*(15), 1286–1297.

Wilson, G. M., Fielding, A. B., Simon, G. C., Yu, X., Andrews, P. D., Hames, R. S., Frey, A. M., Peden, A. A., Gould, G. W., & Prekeris, R. (2005). The FIP3-Rab11 protein complex regulates recycling endosome targeting to the cleavage furrow during late cytokinesis. *Molecular Biology of the Cell*, *16*(2), 849–860.

Wojciak-Stothard, B., & Ridley, A. J. (2003). Shear stress-induced endothelial cell polarization is mediated by Rho and Rac but not Cdc42 or PI 3-kinases. *The Journal of Cell Biology*, *161*(2), 429–439.

Wolfenson, H., Yang, B., & Sheetz, M. P. (2019). Steps in Mechanotransduction Pathways that Control Cell Morphology. *Annual Review of Physiology*, *81*, 585–605.

Wollert, T., Wunder, C., Lippincott-Schwartz, J., & Hurley, J. H. (2009). Membrane scission by the ESCRT-III complex. *Nature*, *458*(7235), 172–177.

Wong, R., Hadjiyanni, I., Wei, H.-C., Polevoy, G., McBride, R., Sem, K.-P., & Brill, J. A. (2005). PIP2 hydrolysis and calcium release are required for cytokinesis in Drosophila spermatocytes. *Current Biology: CB*, *15*(15), 1401–1406.

Woodham, E. F., Paul, N. R., Tyrrell, B., Spence, H. J., Swaminathan, K., Scribner, M. R., Giampazolias, E., Hedley, A., Clark, W., Kage, F., Marston, D. J., Hahn, K. M., Tait, S. W. G., Larue, L., Brakebusch,

C. H., Insall, R. H., & Machesky, L. M. (2017). Coordination by Cdc42 of Actin, Contractility, and Adhesion for Melanoblast Movement in Mouse Skin. *Current Biology: CB*, *27*(5), 624–637.

Woo, S.-H., Lukacs, V., de Nooij, J. C., Zaytseva, D., Criddle, C. R., Francisco, A., Jessell, T. M., Wilkinson, K. A., & Patapoutian, A. (2015). Piezo2 is the principal mechanotransduction channel for proprioception. *Nature Neuroscience*, *18*(12), 1756–1762.

Woo, S.-H., Ranade, S., Weyer, A. D., Dubin, A. E., Baba, Y., Qiu, Z., Petrus, M., Miyamoto, T., Reddy, K., Lumpkin, E. A., Stucky, C. L., & Patapoutian, A. (2014). Piezo2 is required for Merkel-cell mechanotransduction. *Nature*, *509*(7502), 622–626.

Wu, C.-Y., Lin, M.-W., Wu, D.-C., Huang, Y.-B., Huang, H.-T., & Chen, C.-L. (2014). The role of phosphoinositide-regulated actin reorganization in chemotaxis and cell migration. *British Journal of Pharmacology*, *171*(24), 5541–5554.

Wu, J., Young, M., Lewis, A. H., Martfeld, A. N., Kalmeta, B., & Grandl, J. (2017). Inactivation of Mechanically Activated Piezo1 Ion Channels Is Determined by the C-Terminal Extracellular Domain and the Inner Pore Helix. *Cell Reports*, *21*(9), 2357–2366.

Xue, F., Cox, C. D., Bavi, N., Rohde, P. R., Nakayama, Y., & Martinac, B. (2020). Membrane stiffness is one of the key determinants of E. coli MscS channel mechanosensitivity. *Biochimica et Biophysica Acta, Biomembranes*, *1862*(5), 183203.

Yaganoglu, S., Helassa, N., Gaub, B., Welling, M., Shi, J., Müller, D., Török, K., & Pantazis, P. (2019). *GenEPi: Piezo1-based fluorescent reporter for visualizing mechanical stimuli with high spatiotemporal resolution*. https://livrepository.liverpool.ac.uk/3099700

Yamada, K. M., Collins, J. W., Cruz Walma, D. A., Doyle, A. D., Morales, S. G., Lu, J., Matsumoto, K., Nazari, S. S., Sekiguchi, R., Shinsato, Y., & Wang, S. (2019). Extracellular matrix dynamics in cell migration, invasion and tissue morphogenesis. *International Journal of Experimental Pathology*, *100*(3), 144–152.

Yang, H., Liu, C., Zhou, R.-M., Yao, J., Li, X.-M., Shen, Y., Cheng, H., Yuan, J., Yan, B., & Jiang, Q. (2016). Piezo2 protein: A novel regulator of tumor angiogenesis and hyperpermeability. *Oncotarget*, *7*(28), 44630–44643.

Yee, N. S., Zhou, W., & Liang, I.-C. (2011). Transient receptor potential ion channel Trpm7 regulates exocrine pancreatic epithelial proliferation by Mg2+-sensitive Socs3a signaling in development and cancer. *Disease Models & Mechanisms*, *4*(2), 240–254.

You, S. Y., Park, Y. S., Jeon, H.-J., Cho, D.-H., Jeon, H. B., Kim, S. H., Chang, J. W., Kim, J.-S., & Oh, J. S. (2016). Beclin-1 knockdown shows abscission failure but not autophagy defect during oocyte meiotic maturation. *Cell Cycle* , *15*(12), 1611–1619.

Yüce, Ö., Piekny, A., & Glotzer, M. (2005). An ECT2–centralspindlin complex regulates the localization and function of RhoA. *The Journal of Cell Biology*, *170*(4), 571–582.

Yu, Y.-Y., Chen, Y., Dai, G., Chen, J., Sun, X.-M., Wen, C.-J., Zhao, D.-H., Chang, D. C., & Li, C.-J. (2004). The association of calmodulin with central spindle regulates the initiation of cytokinesis in HeLa cells. *The International Journal of Biochemistry & Cell Biology*, *36*(8), 1562–1572.

Zang, J.-H., Cavet, G., Sabry, J. H., Wagner, P., Moores, S. L., & Spudich, J. A. (1997). On the Role of Myosin-II in Cytokinesis: Division ofDictyostelium Cells under Adhesive and Nonadhesive Conditions. *Molecular Biology of the Cell*, *8*(12), 2617–2629.

Zerial, M., & McBride, H. (2001). Rab proteins as membrane organizers. *Nature Reviews. Molecular Cell Biology*, *2*(2), 107–117.

Zhang, T., Chi, S., Jiang, F., Zhao, Q., & Xiao, B. (2017). A protein interaction mechanism for suppressing the mechanosensitive Piezo channels. *Nature Communications*, *8*(1), 1797.

Zhang, W., & Robinson, D. N. (2005). Balance of actively generated contractile and resistive forces controls cytokinesis dynamics. *Proceedings of the National Academy of Sciences of the United States of America*, *102*(20), 7186–7191.

Zhao, H., Michelot, A., Koskela, E. V., Tkach, V., Stamou, D., Drubin, D. G., & Lappalainen, P. (2013). Membrane-Sculpting BAR Domains Generate Stable Lipid Microdomains. In *Cell Reports* (Vol. 4, Issue 6, pp. 1213–1223). https://doi.org/10.1016/j.celrep.2013.08.024

Zhao, Q., Wu, K., Geng, J., Chi, S., Wang, Y., Zhi, P., Zhang, M., & Xiao, B. (2016). Ion Permeation and Mechanotransduction Mechanisms of Mechanosensitive Piezo Channels. *Neuron*, *89*(6),

1248–1263.

Zhao, Q., Zhou, H., Chi, S., Wang, Y., Wang, J., Geng, J., Wu, K., Liu, W., Zhang, T., Dong, M.-Q., Wang, J., Li, X., & Xiao, B. (2018). Structure and mechanogating mechanism of the Piezo1 channel. *Nature*, *554*(7693), 487–492.

Zhao, W.-M., Seki, A., & Fang, G. (2006). Cep55, a microtubule-bundling protein, associates with centralspindlin to control the midbody integrity and cell abscission during cytokinesis. *Molecular Biology of the Cell*, *17*(9), 3881–3896.

Zheng, W., Gracheva, E. O., & Bagriantsev, S. N. (2019). A hydrophobic gate in the inner pore helix is the major determinant of inactivation in mechanosensitive Piezo channels. *eLife*, *8*. https://doi.org/10.7554/eLife.44003

Zhong, Q., Watson, M. J., Lazar, C. S., Hounslow, A. M., Waltho, J. P., & Gill, G. N. (2005). Determinants of the endosomal localization of sorting nexin 1. *Molecular Biology of the Cell*, *16*(4), 2049–2057.

Zhou, W., Liu, X., van Wijnbergen, J. W. M., Yuan, L., Liu, Y., Zhang, C., & Jia, W. (2020). Identification of PIEZO1 as a potential prognostic marker in gliomas. In *Scientific Reports* (Vol. 10, Issue 1). https://doi.org/10.1038/s41598-020-72886-8

Zlotek-Zlotkiewicz, E., Monnier, S., Cappello, G., Le Berre, M., & Piel, M. (2015). Optical volume and mass measurements show that mammalian cells swell during mitosis. *The Journal of Cell Biology*, *211*(4), 765–774.

Zuccala, E. S., Satchwell, T. J., Angrisano, F., Tan, Y. H., Wilson, M. C., Heesom, K. J., & Baum, J. (2016). Quantitative phospho-proteomics reveals the Plasmodium merozoite triggers pre-invasion host kinase modification of the red cell cytoskeleton. *Scientific Reports*, *6*, 19766.